AN ACOUSTIC EMISSION AND HYGROTHERMAL AGING STUDY OF FIBER REINFORCED POLYMER COMPOSITES

by

Kai Jeffrey Newhouse

A thesis submitted in partial fulfillment
of the requirements for the degree

of

Master of Science

in

Mechanical Engineering

MONTANA STATE UNIVERSITY
Bozeman, Montana

April 2019

ACKNOWLEDGEMENTS

I am surrounded by supportive, helpful, and caring people who have all made sacrifices to help me succeed. For this I am grateful. I would like to thank Dr. David Miller for kindling my interest in composite materials and guiding my research with patience. Thanks to Dan Samborsky for helping to cultivate good habits in practical aspects of research. Thank you to my parents Ken and Debbie Newhouse for their lasting support and guidance in all areas of my life. I would also like to thank Laura Merchak for always showing happiness and support and helping the days move easy. Lastly, I would like to thank my cat Buddy. I'm glad you stayed alive long enough in the woods for me to find you.

TABLE OF CONTENTS

TABLE OF CONTENTS – CONTINUED

LIST OF TABLES

LIST OF FIGURES

Figure Page

LIST OF FIGURES – CONTINUED

Table Page

LIST OF FIGURES – CONTINUED

Table Page

LIST OF FIGURES – CONTINUED

Table Page

ABSTRACT

Fiber reinforced polymer matrix composites are a premier choice for offshore wind turbines and Marine Hydro-Kinetic Devices, which operate in harsh and isolated marine environments. These factors combined with decades long target service life make imperative the understanding of damage mechanisms and the environmental effects thereof. Acoustic emission monitoring is a research technology that uses specialized sensors to detect transient elastic waves in a material which originate from damage sources. Waveform parameters have been correlated with different damage mechanisms in fibrous composites.

A diverse set of fiber-matrix combinations configured into a variety of layups totaling more than 30 laminates were mechanically tested in quasi-static uniaxial tension while monitoring acoustic emission. A subset of these materials was aged prior to testing in an artificial marine environment by soaking in a water bath of simulated seawater at 50 degrees Celsius. Various acoustic emission waveform parameters were investigated with respect to expected damage between layups and possible material-based differences.

Among the conditioned material set, mechanical changes from moisture absorption shows mixed levels of degradation among different material systems. Moduli were generally unaffected with a few minor decreases. Strengths were reduced by as much as 41%, and failure strains fell as much as 47%.

From acoustic emission investigation, good correlation is found between Fast Fourier Transform peak spectral frequency bands and expected damage mechanisms between layups. Material based peak frequency differences are found exclusively in interphase failures (de-bond and fiber pullout). Layup-based correlations in conjunction with elastic wave theory were used to put forth new frequency band ranges associated with damage types.

INTRODUCTION

A Need for Clean Energy

The United States has formidable energy demand, near 30,000 TWh/year, which is projected to increase [1]. Additionally, large and ever-growing body of environmental research shows that humans have a significant effect on climate change in part caused by combustion-type energy production methods, which constitute 80 percent of the US energy supply [2],[3],[4]. Finally, fossil fuels are subject to scarcity. These circumstances have created a great need for clean and renewable energy.

Marine Hydro Kinetic Devices and Offshore Wind Turbines

The movement of wind and water currents around the globe is a tremendous source of renewable energy. Marine Hydrokinetic (MHK) Devices harness a portion of energy in moving water. Ocean currents, waves, and tidal streams are predictable and consistent, providing a reliable energy source in coastal regions. This is convenient as many coastal regions have high population and thus high energy demand. Ocean currents and waves on the coasts of the United States are estimated between 1168 and 1670 TWh/year in technical potential [5], [6]. Offshore wind turbines harvest energy from moving air currents over the ocean and are estimated to hold another 2,000 GWh/year in technical potential [7]. Offshore wind is also candidate for coastal regions power supply, but offshore wind is less consistent than water currents and waves.

The ultimate shortcoming of offshore wind and MHK energy is projected levelized cost of electricity (LCOE). LCOE estimates vary widely (>1000-100 $/MWh) between

institutions, which assess based on: deployment site, design, and array size. Very few estimates describe MHK or offshore wind to be economically competitive with combustion-type power generation within the next twenty years [6], [8]. Projected LCOE estimates for popular combustion type generation are near 50-100 $/MWh [9]. LCOE is affected by the costs of building and operating a generation site over a certain financial life and duty cycle. Because wind and water power have no fuel costs, the primary factor is capital cost: what it takes to build and maintain a site.

To build an efficient turbine array, devices should maximize power generation and service life and minimize maintenance. With respect to wind power, larger turbines produce more energy. Therefore, wind turbine rotor diameters have increased since their inception with current rotor diameters reaching upwards of 200 meters, but these structures must be light weight enough to capture wind energy efficiently.

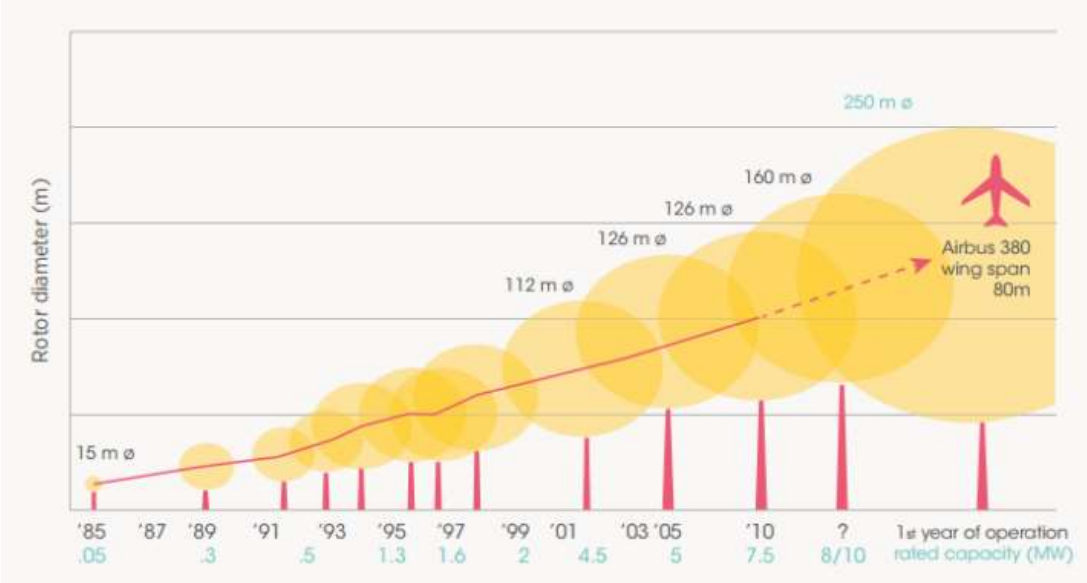

Figure 1: Progression of wind turbine blade size indicated the need for high performance composites

Composite materials are the premier choice for wind turbines and MHK devices for their high specific stiffness and strength, qualities essential for such specialized applications. Composites also lend themselves to manufacturability into complex 3D shapes and can be tailored to have high fatigue performance. However, response to environmental conditions is an important factor in establishing service life of offshore turbines and MHK devices. Therefore, fully characterizing and understanding these materials is essential to advancing technology and lowering the cost of these renewable energies.

Composite Materials Research

Fiber reinforced polymer matrix composites are versatile materials employed in a myriad of industries because of their high specific strength, specific stiffness, durability, and formability. Among these industries are marine, aerospace, recreation, and renewable energy production. Each application requires slightly different tailored characteristics. Aerospace structures must be light, stiff, strong, and durable. Marine structures must be inexpensive, easily integrated into manufacturing, and resist environmental degradation. MHK structures require a combination of all these properties. Turbine blades must be light, strong, inexpensive, durable, and environmentally stable to be an efficient and long-lasting structure. This unique set of requirements necessitates development of a specialized class of composite materials tailored for such an application.

In this field of materials research various fiber-matrix combinations are selected and evaluated with respect to stiffness, strength, damage tolerance, manufacturability, and susceptibility to environmental degradation. This research is preformed empirically as theoretical methods are insufficient. Generalized theories for homogenized stiffness, strength, moisture effects, temperature effects, and fatigue life exist [10] but these methods are ultimately unreliable as composite materials are complex mechanical systems which behave very differently depending on fiber type, fiber form & shape, fiber orientation, matrix type, and fiber matrix interaction.

Structural Health Monitoring

MHK devices and offshore wind turbines, the target applications for the materials studied in this work, are very difficult to manually maintain and inspect for damage. Offshore turbines are far from land and MHK devices are submerged, making accessibility difficult and expensive. This expense increases LCOE and reduces the appeal of the energy source. Therefore, it is advantageous to create a system by which structural integrity can be assessed remotely. This is referred to as structural health monitoring (SHM). For example, in bridges SHM has been achieved by measuring load, displacement, strain, vibration etc. by implementation of anemometers, seismometers, accelerometers, temperature sensors, humidity sensors, pressure sensors, and others [11]. This array of data yields a detailed picture of loads and structure response which is used to determine structural health and necessary manual maintenance. A similar system could be implemented in composite structures but assessing structural health is far more challenging. Acoustic Emission, a field explained more thoroughly later in this work, has shown promise in detecting damage in many material types. However, this information is still limited. Damage information is also difficult to use as damage progression and damage tolerance is not fully defined for all composite systems. Therefore, developing damage detection technology in tandem with damage models is an importance science to advance this class of materials for renewable energy and moving toward a more sustainable future.

BACKGROUND

Composite Materials

Composite materials are the combination of two or more materials, which have superior properties than their constituents. Composites have a matrix phase and one or more reinforcement phase. Reinforcement can be particulate or fibers. From a mechanical perspective, the reinforcement phase(s) bare the load, and the matrix phase acts to transmit the load to the reinforcement. Particulate reinforcement often creates an isotropic material where mechanical properties are the same on all directions. Fibrous reinforcement can create nearly isotropic materials with random orientation, but they can also create anisotropic materials where mechanical properties vary with direction. Strength and stiffness are higher along fiber axis. Using anisotropic materials is appealing from a structural engineering perspective because fibers can be oriented along primary load paths providing stiffness and strength in the directions where they are needed while reducing material use and weight in less critical areas.

Many types of composites exist. Some common examples are concrete, plywood, and fiber reinforced polymer. Concrete has hard mineral particulate reinforcement with a cement matrix phase. Concrete also uses steel rebar as directional reinforcement. Plywood uses thin wood plies held together with glue. There are a multitude of fiber reinforced polymer matrix composites with fibers ranging from engineered continuous strand glass, quartz, carbon, metallics, and plastics to chopped natural fibers. All of which are embedded in a plethora of matrix materials, which include: thermoplastics, thermosets, ceramics, and metals.

Although there are a multitude of fiber and plastic matrix combinations, the fibers and plastic matrices covered here are not an exhaustive list but are only those applicable to this work. Glass and/or carbon fiber reinforced polymer matrix composites are the focus of this thesis. There are several varieties of glass fibers which have different physical, chemical, electrical, and mechanical properties. E-glass is the most commonly used for its high tensile strength, low cost, and good corrosion resistance. S-glass, C-glass, D-glass, A-glass, and AR-glass are other types of glass which are tailored to accentuate strength, corrosion resistance, or electrical insulation. Glass fiber diameter range from 9 to 25 microns [10].

Carbon fibers are lighter, stiffer, stronger, and have better chemical resistance than glass fibers, but they are more expensive. Carbon fibers are made from two different raw materials, often called precursors: polyacrylonitrile (PAN) and pitch. In general, PAN fibers are stronger than pitch but more expensive. Even within a precursor family, carbon fiber stiffness and strength can vary widely, which is largely influenced by thermal treatment. Different grades of carbon fiber are classified by their modulus and strength or tenacity. Carbon fiber are typically thinner than glass, ranging from 5 to 10 microns [10]. It is also important to note that carbon fibers are electrical conductors and therefore can create galvanic corrosion when in contact with metal parts.

Fibers exist in continuous and discontinuous forms. Chopped versus continuous is a major distinction. Chopped fibers are usually used in injection molding (short fibers) or in veils and mats (long fibers). Within continuous fibers, the varieties are boundless, but there are common types and groupings. They are typically formed into a continuous sheet,

called a ply. Plies are stacked on top of one another as a plate or curved part orienting fibers in the desired directions. Ply pattern and orientation is called the layup and has a specific notation, exemplified in Figure 2 which shows a quasi-isotropic and symmetric layup. It is quasi-isotropic because there are fibers oriented longitudinally, transversely, and along the 45. It is symmetric because the stacking sequence is repeated in reverse at half way. This is denoted by the subscript 's' after the bracketed layup. Subscripts are also used to denote multiple plies in the same orientation as well as a change in fabric type.

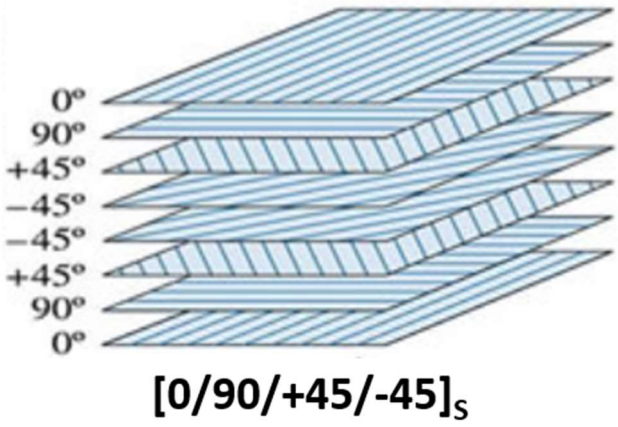

Figure 2: Quasi-isotropic symmetric layup example with notation

A common composite form is prepreg, in which fibers are impregnated with an epoxy matrix and aligned onto a removable backing sheet for easy handling. Fibers also come collected into workable bundles, called tows. Tows come in different diameters and are often woven or stitched into sheets with fibers oriented in a single direction or several

directions. Very thin tows also come in randomly oriented mats called veil. Examples of such forms are shown in Figure 3.

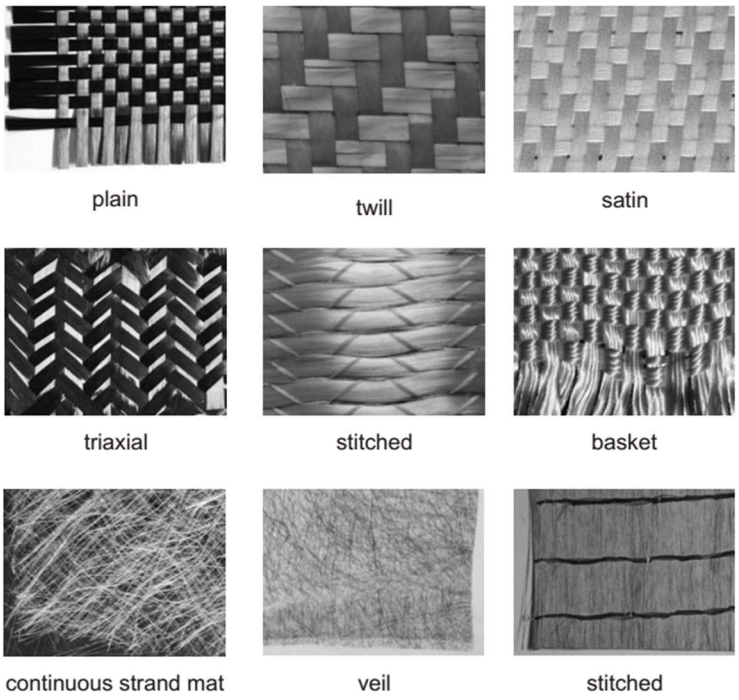

Figure 3: Examples of fiber forms [10]

There are many different weaves, which provide different advantages. Stitched fabrics are usually unidirectional, but also exist in multi-directional plies. Both families suffer from 'pre-buckling' and crimp. When tows are not completely straight, the fabric is pre-buckled. In weaves, tows are deflected out of plane as they pass over another tow, also considered pre-buckling. This greatly reduces compressive strength of the fiber. A stitched fabric ameliorates some amount of pre-buckling, but can still suffer from crimp. Crimp is

when the tow is strangled by the stitching. Crimp causes problems because it can impede complete resin saturation, causing dry spots. It also creates a stress concentration by slightly deforming the load path. Crimp effects woven and stitched fabrics.

Fibers must bond to the matrix for load transfer to occur. Glass and carbon fibers do not naturally bond well to every type of plastic and are therefore coated in a special chemical compound, called sizing, which enables bonding. This chemical compound varies from different fiber types and matrix materials to accommodate different fiber and matrix surface chemistry. Sizing is also used to aid manufacturing. Raw glass fibers are abrasive and do not slide past one another easily. Sizing reduces the friction thus easing the weaving and stitching process. In the composites industry each fabric manufacturer often creates their own sizing compound and tends to guard its formulation closely. Therefore, sizing development is not well documented in the public domain. It is known that it can be contaminated, washed off, and/or expire.

Many different plastics are used as matrix materials, all of which fall into thermosets or thermoplastics. Thermoset plastics are created by inducing a curing agent into a resin which facilitates creation of chemical links between polymer chains or individual monomers in the resin. This process is called crosslinking. The most common classes of thermosets used in composites are polyesters, vinyl esters, and epoxies.

Polyesters are a class of low-cost thermosets which provide a good cost/performance ratio and good environmental degradation resistance. Polyester resins are low viscosity which aids in manufacturing, covered later in manufacturing of composites. Vinyl esters are another thermoset with a slightly higher cost than polyesters but provide

higher failure strain and resistance to chemical corrosion. Epoxies are the highest cost but highest performing thermoset with good mechanical properties, low resin viscosity, good environmental properties, and good chemical resistance. Epoxies are a diverse and highly modifiable family of polymers. It is for these reasons that epoxies are the most widely used in high performance applications.

Thermoplastics are also used in composites, but usually for less demanding applications as they have lower mechanical properties and are more vulnerable to chemical and environmental degradation. They can have higher damage tolerance as cracks propagate slower through a softer matrix, but this matrix ductility must be accompanied by strong bonding to the fibers for efficient load transfer.

Any of these material classes are modified chemically, hybridized by combining with other plastics, or altered with fillers/additives to tailor mechanical, physical, or chemical properties. Polymer science is a vast and complicated stand-alone field parts of which support the composites industry. The information provided here is a generalized and simplistic overview of the plastics used in composites. Later sections will delve into physical, chemical, and mechanical properties relevant to this work.

Manufacturing Composites

There is a myriad of methods for creating composite forms, which depend on the application, the form, and the materials used. In all cases, the material is shaped by a forming the material around an existing mold, often called a tool. Tools can be male or female and open or closed. These choices are made depending on geometry complexity, desired cost, desired surface finish, desired tolerances, and manufacturing methods.

The two main categories for creating composite parts are wet-layup and dry-layup, which refers to if the fibers are dry or they have been covered in resin. Wet-layup methods include pre-preg manufacturing, which eliminates the 'messy' element of wet-layup but requires a pressurized high temperature cure. Prepreg layup can be done by hand but is also automated for very high-performance applications. Other wet layup techniques include wet hand-layup, where plies are saturated with resin and laid onto the tool. This is usually confined to use in home projects and low-tech jobs. Pultrusion is a wet process by which a length of constant cross-section is created by pulling saturated fibers through a die. Filament winding is a method used for radial parts turned on a mandrel where a tow is wound around the piece. This is done wet or dry. Dry-layup can be done by hand or automated, but these methods require that resin is transferred to the fibers after they have been put down on the part, which creates an engineering challenge of fully saturating the fiber stack without leaving dry spots or creating resin-rich areas. Resin can be transferred by pouring or spraying and using a squeegee/roller (low-tech), or the piece is sealed with a plastic membrane or hard face. For the latter cases, a vacuum pump is used to transfer resin from a reservoir to and through the part. This is referred to and vacuum assisted resin transfer molding (VARTM), and an example of such is illustrated below. For this process a film of chemical releasing agent is applied to the mold so that the cured (or semi-cured resin can be easily removed. The material is then laid down in the prescribed stacking sequence. Next, an adhesion resistant peel ply is put on the part followed by a resin diffusion fabric or flow media to facilitate resin flow over the entire part. Finally, the stack is closed with a vacuum bag or another hard side of the mold and sealed with a sealant tape.

Vacuum is pulled at one end of the mold, and the other end is connected to a resin reservoir. When the part is fully infused, the connection is closed to the resin bath, and the resin is allowed to gel. All these processes that use a thermosetting plastic require a curing cycle wherein the plastic is cured to its structural form.

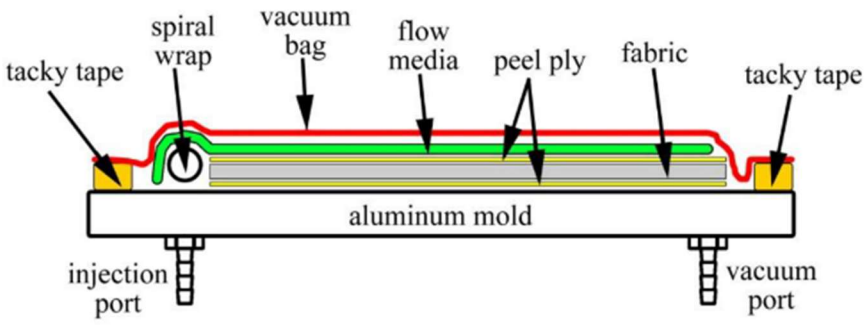

Figure 4: Vacuum assisted resin transfer molding (VARTM) illustration

Thermoplastic composite parts are also infused, but due to their high viscosity VARTM is impractical. Instead, thin sheets of matrix plastic are alternated into the stacking sequence, and the complete layup is heated and pressurized to force matrix amidst the fibers. This is not a comprehensive review of manufacturing methods but is simply meant to familiarize the reader with common methods.

The amount of machining done on a composite part is kept to a minimum. Composites are especially susceptible to cracking, and machined surfaces are common crack initiation sites. If two parts are to be joined, it is best practice to use a bonded joint instead of a bolt/fastener.

Damage Mechanisms in Composites

Damage in composite materials is a complex phenomenon. Their heterogeneity creates more damage mechanisms than in a single constituent. Where metals and plastics experience cracking and widespread plastic deformation, composites experience matrix cracking, fiber breakage, and failure of the fiber-matrix interphase. Interphase failure can occur in shear, creating fiber pullout, or by normal stress common in delamination. Delamination is a form of damage where a large crack is created between plies. Fiber bridging occurs when a crack propagates through the matrix, but fibers remain intact and bridge the gap. This is often seen in delamination. In this way, fibers can stop crack growth. Depictions of these mechanisms are shown in Figure 5.

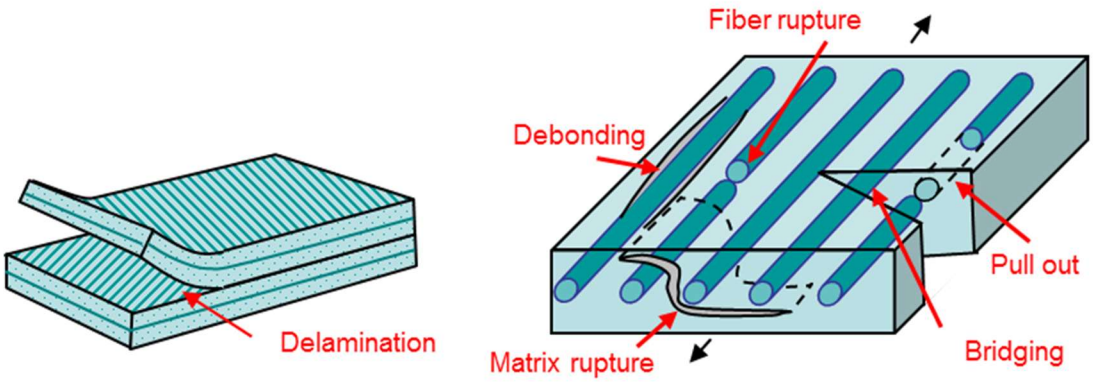

Figure 5: Damage mechanisms in composites [12]

Where damage appears, the form it takes, and stress/strain level at which it occurs is largely a function of fiber orientation and ply stacking sequence as much as loading type.

Matrix cracks develop in resin rich regions. Delamination grows from matrix cracks and small interphase failures. Unidirectional laminates typically show very little damage until final failure. If fibers are not completely straight, longitudinal shear cracks can develop as the fibers are pulled straight in tension. Delamination can also grow in woven fabrics for the same reason. Straightening of the tows induces out of plane normal stresses, which can cause delamination. These effects are exemplified in figure 6. Shear matrix cracking is apparent in the [+45/-45] (right) and transverse matrix cracking in the [90/0] laminate (second from right). Wide spread delamination is present in the quasi-isotropic laminate (second from left), and catastrophic failure is clear in the unidirectional coupon (left).

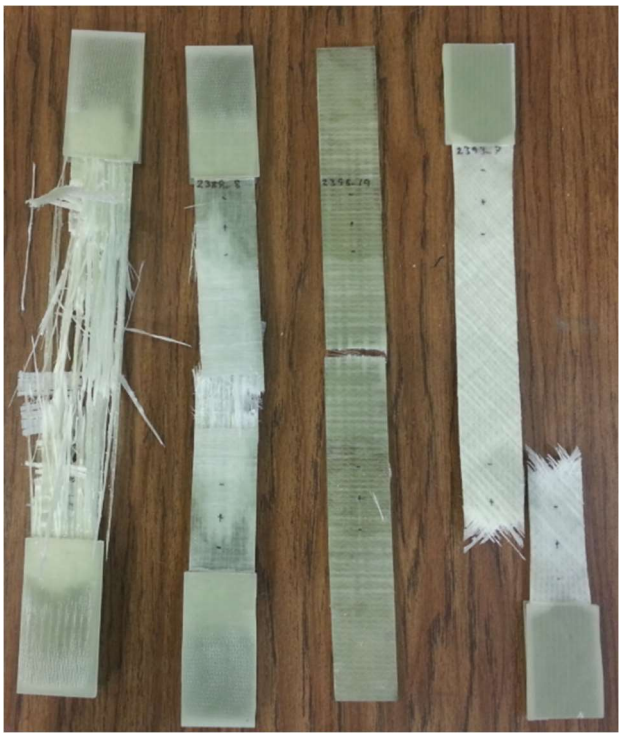

Figure 6: Damage in different layups in uniaxial tension: left [0]n catastrophic failure, left of center [0/90/45/-45] delamination, right of center [0/90]s transverse cracking, right [45/-45]s shear cracks [13]

Damage tolerance in a composite system is governed by the fiber-matrix interface and failure strain of the matrix. Stress is transmitted from matrix to fiber via shear. Considering a discontinuous fiber, not all the fiber length is used for load carrying. There is a minimum length at which the fiber reaches its load carrying potential. This critical length is based on fiber and matrix properties, fiber dimensions, and ultimately interphase strength. This critical length is on the order of millimeters [10]. Continuous fibers are subject to the same mechanical principal, which is an important factor in damage tolerance. When a fiber brakes, the load path (fiber) is interrupted, and load is transmitted back to the matrix via shear and then into the next segment of fiber. This process is called shear lag.

Under normal fatigue loading, small damage sites accumulate to degrade the stiffness of the gross material. These damage sites grow with load cycling, combine to form large damage conglomerations and lead to ultimate failure. This process is illustrated in Figure 7.

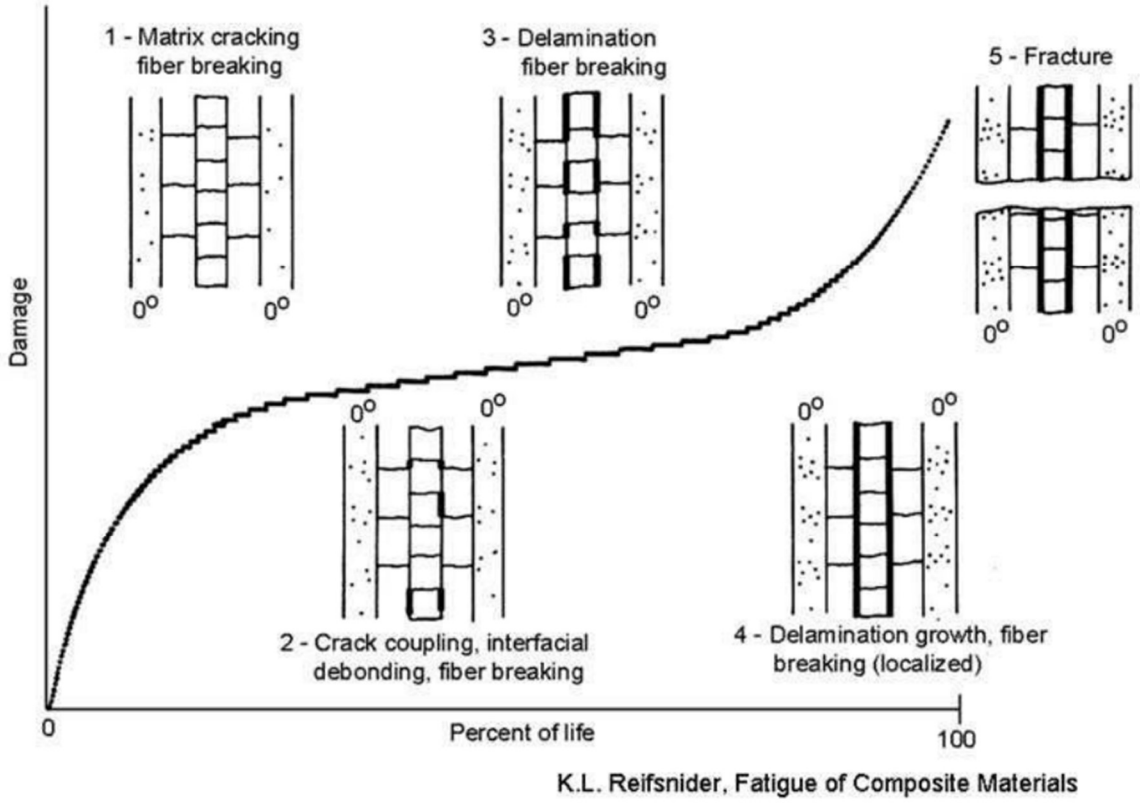

Figure 7: Damage progression under fatigue loading for non-unidirectional laminates [14]

Hygrothermal Aging

Hygrothermal aging is a method by which samples are saturated with water by prolonged exposure to a heated humid environment. This method is employed as a tool to study the effects of water on a material sample.

Moisture Diffusion

Diffusion is a process of random-walk motion whereby a substance in high concentration is distributed toward an area of low concentration to achieve equilibrium. For composite material systems in marine environment, the polymer matrix is the primary influencer in moisture diffusion/uptake, though reinforcement type and sizing formulation have been shown to affect moisture uptake [15][16][17].

Fickian Diffusion Most moisture uptake regimes are modeled with Fickian Diffusion. Fick's first and second laws of diffusion simplified for one dimensional diffusion are shown in equations (1) and (2).

$$J = -D\frac{\partial C}{\partial x} \tag{1}$$

$$\frac{\partial C}{\partial t} = -D\frac{\partial^2 C}{\partial x^2} \tag{2}$$

Where J is flux of mass transport, D is diffusion constant, C is concentration, and x is position. The negative sign indicates that mass will trend from areas of high to low concentration. It is important to note that moisture diffusion rate into a non-isotropic material such as a composite laminate will vary significantly depending on orientation described by the second order diffusion tensor Dij. The effects of the one dimensional and isotopic assumptions are significant for geometries and materials used in this work.

However, moisture effects in the materials studied here are assessed relative to mechanical and acoustic properties instead of absolute chemical or physical effects.

For empirical measurements of moisture absorption in a laboratory situation, samples are exposed to a humid environment and mass measurements are taken at different time intervals and compared to original mass to determine moisture absorption level. If these mass measurements are plotted against the square root of exposure time, like in Figure 8, the diffusion constant for the system can be calculated with the slope equation, where L is the sample thickness. It is important to note that the slope method for finding diffusion constants is only valid for the linear portion of the diffusion curve. In practice, the first mass measurement is used to determine slope.

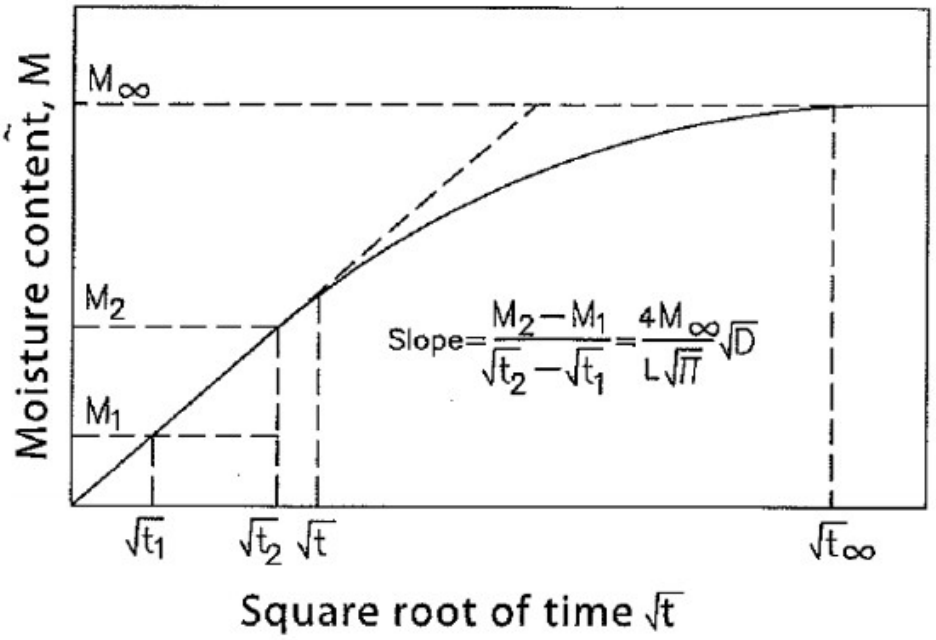

Figure 8: Diffusion concentration curve for theoretical 1-D Fickian diffusion [18]

Another practical consideration for moisture mass uptake measurements is the effect of surface imperfections. Cracks and porosity will affect measurements as voids on/near the surface will fill quickly and expedite diffusion by effectively increasing the exposed surface area.

Temperature Effects on Diffusion Diffusion is greatly influenced by temperature, described by the Arrhenius relation in equation (3).

$$D_t = D_o * exp\left(\frac{E}{RT}\right) \tag{3}$$

Where D_t is diffusivity at an arbitrary temperature, D_o is a reference diffusivity, E is activation energy for diffusion, R is the universal gas constant, and T is absolute temperature. Activation energy for diffusion is not a readily tabulated value for all polymers employed in composites. In practice, separate samples of a polymer are hygrothermally aged to full saturation at two different temperatures, T_1 & T_2, while collecting water mass uptake data. The slope method is used to determine respective diffusivity coefficients D_1 & D_2. Then if E/R is combined into a single constant C, equations (4) and (5) are used to determine C and the reference diffusivity, D_o.

$$C = \frac{ln\frac{D_1}{D_2}}{\frac{1}{T_1} - \frac{1}{T_2}} \tag{4}$$

$$D_o = \frac{D_1}{exp\left(\frac{-C}{T_1}\right)} \tag{5}$$

Mechanical Effects of Moisture Uptake

Moisture diffusion in to a composite laminate causes swelling which will induce stresses near geometry changes and between plies because of the strain mismatch. The polymer swells, but a glass or carbon fiber reinforcement will not, constraining the polymer and inducing a stress.

The presence of water in polymer structure can also have chemical repercussions affecting strength and modulus. Plasticization of the matrix and interphase degradation are two such examples. Plasticization is a process by which water molecules occupy free volume between polymer chains acting as an interstitial lubricant thereby increasing chain mobility. Increased chain mobility reduces stiffness and strength [19], [20].

Interphase degradation occurs when the sizing formulation is chemically favored to interact with water, attracting water to the interphase and degrading the bond strength [21]. Reduced interphase strength decreases overall performance of the composite because this is a critical element of load introduction and damage tolerance.

Acoustic Emission

Lamb Waves

Lamb waves are transient elastic vibrations in a material produced by a sudden release or impartment of energy, like the rapid redistribution of stress in a material caused by cracking. These waves exist in different modes, two of which are pictured in Figure 9, but shear mode waves also exist. These modes have different wave speeds, which are

dependent on material properties. For an infinite plate, the equations for extensional and flexural modes are described by equations (6) & (7) respectively. Where, A_{11} and D_{11} are extensional and flexural rigidity, ρ is density, d is thickness, and ω is frequency [22]. Though directional wave speed is readily defined other wave propagation features are far more complex. Reflection and refraction due to finite geometry, material heterogeneity, and large defects are more difficult to define.

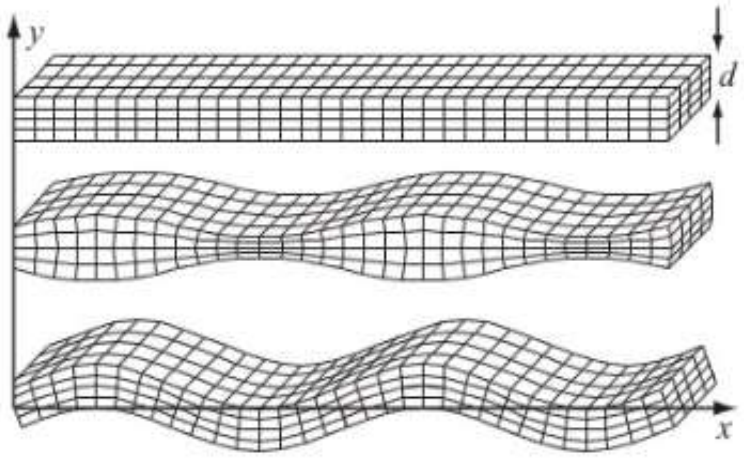

Figure 9: Lamb Wave modes (top) undeformed (middle) extensional/symmetric (bottom) flexural/antisymmetric mode

$$c_e = \sqrt{\frac{A_{11}}{\rho d}} \tag{6}$$

$$c_f = \sqrt[4]{\frac{D_{11}}{\rho d}} * \sqrt{\omega} \tag{7}$$

[22]

Acoustic Emission Data Collection and Waveform Analysis

AE monitoring is a real time damage detection technique that measures the transient elastic waves originating from damage sites. These waves are detected by piezoelectric sensors adhered to the surface of the material under load. When deformed, piezoelectric crystals produce a voltage proportional to their deformation. When a piezoelectric sensor is attached to the surface of a material, a passing elastic wave acts to deform the sensor producing a voltage signal which is representative of the passing wave. These signals are referred to as hits or events, and they can be complex, exhibiting different lamb waves modes: extensional, flexural, as well as reflections. An example of an event is shown in Figure 10. Considering equations (6) & (7), it is not surprising that extensional waves are typically the first features in a signal followed by flexural then reflections. Reflections are primarily the results of finite coupon boundaries but can also be caused by large discontinuities.

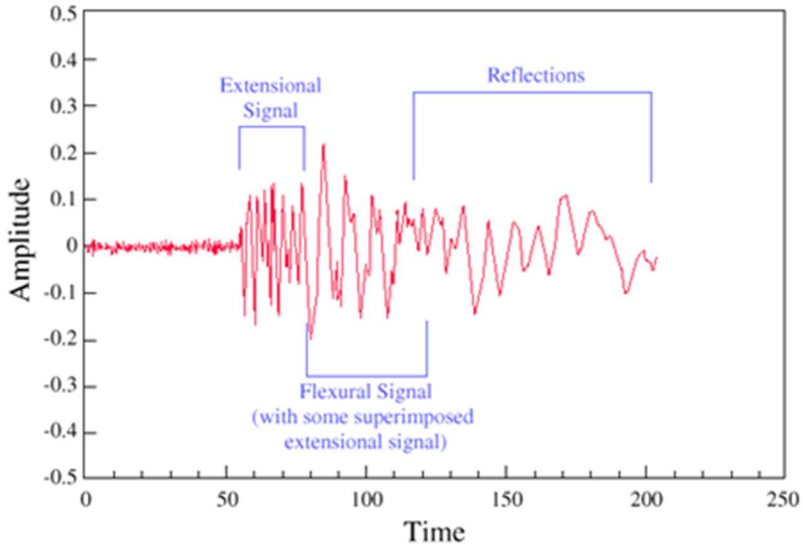

Figure 10: Example of an acoustic event voltage signal with wave mode annotations [23]

Several different metrics are used to describe these event waveforms. Most as depicted in Figure 11. Missing from this figure is absolute energy, which is true area under the curve. This is reconstructed from frequency and amplitude data. Absolute energy will differ from MARSE energy, which is shown in the figure (the shaded blue area). Other important metrics used in characterizing an event are peak spectral frequency and frequency centroid, which are derived from the Fourier Transform of the voltage signal. An example of the frequency domain data from an event signal is shown in Figure 12.

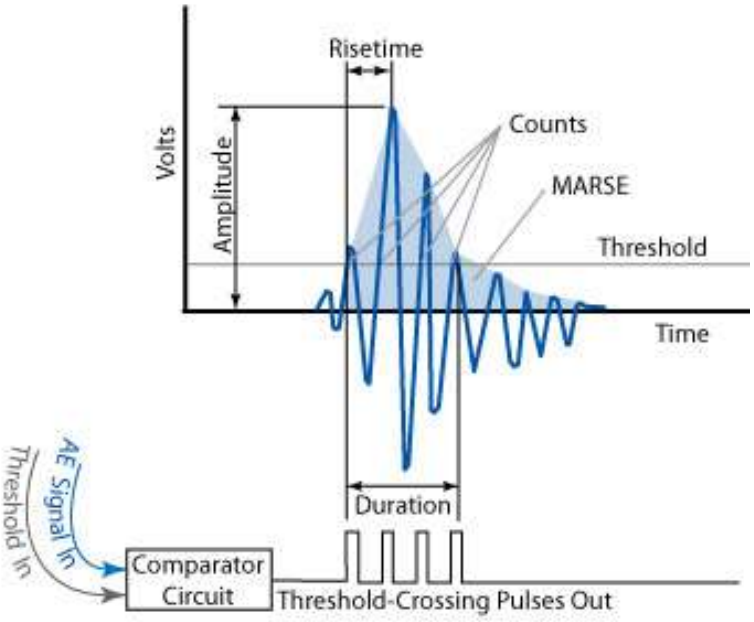

Figure 11: Visual aid and annotation for AE wave form metrics [24]

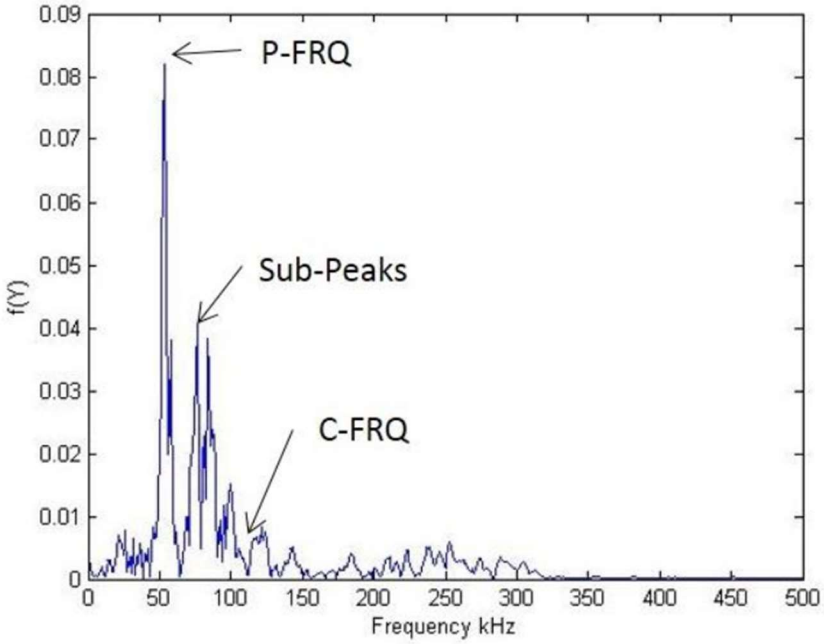

Figure 12: Frequency domain data from an acoustic event derived from Fast Fourier Transform (FFT) analysis with annotations for peak spectral frequency (P-FRQ), subpeaks, and Frequency Centroid (C-FRQ) [13]

Identifying Damage with AE

The explicit goal of acoustic emission monitoring is to identify the type and or severity of damage. To this end, researchers have developed methods which fall into three major groups: single parameter, multi-parameter, and waveform analysis. In general,

Among single parameter methods, peak spectral frequency of an event, obtained through fast Fourier transform (FFT), is the most common. Researchers have observed correlation between damage mechanisms and peak spectral frequency and have associated frequency ranges with different damage types [25]–[32]. While frequency ranges are variable, matrix cracking is generally associated with 50 to 150 kHz, interphase failure/de-bond with 150 to 350 kHz, and fiber failure from 350 kHz upwards. de Groot authored an oft-cited publication which compared peak frequency from different materials and layups to correlate frequency ranges with expected damage types [25]. Research stemming from this seminal work has yielded mixed results with varying levels of agreement, but the work has never been fully reproduced. It is also speculated that different damage types produce different frequencies due to differences according to equation (8) [29]. Where f is frequency, τ is relaxation time, c is elastic acoustic velocity, E is elastic modulus, and ρ is density.

$$f_i \sim \frac{1}{\tau_i} \sim c_i \sim \sqrt{\frac{E_i}{\rho_i}} \tag{8}$$

Though there is a large body of literature correlating damage types with frequency content through layup comparison, damage type isolation, and optical investigation, the

correlation has not extended to fool-proof evidence of causation. Deriving the frequency of a single damage event from first principle is possible, but damage in composite materials is more likely to occur in a rapid cascade if damage however localized. Therefore, it is not uncommon to have overlapping or slightly staggered damage waveforms even with correctly applied AE timing parameters. Through FFT and peak frequency extraction information about lower amplitude event(s) can be lost. It is reasonable to assume that a higher amplitude event is more significant, but unintentionally filtering out information of lower amplitude events changes the picture of damage in the coupon. This would be especially detrimental to understanding of damage initiation and progression if low amplitude damage events were acting to initiate larger damage events.

Some additional doubt is shed on the frequency method for damage mode identification as frequency bands have been shown to be somewhat dependent on sensor sensitivity curves which may contribute to the differences in band centers reported in different studies. Though this effect of sensor sensitivity is of minor concern as general agreement is found between researchers despite these differences.

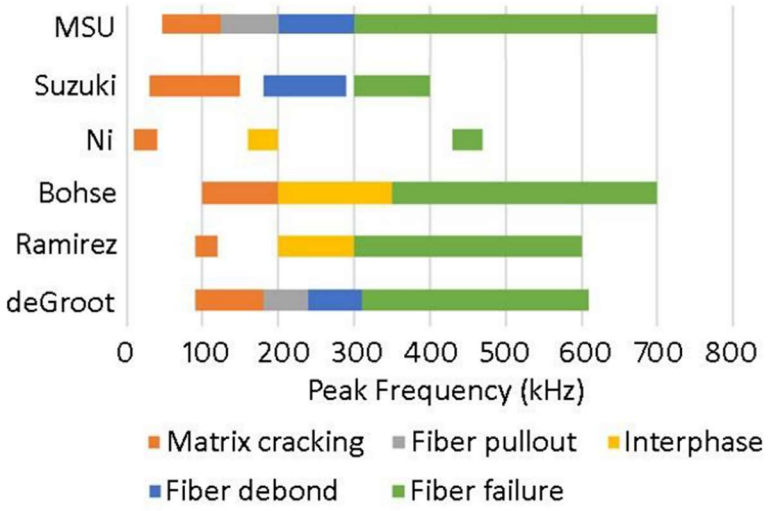

Figure 13: Frequency range damage mode association summary [13]

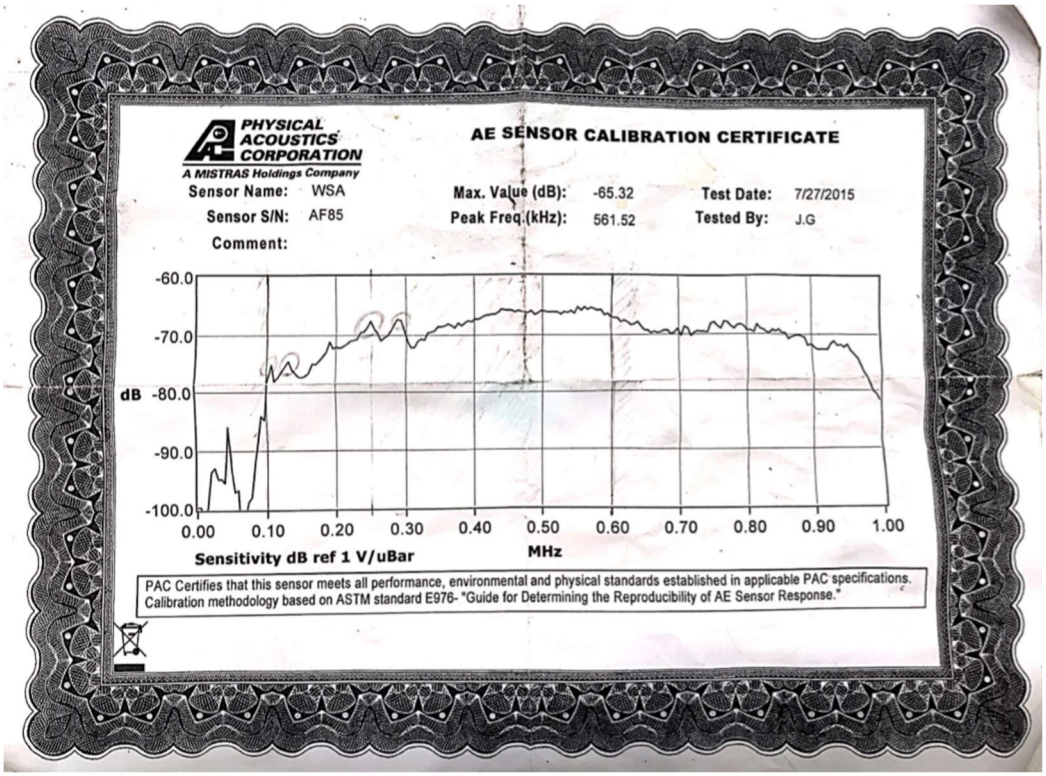

Figure 14: WSA-type sensor sensitivity curve example

Absolute event energy is another common single parameter method. Schuster investigated absolute event energy, with mild success, by comparing absolute accumulated AE energy to dissipated mechanical energy during a load-unload-reload test [13]. Barré *et al.* had success is identifying damage with amplitude [33].

Multiparameter methods vary greatly in complexity and implementation. Haselbach and Lauke associated frequency ranges, duration, and amplitude with different damage modes [30]. Sause *et al.* implemented a clustering algorithm to identify appropriate waveform parameters to identify damage types [34]. Other researchers employ artificial neural networks to identify damage modes from patterns in different waveform parameters [35], [36]. Recent work by Murdy used statistical models to select parameters from AE and guided ultrasonic data for a multivariate linear regression model to predict modulus degradation under fatigue loading from load-unload-reload tests [37].

Lastly, many researchers have performed wavelet analysis of individual waveforms to identify different wave modes (extensional vs. flexural) to correlate with damage types [26], [28], [32], [38], [39].

Influence of Hygrothermal Aging

All research referenced for this work reports a reduction in AE energy from hygrothermally aged samples [40]–[45]. This is most likely due to changes in the polymer due to moisture absorption. As mentioned, water acts to plasticize/soften the polymer therefore creating a more ductile material. The plasticization effect also increases attenuation in polymer, which will result in lower energy AE events even from an

unchanged damage source. Fiber-matrix interphase is also degraded by moisture absorption, thus effecting damage progression. This effect could manifest as more events from a slightly degraded interphase or less events from a heavily degraded interphase. Inter versus intralaminar failure is investigated by Garg *et al.* who found a decrease in number of events in conditioned samples, resulting in reduced overall energy [41], [42].

Acoustic Emission in Different Materials

Differences in acoustic emission between material types stem from wave propagation (attenuation) and the damage progression from preferred damage modes. On a basic level, composite systems with ductile matrix materials should exhibit relatively more and low energy events than a brittle system as a ductile material will experience more frequent and less energetic crack propagation. This is due to energy dissipation at the crack tip due to plastic flow. A softer material will yield lower energy events also because of greater attenuation in the signal. Referring to equation (8), softer materials of comparable density to a stiff counterpart should produce lower frequency events. Differences in matrix properties, fiber properties, and fiber-matrix bond strength will create a unique regime for preferred damage types and therefore damage progression.

Thesis Goals

This work aims to empirically elucidate differences in acoustic emission signals from different material configurations to advance the understanding of damage progression in different material types. This shall be achieved by examination of various acoustic emission waveform metrics from a diverse set of materials, applicable to structural

applications such as offshore wind turbines and MHK devices. Gaining a more thorough understanding of damage progression in these materials and the acoustic emission resulting there from, aims to advance the field of structural health monitoring.

To that end, elements of this work are included to reinforce and augment prior research into the effect of hygrothermal aging on mechanical properties and acoustic emission of composites materials.

ACOUSTIC EMISSION METHODOLOGY

Mechanical Testing Procedure

Samples were tested in uniaxial tension in Instron 8562 at a rate of 1.8 mm per minute until complete failure or a significant decrease in load. AE sensors were removed before failure if load exceeded 4.45 kN (10 kips) to avoid possible damage from being ejected off the coupon surface at failure. Actual testing configuration is pictured in Figure 15. A number of coupons cut and prepared by other researchers deviated from the coupon dimensions outlined here, but the acoustic emission gage section and set-up was maintained.

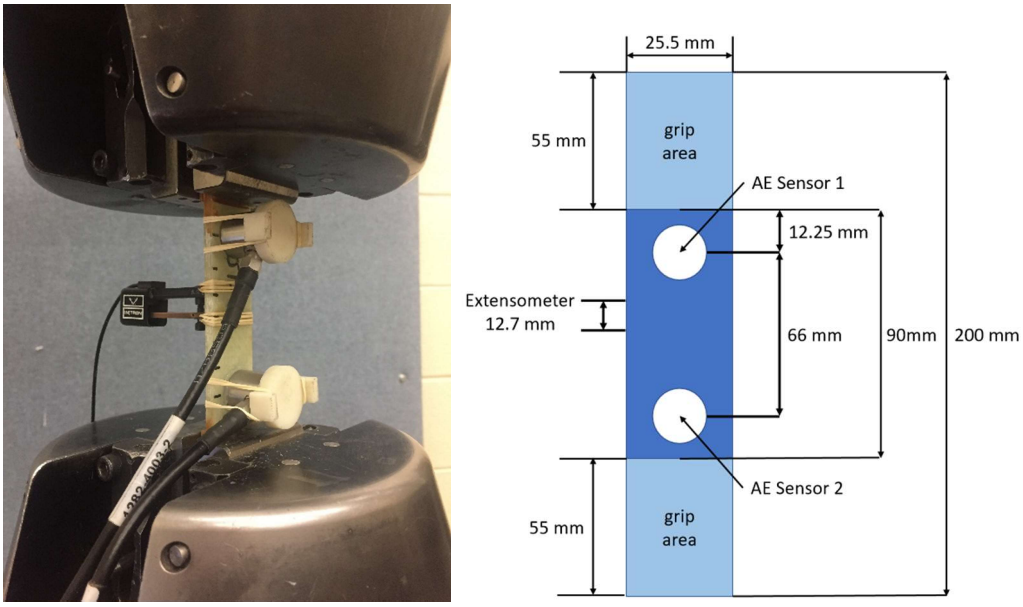

Figure 15: Static tensile testing configuration

Acoustic Emission Hardware & Data Collection Procedure

Before testing, speed of sound in each material was measured with a Physical Acoutics Micro-II Digital AE data acquisition system. Measured wave speed was input into AEwin™ fir USB™ with Physical Acoustics 1283 USB-AE Nodes™ for testing. Two Physical Acoustics WSα sensors were applied to the coupon surface with a spacing of 66 mm with a vacuum grease couplant and plastic retention caps with elastic bands. In the AE software the event definition window was set to 56mm to eliminate the region directly beneath the sensors. This two-sensor system was used to reduce grip noise via linear location. By adjusting an acquisition parameter in the software, wave velocity and time of flight data is used to filter out events originating from outside the sensor gage section. Couplant is used as standard procedure for AE monitoring. A highly viscous and incompressible fluid creates gentle adhesion between the sensor and coupon surface and facilitates efficient wave transmission to the sensor.

Aside from sampling rate, data acquisition and timing parameters were identical to those used by [46] and are listed in Table 1. Pencil lead break tests (PLBs) are a common sensor test procedure, where pencil lead is broken against the surface of the testing coupon at known locations. The location recorded by the AE systems is compared to the actual location. PLBs were performed before every coupon test to ensure proper sensor spacing, adhesion, and functionality.

Table 1. Acoustic emission data acquisition and timing parameters

Parameter	**value (units)**
Peak Definition Time	50 (μs)
Hit Definition Time	100 (μs)
Hit Lockout Time	500 (μs)
Max Duration	1000 (ms)
Threshold	50 (dB)
Sampling Rate	5 (MHZ)

Mechanical and acoustic emission results were saved as a .TXT file and imported using MATLAB R2017b. This input creates MATLAB data as well as excel files with the same data. All post processing was performed with the same MATLAB software. Data from this study (MATLAB and excel) are available on the MSU composites drive in a folder under the authors last name. They are saved as a MATLAB data file. Each laminate is saved as a separate structure with information about the laminate and a sub-structure of tested coupons. Information on each coupon is listed as fieldnames. Test data are separated by each coupon substructure and are subdivided into two types “para” and “event”. The data is organized into a matrix where each column is a parameter and rows are a sampling times. “para” holds time, strain, load, and stress for the entirety of each test. “event” holds acoustic emission data for each event or hit. Content and organization of these columns is found in the “headers” field of each data structure.

ACOUSTIC EMISSION DATA AQUASITION SYSTEM STUDY

All materials considered in this body of work are not unique to this acoustic emission study. Composite forms identical or very similar to these have been investigated in other acoustic emission studies. Though many studies have investigated these materials, AE results are highly varied in energy release, frequency content, amplitudes, etc. (SOURCES). These variations stem from material variations as well as AE set-up differences: timing parameters, sampling rate, threshold, pre-amplifier, sensor sensitivity, number of sensors, couplant type, couplant thickness, and other factors. Therefore, direct comparison of data from different sources is difficult and relatively suspect. It is near impossible to differentiate between variations in materials and coupons versus those between AE systems. Even two AE systems configured with the closest possible acquisition parameters will measure different events. This sub-study is included to illustrate this point by comparing data between two different AE data acquisition systems monitoring the same coupons.

Experimental Methods

There are two separate AE data acquisition systems at MSU. The first is a Physical Acoustics Micro-II Digital AE data acquisition system. The other is a trio of Physical Acoustics 1283 USB-AE Nodes. Both run separate versions of MISTRAS AEwin software. For this study, both systems were configured with the same timing and acquisition parameters, listed in Table 1, except for sampling rate. The Micro-II Digital AE system has a maximum sampling rate of 3 MHz. The USB AE Nodes have a maximum

sampling rate of 5 MHz, and the software for the latter does not allow the sampling rate to be set to 3 MHz. The lower sampling rate for the Micro-II Digital AE system limits the systems detectable frequency range to those less than 400 kHz. There should be no other effects. Therefore, the data collected from the USB AE nodes was filtered to eliminate frequencies above 400 kHz.

Another major difference between these systems was sensor type. Sensors used with the USB Node system were WSα type single input, and those used with the Micro-II system were WD type differential type. Because the two sensor types have very similar sensitivity curves (see appendix B), the only effective difference is input type. Differential input sensors are more resistant to common-mode noise. Therefore, the only sensor-based difference that might be expected in this data would be noise in the USB node system, but this is not the case.

The laminate used in this study was manufactured by VARTM at MSU, plate number: 4149. The plate was made from Vectorply E-LT 3800 infused with Hexion 135/1366 resin with a layup of [0b]s. Three coupons were cut with a water lubricated diamond saw to dimensions of 25.5x200mm. Tabs of G10 material were adhered with epoxy adhesive to the 55mm at either end, leaving 90mm of total gage section. This geometry matches that depicted in Figure 15.

For testing, the procedure outlined in the previous section was implemented simultaneously with both AE systems. Two sensors from each system were applied to the coupon surface on opposing faces so each system could collect data from the 56mm AE gage section from opposite sides. This Samples were pulled in uniaxial tension to failure

at a rate of 1.8 mm per minute using the Instron 8562 screw actuation machine. The raw data is available under the laminate name (4149) in the data structure mentioned in the Acoustic Emission Methodology section.

Results

Results collected by this investigation are similar but bare numerous and severe enough differences to warrant comparison and comment. The first obvious difference between the acquisition systems is total number of events collected during testing.

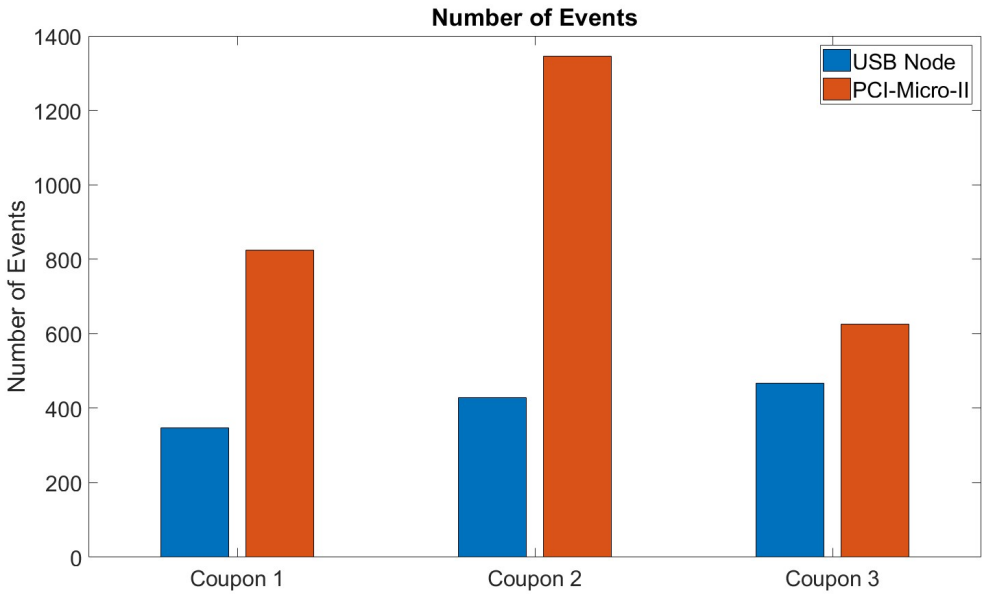

Figure 16. Number of events captured by different AE systems monitoring the same coupons showing the difference between the two AE DAQ systems

The USB-node system consistently collected fewer events. Detecting different numbers of events is especially concerning because of the implications in damage detection for any AE system. If one system is collecting more events then the other, some damage events are undetected by the other system. It is easily suggested that still more damage events go undetected by both systems. This casts doubt on the capabilities of an AE system collecting a comprehensive image of damage in a composite. Still, past research has shown that a well configured AE system can detect enough events to help predict modulus degradation [37].

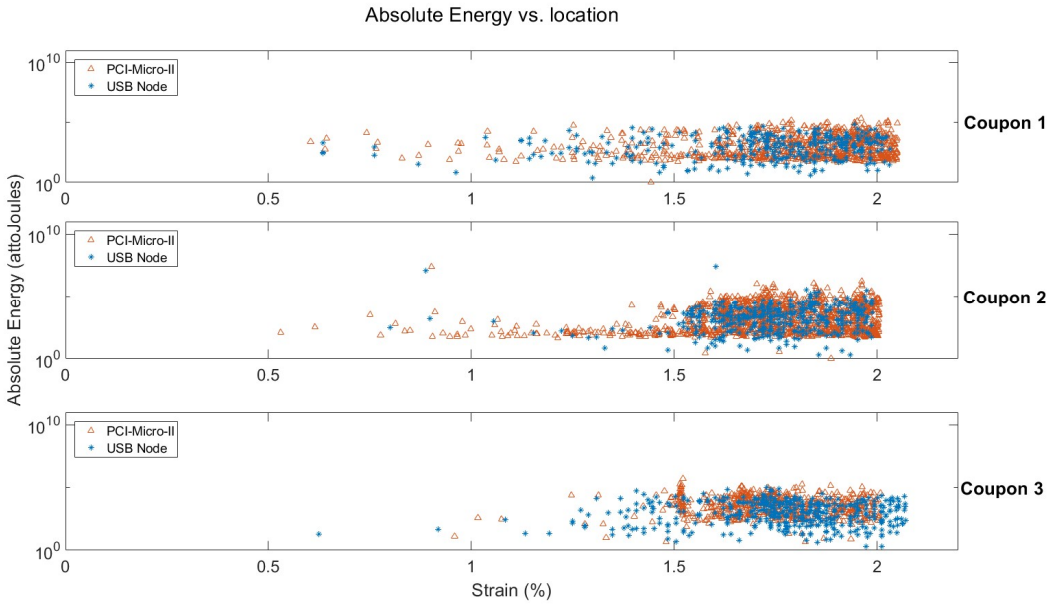

Figure 17: Absolute energy versus strain comparison between AE systems showing inconsistency in event energy detection

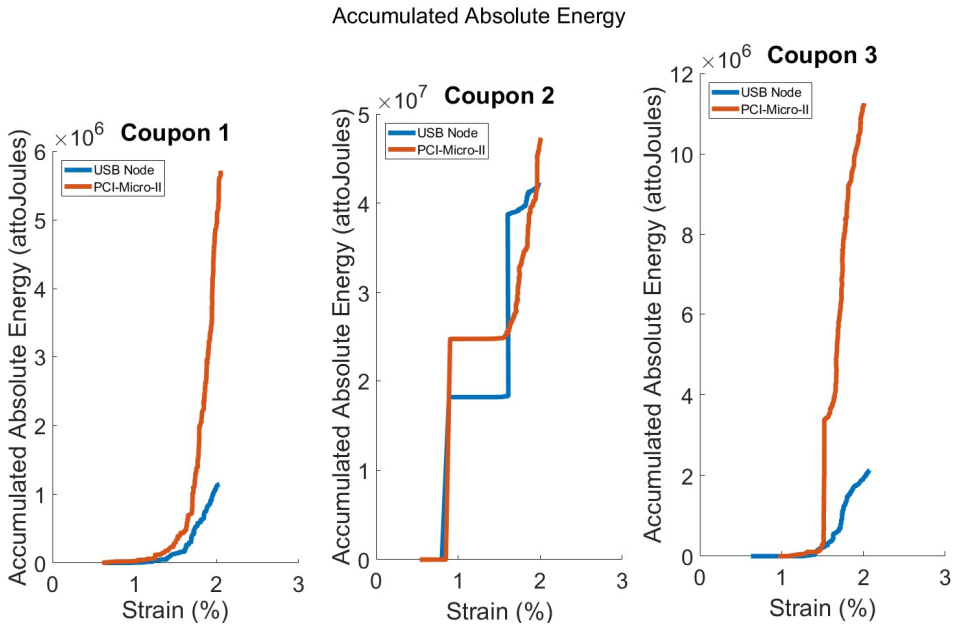

Figure 18: Accumulated absolute energy comparison between AE systems indicating further inconsistency in energy detection between AE systems

Another difference between the systems was accumulated absolute energy, shown in Figure 18. The main contributor to this effect is differing number of events, but mean absolute energy was also significantly different between systems for each coupon. Another concerning feature, which requires a closer look at Figure 17, is absolute energy of events and severity of the damage during a test. The damage initiation strain concurs well between the systems in the first coupon, but it does not for the other coupons. In addition, there are many high energy events detected by the Micro-I system only.

Still another area of disparity in the data is frequency content, shown best in Figure 20, and damage detection during testing. There is reasonable agreement in the strain at which damage is first detected, see Figure 19, but through the remainder of resting, there

is significant divergence in type of damage detected (delineated by peak-frequency). The USB node system records far more high frequency fiber failure events (>300 kHz), whereas the Micro-II system detects far more low frequency matrix cracking events (<150 kHz). Intermediate frequency events between 150 and 300 kHz, which have been associated with interphase failures, are relatively constant, though still different in range and count. These inconsistencies in frequency content are also cast doubt on the ability of AE monitoring to always detect an accurate picture of the damage state within a coupon. While frequency ranges are in good agreement between AE systems, but drastic variations in proportion of events in any 'bin' will yield vastly different conclusions on the prevailing damage mode in the test coupon. For example, in coupon 1 the Micro-II system a very large proportion of matrix events and very few fiber failures, indicating prevalent matrix cracking as a source of softening. Whereas, the USB-Node system detects a nearly equal proportion of matrix cracking and fiber failures. For the unidirectional laminate tested there, it can be asserted that the latter is a more accurate picture.

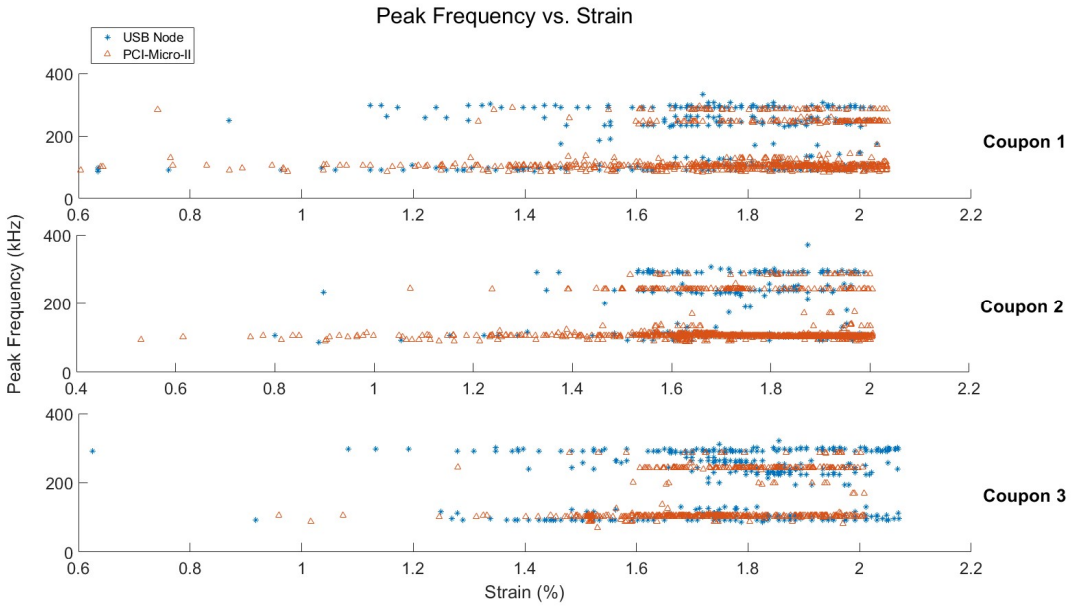

Figure 19: Peak spectral frequency versus strain scatter plot comparison between AE systems

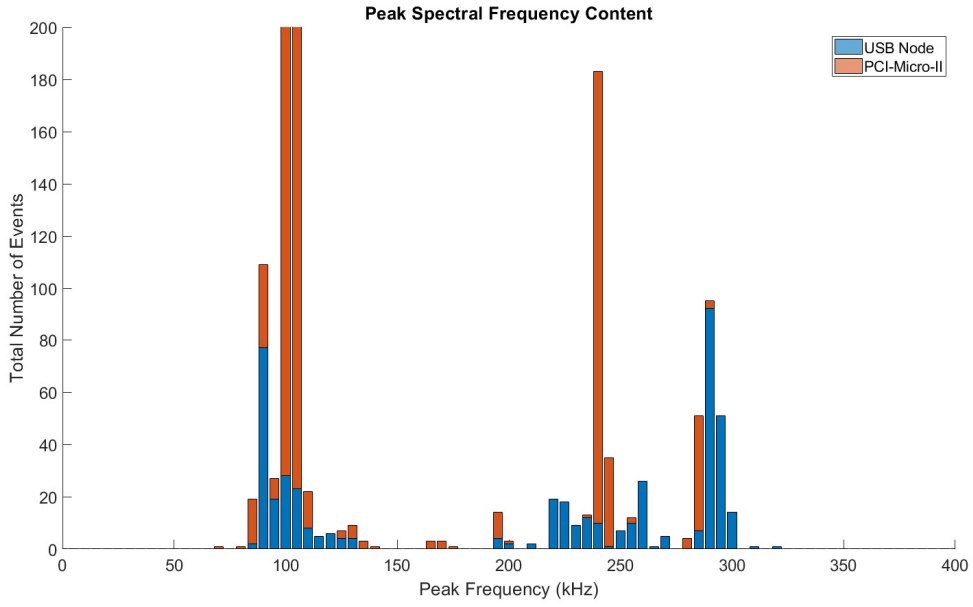

Figure 20: Peak spectral frequency content comparison between AE systems

Several discrepancies between these data have been illustrated here. Because of the differences seen in number of events and frequency content, the necessary operating assumption for this area of research is that any system configured correctly is measuring a portion of the whole complete picture of damage progression in a composite laminate, and this partial account is fully representative of the whole. Under this assumption, we can use any AE system to monitor the damage state in these materials, but to effectively identify variations between materials, all must be tested with the same equipment to eliminate those possible differences between systems.

HYGROTHERMAL AGING & ACOUSTIC EMISSION STUDY OF MATERIALS FOR MHK APPLICATIONS

Material Summary

The MSU composites group received funding from the U.S. DOE Water Power Office and has solicited various industry contacts to provide composite materials for mechanical characterization which are applicable for MHK devices. A summary list of these materials is provided in Table 2. Materials were received in plate and coupon form.

Table 2. Summary of materials included in MHK study

LABEL	Resin	Fabric Info	Layup	Volume Fraction
J1	Eastman Copolyester 5011, PETG	Vectorply E-QX 4800	[0/45/90/-45]4	53.8
J2	Derakane 470 HT-400 VE	Vectorply E-QX 4800	[0/45/90/-45]4	54.6
J3	Applied Poleramic SC18	Vectorply E-QX 4800	[0/45/90/-45]4	53.6
J4	Derakane 470 HT-400 VE	OCV WR27TW	[(0/90/)(45/-45)]4	58.4
J5	Applied Poleramic SC18	OCV WR27TW	[(0/90/)(45/-45)]4	59.1
J6	Applied Poleramic SC18	TPI 4582 (2x2 twill), T700 12K 670 gsm	[(0/90/)(45/-45)]4	60
J7	Applied Poleramic SC18	Vectorply C-QX 2300, T700 12K Quad	[(0/45/90/-45]4	59.5
J8	Derakane 470 HT-400 VE	TPI 4582 (2x2 twill), T700 12K 670 gsm	[(0/45/90/-45]4	60
CE1	Pro-set INF 114/211	Zoltek UD600, E-BX 1700	[(+45/-45)g/0c]s	55
CE2	Pro-set INF 114/211	Vectorply CLA 1812, E-BX 1700	[(+45/-45)g/0c]s	55
CE3	Hexion RIMR 035c/RIMH 0366	Zoltek UD600, E-BX 1700	[(+45/-45)g/0c]s	55

Table 2 Continued

CE4	Hexion RIMR 035c/RIMH 0366	Vectorply CLA 1812, E-BX 1700	[(+45/-45)g/0c]s	55
CE5	Crestapol 1250PUL urethane Acrylate	CLA 1812, E-BX 1700	[(+45/-45)g/0c]s	55
CE6	AME 6001 VE +1.5% MCP	ELT-2900, E-BX 1700, ELT-2900	[0/+45/-45/0]	55
N1	Elium	JM 086 - 4 layers	[0b]2s	56.7
P1	PP	E-glass w/AMB	[0/90]3	33.6
P4	PA6	E-glass	[0/90]3	34
P5	PA11	E-glass	[0/90]3	47.6
P6	PET	E-glass	[0/90]3	49.5
P9	PETG	E-glass	[0/90]3	37.3
P11	HDPE	E-glass	[0/90]3	38.8
P13	PP	E-glass	[0/90]3	38

Experimental Methods

Sample Preparation

No composites used in this study were manufactured at MSU, and manufacturing details are not explicitly known. Surface finish, materials used, and other characteristics such as volume fraction can be indicative of how a laminate was made. Using these indications, it is suspected that J1-8, CE1-6, and N1 were made by hand layup and vacuum assisted resin infusion, a method described in the background of this work. The remaining materials (P series) were made by heated press resin infusion. Wherein, thin sheets of the

thermoplastic resin are alternated into fiber layup and a heated tool applies pressure, melting the resin, and forcing infusion.

Coupons of each system were cut with a water lubricated diamond abrasion saw to target geometries of 200 x 25mm. After cutting thickness and width measurements were made of each coupon with digital caliper and recorded. Theses dimensions were used in calculating modulus and stress after testing. Mass of each coupon was also measured with a digital scale with resolution of 1E-3 grams. Mass of each coupon was used in calculated moisture uptake. For J1-8, CE1-6, and N1, tabs were adhered with epoxy to the gripping are at each end, leaving a total gage section of 90 mm. The remaining systems (P1,4,5,6,9,11, &13) were left without tabs.

Conditioning and Moisture Uptake Measurements

A portion of the samples from each material system were conditioned in ASTM D1141 (without heavy metals) synthetic seawater (SSW) at 50°C to complete saturation. SSW was created by mixing the prescribed quantity and amounts of salts with distilled water. Previous research at MSU found that salt buildup in SSW can affect moisture uptake measurements. Despite this added complexity, SSW was selected to maintain consistency and comparability to a study conducted by Dan Samborsky on these same materials. Samples were stored in a sealed bath of SSW inside a temperature-controlled oven. Samples were removed from the oven at arbitrary sampling intervals to be dried of surface moisture and weighed for water uptake. These measurements were made with the same digital scale used to take initial measurements (1E-3 gram resolution). After weighing, samples were returned to the water bath in the oven.

Moisture uptake measurements for this study were taken from tabbed samples. This method is not recommended as tabbing material and epoxy adhesive absorb moisture at different rates than any of the materials here. It is best practice to take measurements from un-tabbed samples which have been conditioned in the same bath alongside tabbed samples. The technician conducting this study was not aware of these effects at the outset, and there were not enough materials or time to correct this mistake after it was realized.

Results

Moisture Absorption

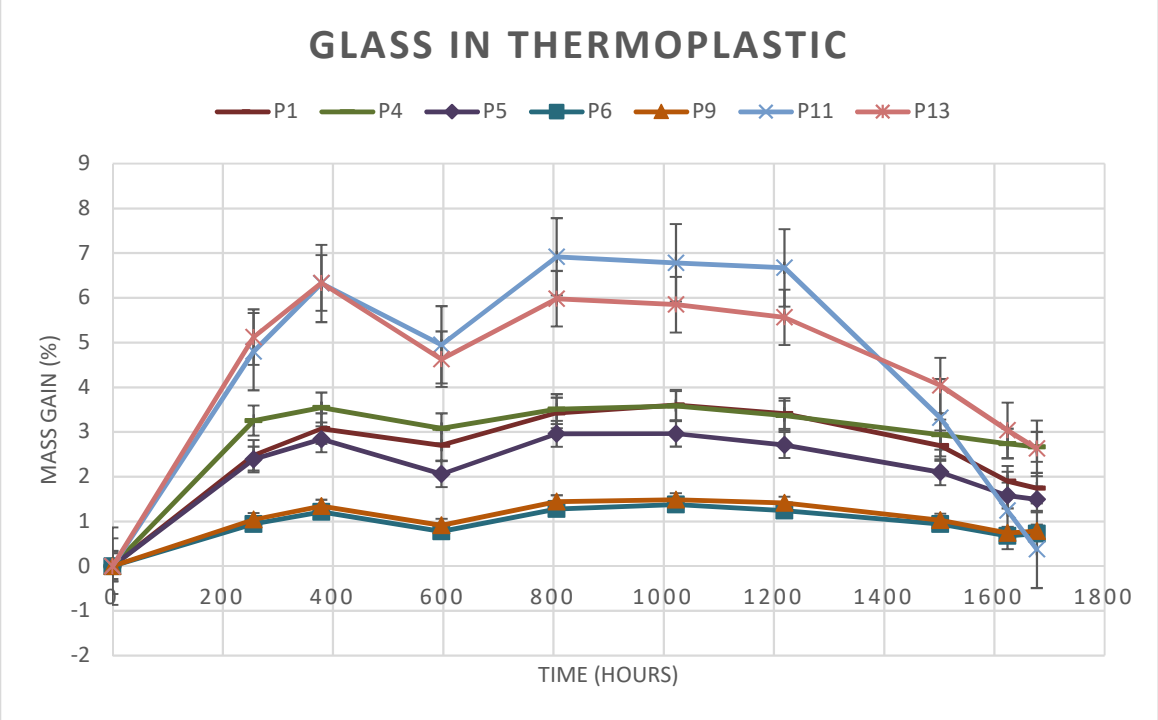

Figure 21: Mass uptake measurement curves for thermoplastic matrix systems.

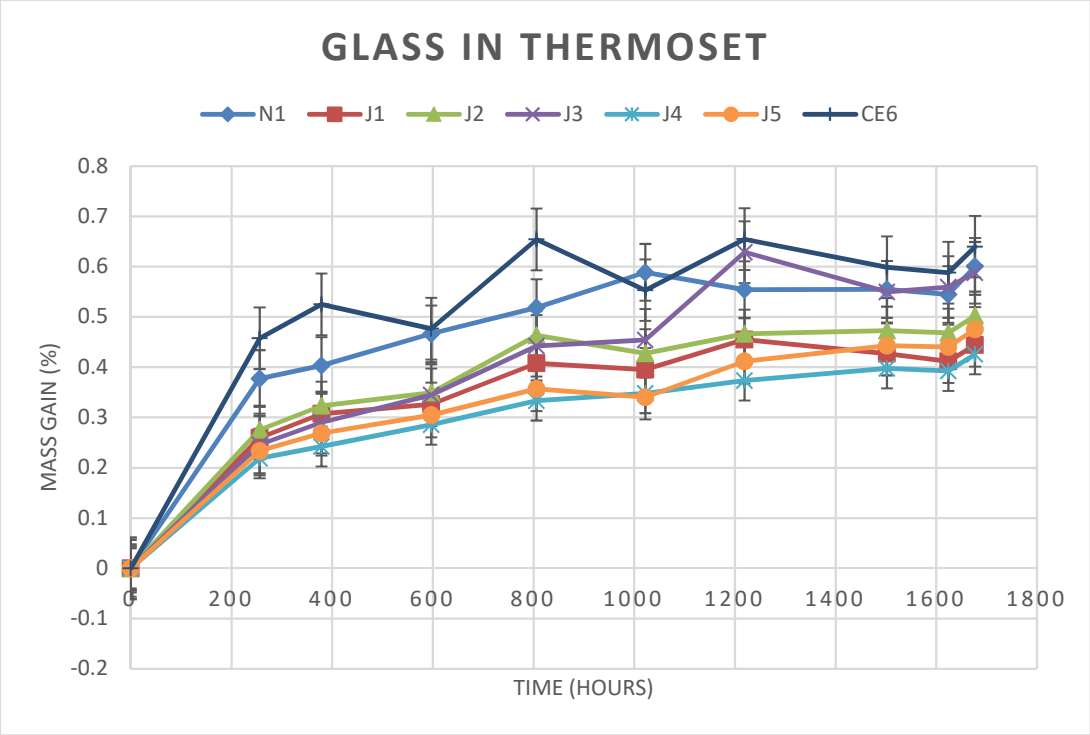

Figure 22: Mass uptake measurement curves for thermoset matrix systems.

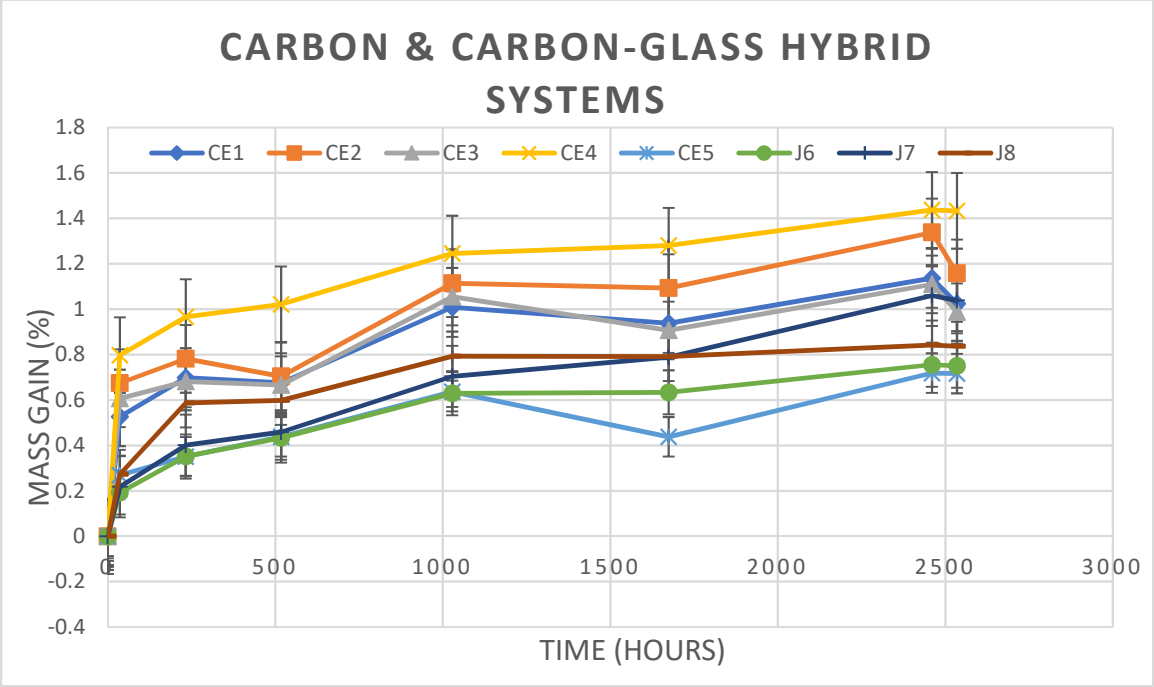

Figure 23: Mass uptake measurement curves for carbon and carbon-glass hybrid systems.

Considering these saturation curves (Figure 21, Figure 22, and Figure 23), significant inaccuracies occurred in moisture uptake measurements. The true cause of these imprecisions is not known but is likely due to inconsistent procedure. It is important to allow plenty of time for surface moisture to evaporate from the samples before weighing, especially for the thermoplastic samples as they have significant surface porosity. Varying amounts of surface moisture between sampling times would cause the sharp increases and decreases in moisture.

Referring to Figure 21, it is interesting to note the consistent decrease in mass past approximately 1000 hours. Because the trend is smooth, it is unlikely this is a measurement artifact. There are multiple possible causes for this mass loss. Hydrolysis could have

occurred in the matrix resulting in subsequent leaching of lysed monomers into the water bath. This process is commonly called ‘leeching,’ and it is the most likely culprit. Another possibility is loss of discrete particles or flakes into the water bath. Plastic and fiber near edges and corners would easily crack and slough off into the water bath as a result of swelling and/or handling during mass measurements. Still another, possibility is biological degradation. Bacterial contamination of the water bath is common. Biofilm growth in/on samples could be acting to degrade the polymer and expel biproduct into the water bath. However, this is especially unlikely as bacteria capable of breaking down these polymers are highly rare, and the process is very slow. Hydrolysis in combination with loss of discrete particles is the most likely possibility. It can be confidently stated that moisture was absorbed into these samples. Therefore, testing these samples does achieve the stated goal of investigating the effects of moisture absorption on mechanical properties and acoustic emission.

Moisture absorption between laminates with the same matrix should be similar, while considering volume fraction effects. This is not fully reflected in the saturation data. Starting with the thermoplastic matrices, there is a significant difference between P1 and P13, which are both polypropylene (PP) materials, but P1 has an unknown additive called AMB, which has shown here to reduce moisture absorption. Nylon 6 is shown to absorb similar amount to Nylon 11. The mass uptake for P4 (PA6) is slightly greater than P5 (PA11), but P4 has a lower volume fraction and should therefore absorb more moisture. So, the difference is insignificant. There is no discernable difference between polyethylene terephthalate (PET) and polyethylene terephthalate glycol (PETG), which is P6 versus P9.

Finally, high density polyethylene (HDPE) in P11 absorbs the most water and is shown to lose the most mass near the end of conditioning. This is unexpected as HDPE is known for having good performance in water and a lower moisture permeability than many of the other plastics included here [47].

The thermoset matrix laminates absorbed less water than the thermoplastics, which follows expectations. Comparing between thermosets, all laminates with Applied Poleramic SC18 (J3, J5, J6, & J7) absorb similar amount of moisture. Laminates of Derakane vinyl ester have similar absorption between glasses (J2 & J4), but the carbon system, J8, absorbed more water and has a higher volume fraction. This increased absorption would suggest a fabric/fiber effect, but the trend does not appear in comparing to the Applied Poleramic resin. If there was an effect, J6 should have absorbed more than J3, J5, and J7 because it has the same fabric as J8, but this is not the case.

There does seem to be a fabric effect in the CE series. CE1 and CE3 both use the same Zoltek UD600 fabric and absorb more moisture than their counterparts, CE2 and CE4 respectively. This effect may arise from a preferred diffusion path at the interphase where the sizing, specific to that fabric, bonds to the matrix. The impact of sizing could be confirmed by contact angle measurement. Between plastics used in the CE systems, Pro-set INF and Hexion RIMR 035/0366, there is not definitive difference in moisture absorption. There can be no comparison made between these and the J series, as the fiber volume fractions are significantly different and uptake measurements are very inaccurate.

Mechanical Properties

Samples were tested with the procedure outlined in the "Acoustic Emission Methodology" section. Mechanical and acoustic emission results were saved as a .TXT file and imported using MATLAB R2017b. All post processing was performed with the same MATLAB software.

Table 3.Mechanical data summary for materials included in MHK study

Label	Conditioning (% Moisture)	Modulus (GPa)	Ultimate Stress (MPa)	Failure Strain (%)
J1	0.00	21.6	283	1.79
	0.44	19.4	324	2.10
J2	0.00	22.3	365	2.55
	0.50	22.4	339	2.28
J3	0.00	22.5	330	2.53
	0.59	21.5	196	1.13
J4	0.00	22.6	282	2.29
	0.43	25.4	301	1.95
J5	0.00	24.5	293	1.87
	0.48	24.4	291	1.75
J6	0.00	48.3	426	1.51
	0.85	43.6	465	1.72
J7	0.00	41.5	703	2.18
	1.14	41.5	550	1.57
J8	0.00	35.3	493	2.00
	0.84	35.4	510	1.77
CE1	0.00	53.6	781	1.50
	1.02	54.0	742	1.35
CE2	0.00	56.8	780	1.43
	1.44	48.1	695	1.56
CE3	0.00	48.4	739	1.58
	1.13	49.9	643	1.30
CE4	0.00	53.8	773	1.52
	1.07	51.4	748	1.54
CE5	0.00	53.1	744	1.41
	0.79	52.4	678	1.40
CE6	0.00	29.5	626	2.65
	0.64	30.7	621	2.54

Table 3 Continued

N1	**0.00**	**36.6**	**852**	**2.82**
	0.60	41.7	622	1.50
P1	0.00	15.1	321	2.29
	1.75	15.7	230	1.55
P4	0.00	22.2	457	2.33
	2.67	20.5	267	1.33
P5	0.00	17.9	366	2.21
	1.49	18.7	284	1.65
P6	0.00	17.5	395	2.74
	0.73	16.1	313	2.24
P9	0.00	17.1	395	2.70
	0.79	15.6	282	2.05
P11	0.00	14.9	248	1.90
	0.37	15.3	243	1.71
P13	0.00	12.3	277	2.58
	2.63	13.2	229	1.76

The thermoplastic materials had the lowest moduli and low strength. Moduli in these systems are matrix and volume fraction driven. The stiffest and softest were P4 (PA6) and P13 (PP) respectively. P4 was also the strongest P1 and P13 shared a matrix material (PP), but P1 incorporated an unknown additive called AMB, which increased the modulus and strength of the composite. Strength of the other materials did not follow any clear or discernable pattern without knowing the unreinforced strength of the matrix and the bonding quality to the fibers. Their failure strains were lower than their glass counterparts, which is likely a bond strength effect, as thermoplastics are difficult to bond to glass. Reduced bond strength will reduce damage tolerance. Examples of P series failed coupons are shown in Figure 24.

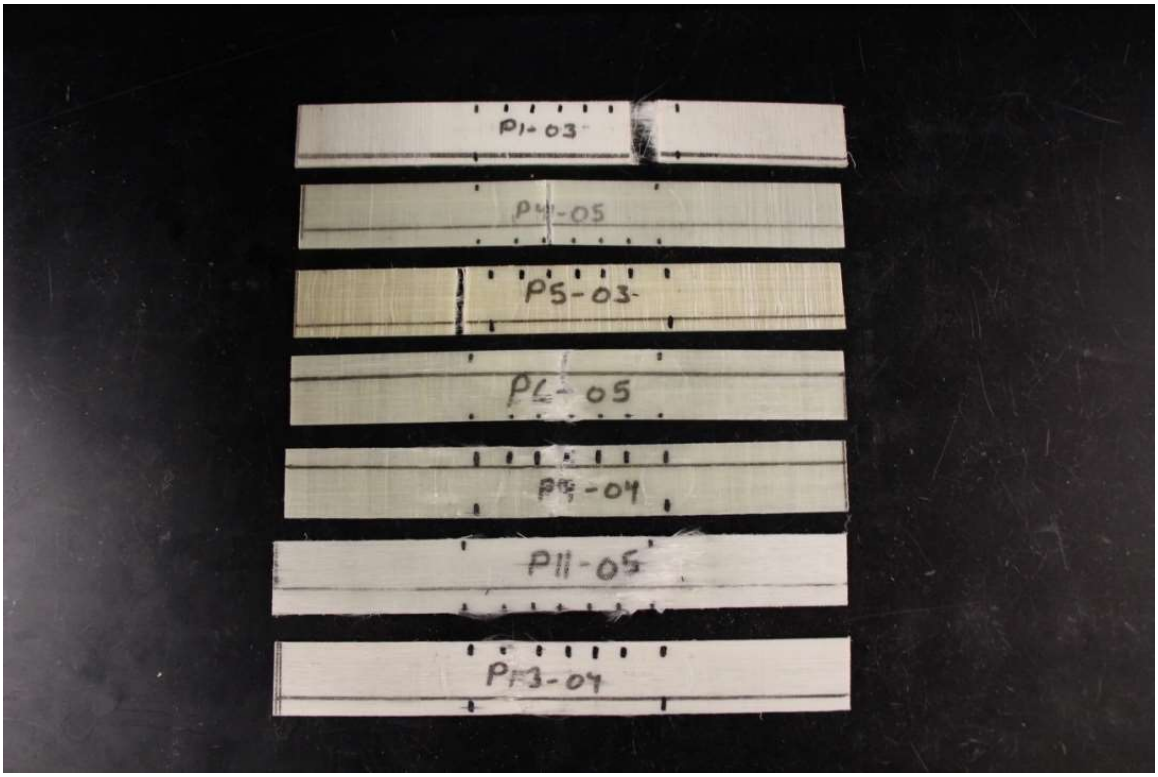

Figure 24: Examples of failed coupons of MHK study materials (P series) showing common failure modes for these materials

J series materials had relatively low moduli and strength and erratic strain to failure. Quasi-isotropic laminates will have lower stiffness and strength, but results are more a consequence of the low quality. Porosity and dry spots were prevalent. These defects produced audible cracking and visible delamination during testing, well before final failure. This indicates a relatively high damage tolerance, but the appearance of such significant damage early in a static test does not bode well for fatigue testing or environmental durability. Early cracking and delamination will propagate and lead to early failure in a

fatigue test and act ac expedited diffusion paths for moisture in a humid environment. Examples of failed coupons are shown in Figure 25.

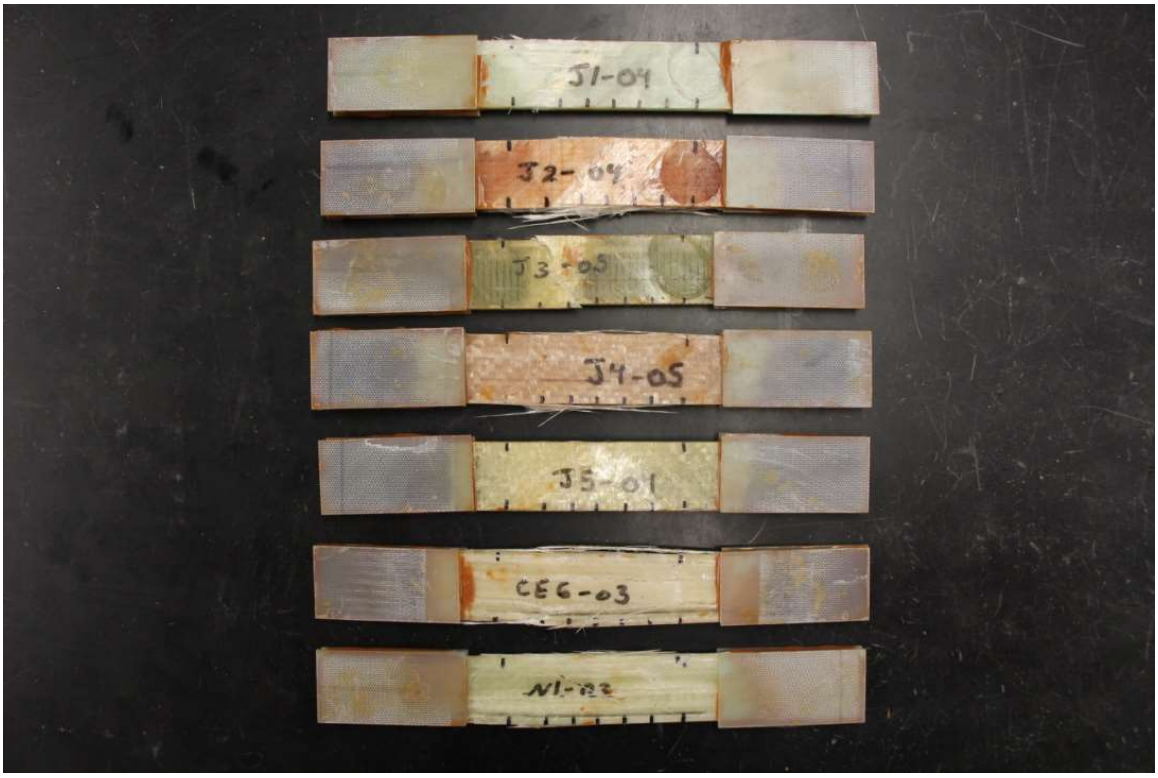

Figure 25: Examples of failed coupons of MHK study materials (J1-5, CE6, & N1) showing typical failure modes

CE series were high performing laminates with high moduli, strength, and strain to failure for carbon reinforcement. These hybrid materials, composed of unidirectional carbon and +-45 glass, performed higher than the other carbon laminates (J6-8) even with lower volume fractions. A contributor to these high values is a high proportion of 0-degree

fibers. The best performing laminate was N1, with high modulus, strength, and strain to failure, though it was the most effected by moisture uptake in strength and strain to failure.

Figure 26: Examples of failed coupons of MHK study materials (J6-8 & CE1-5) showing typical failure modes

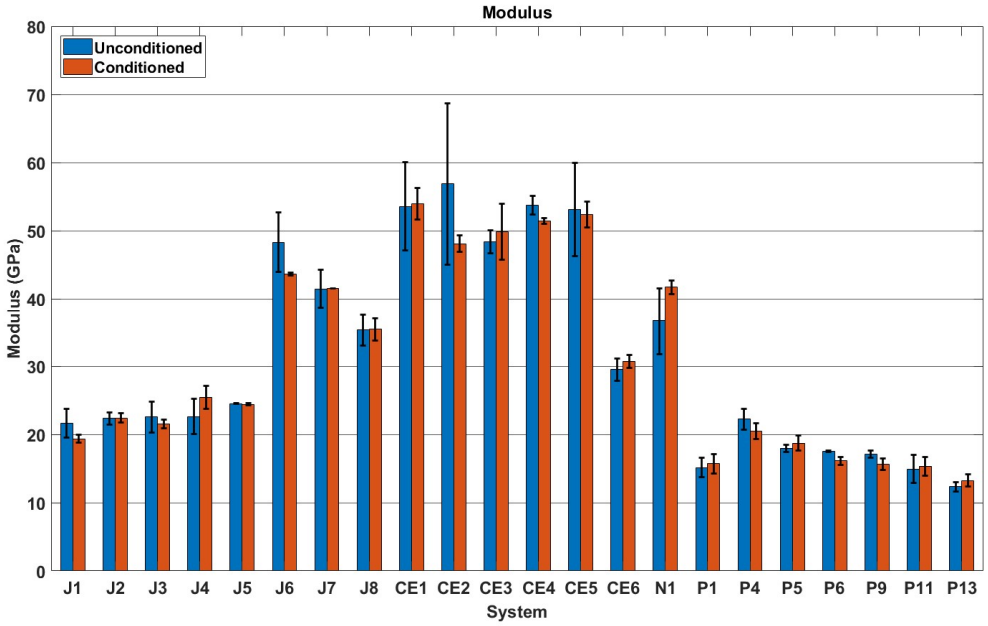

Figure 27: Summary of modulus degradation from conditioning. Error bars are range

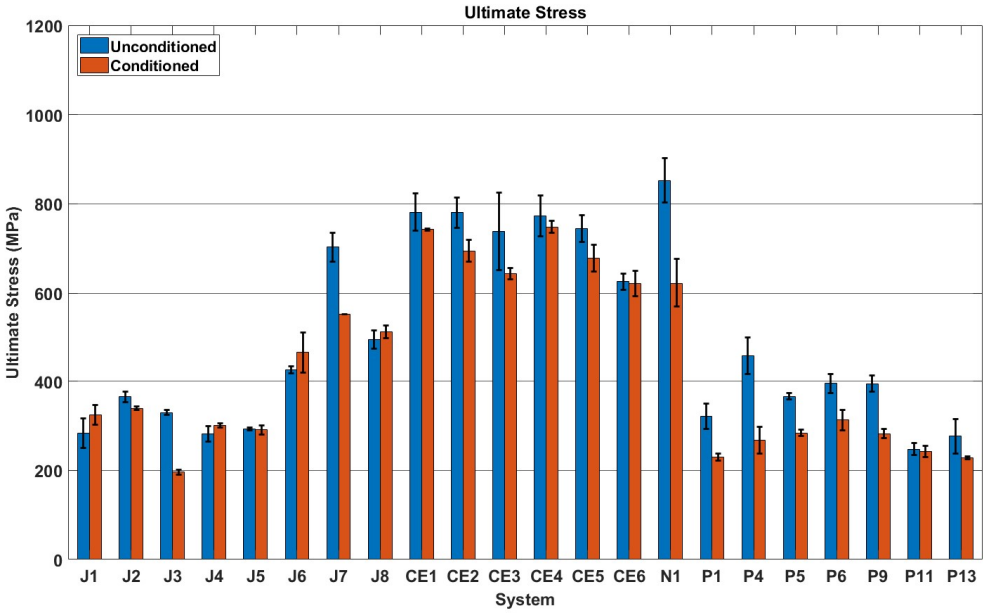

Figure 28: Ultimate strength degradation from conditioning. Error bars are range

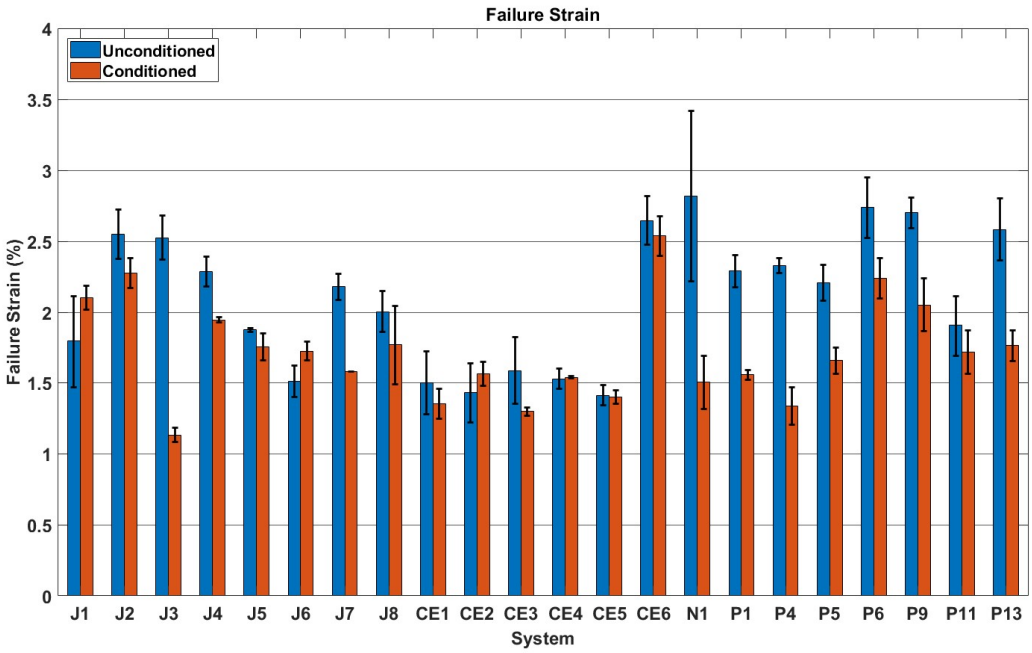

Figure 29: Failure strain degradation from conditioning. Error bars are range

Considering scatter, there is little or no significant effect of conditioning on modulus of any laminate. This is surprising because water is a known plasticizer of polymers and should therefore soften the matrix. This effect may be minimal on the scale of a laminate (amount of plastic versus reinforcement), or the effect is not pronounced at only partial saturation. The proportion of saturation is not exactly known. From the shape of the saturation curve, it can be asserted that these coupons are more than 80% of complete saturation.

There is a general downward trend of strength and failure strain with conditioning. This concurs with previous research at MSU and outside research [39], [46], [48]–[53]. Thermoplastics show the greatest reduction in strength and failure strain. Scatter in these data make it impossible make further comparison of relative mechanical effects between fabrics and matrix materials.

Acoustic Emission

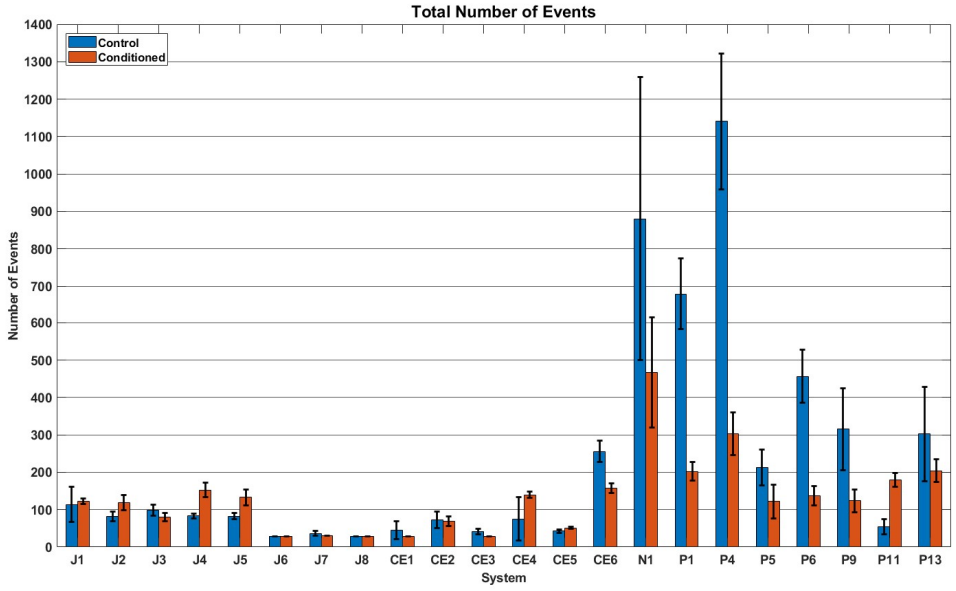

Figure 30: Mean number of AE events for MHK study materials showing variability/consistency and the greater number of events from thermoplastics

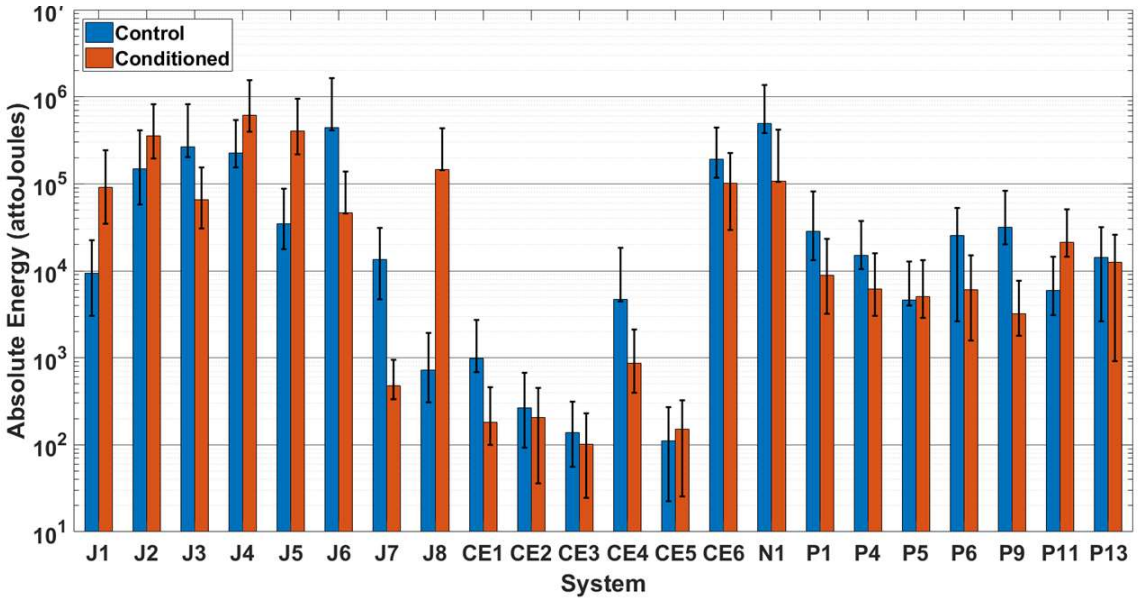

Figure 31: Mean absolute energy per AE event showing variability

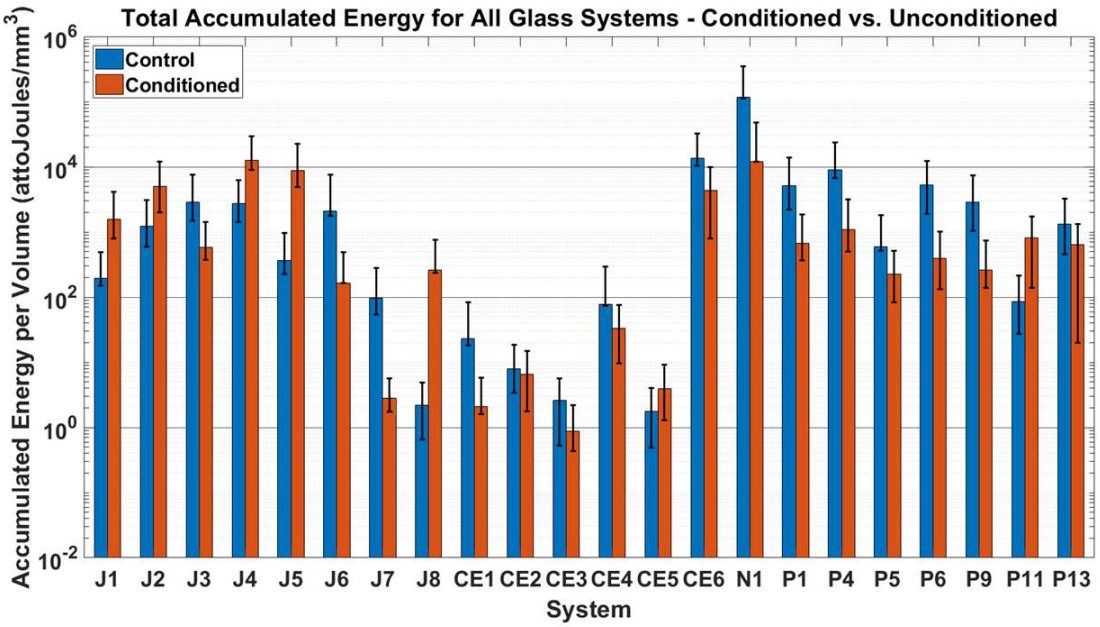

Figure 32: Mean accumulated absolute energy per coupon showing variability

Thermoplastics are found to produce fewer events with conditioning. In all P-series systems excluding P11, accumulated energy release also decreased. Changes in mean absolute energy per event were varied and mostly indeterminate. These changes combined with the loss in ultimate strength indicate increased matrix ductility (plasticization) for most thermoplastics. P11 is anomalous and puzzling, with no real mechanical effects and significant increase in AE activity.

Energy activity effects present no overall, matrix-based, or fabric-based trends in the thermoset laminates. Most systems do no show changes in overall activity (number of events), and the changes in energy yield are erratic. Some materials release more energy with moisture uptake while some release less. Because there is no change in number of events, those changes that occur in accumulated energy are due to a change in mean absolute energy. Further study is required to determine the nature of changing energy release with conditioning.

Frequency Content

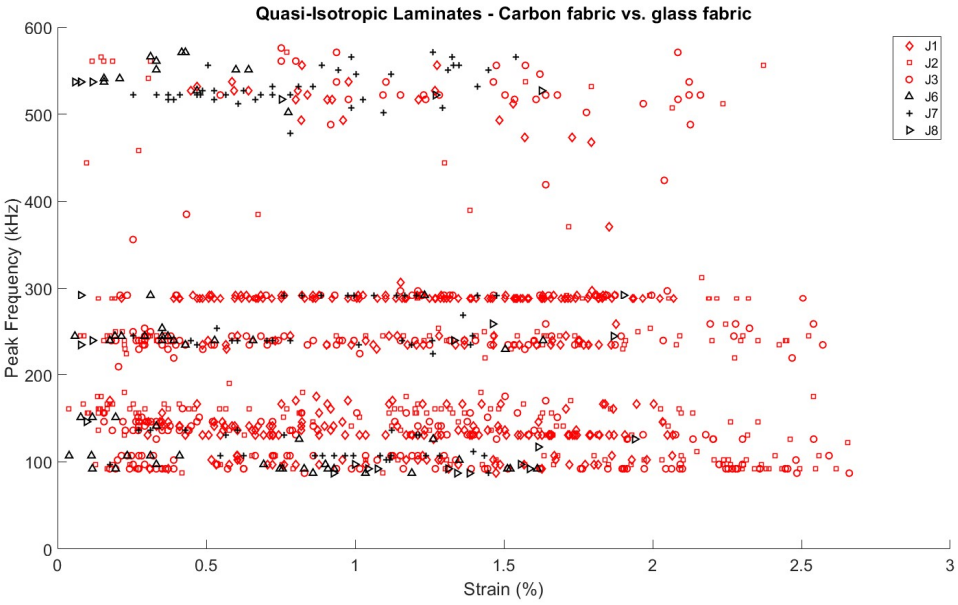

Figure 33: Peak spectral frequency versus strain for glass and carbon fabric quasi-isotropic laminates

All materials are found to have similar but non-identical frequency content. The most general comparison to be made in this material set is carbon versus glass reinforcement. Shown in Figure 33 is a scatter plot of peak spectral frequency versus strain for quasi isotropic laminates of comparable materials. That is J3, 5, 6, & 7 use the same matrix, AP SC18, but different fabrics, Likewise for J2, 4, & 8, using Derakane Vinyl ester but different fabrics. Inspecting this plot, there is no clear difference in frequency content on a reinforcement, fabric, or matrix level. Glass materials show more events between 120 and 200 kHz, but there are simply more events in the glass systems. The probability of

event occurrence in this range for carbon materials is the same. This absence of a difference in frequency content between carbon and glass is unexpected because carbon much stiffer than glass and would be expected to produce higher frequency events. However, this result appears in previous research [13]

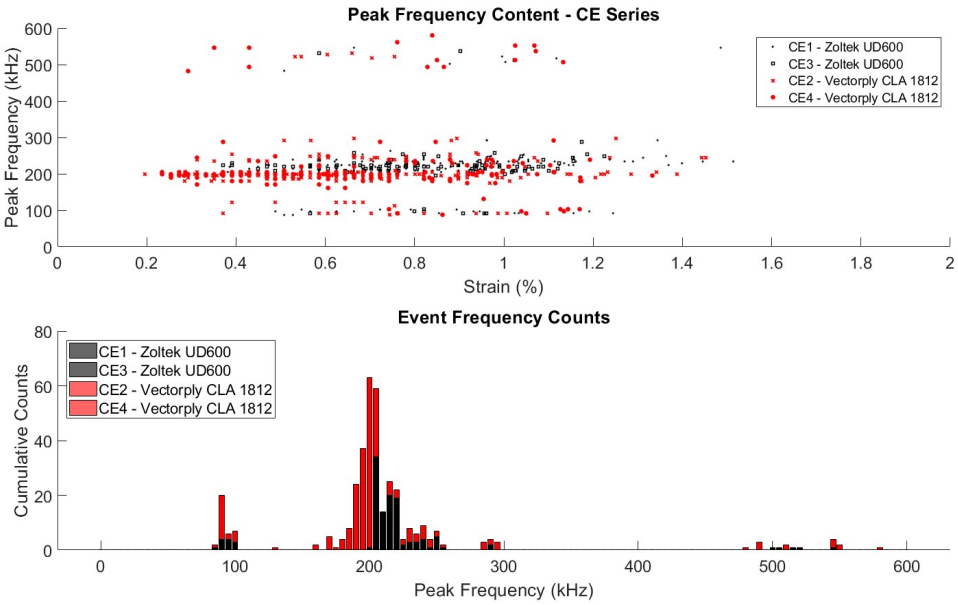

Figure 34: Peak spectral frequency versus Strain (Top) and cumulative peak spectral frequency histogram (Bottom) for CE1, 2, 3, & 4 showing frequency shift in interphase activity (~150-250 kHz)

Many more comparisons are made between similar layups. One result of these investigations was a shift in a sub-range of the mid-level frequency range associated with interphase failures. CE1 and CE3 use the same fabric (Zoltek UD600 with E-LT 1700) but use different resins. CE2 and CE4 also use the same fabric (Vectorply CLA 1812 with E-

LT 1700) and difference resins. In comparing their frequency content based on fabric, there is a shift in the mid-range frequency band ~150-250 kHz associated with interphase failure. This shift appears to be fabric driven with the epoxy resins used for these materials. This assumes that the interphase activity seen here is from the longitudinal fibers, not the glass fibers. The glass fibers are the same biaxial fabric (E-BX 1700 [45/-45]). Because there is a frequency shift in two materials with the same angle-ply fabric and coupon geometry, it will be assumed that the activity originates from longitudinal carbon fibers. There is no appreciable difference in mechanical properties between the materials. So, it would be difficult to make an association with interphase strength and frequency.

ACOUSTIC EMISSION IN A DIVERSE MATERIAL SET

Materials and Preparation

These materials were selected to represent a diverse range of PMC materials applicable to structural applications. This diversity was intended to extend into manufacturing method (prepreg, infusion, etc.), reinforcement type (glass and carbon), and matrix material (infused epoxy, prepreg epoxy, and various thermoplastics). Several layups were selected in order to create a pseudo-control for layup effects in acoustic emission features. Certain layups will produce a greater numbers of different damage types. Angle-ply ([45/-45]n) should experience matrix cracking and interphase failure. Cross-ply ([0/90]n) will experience matrix cracking between transverse tows as well as interphase failures early in the damage progression. Later there should be fiber pullout and fiber failure. Unidirectional transverse layups ([90]n) should only produce transverse matrix cracking and interphase failure, but because fabrics often use transverse backing strands to hold the fabric together longitudinal fibers will produce fiber failures and pullout. Lastly, unidirectional longitudinal layups ([0]n) will produce all types of failures modes: matrix cracking, interphase failure, fiber pullout, and fiber failure.

Table 4. Material summary for AE study of a diverse material set

Label	Resin	Fabric	Layup	Volume Fraction	Material Class
4191	Hexion 135/1366	E-LT 3800	[0]2	50.67	Vacuum Infused
4108	Hexion 135/1366	E-LT 3800	[0/90]s	58.2	Vacuum Infused
4115	Hexion 135/1366	E-LT 3800	[45/-45]s	58.0	Vacuum Infused

Table 4 Continued

4113	Hexion 135/1366	E-LT 3800	[90]4	59.5	Vacuum Infused
GPP1	Newport 301	300 gsm E-glass	[0]8	48.7	Prepreg vacuum
GPP2	Newport 301	300 gsm E-glass	[0/90/0/90]s	44.0	Prepreg vacuum
B15	Hexel 8552	IM7 carbon fiber	[0]8	N/A	Prepreg autoclave
B13	Hexel 8552	IM7 carbon fiber	[0/90/0/90]s	N/A	Prepreg autoclave
B14	Hexel 8552	IM7 carbon fiber	[45/-45/45/-45]s	N/A	Prepreg autoclave
B15t	Hexel 8552	IM7 carbon fiber	[90]8	N/A	Prepreg autoclave

Manufacturing & Sample Preparation

Material systems 4191, 4108, 4115, and 4113 were manufactured by hand layup and VARTM, outlined in the background. A rectangular aluminum plate was used as the mold with a resin inlet at one corner and an outlet at another corner along the long edge. The mold was coated with a wax-solvent releasing agent and allowed to dry. A layer of peel ply was placed below and above the fabric layup. These steps were included to allow easy removal of the plate after curing. A ply of flow media was placed on top of the peel ply to facilitate resin flow over the plate thereby allowing resin diffusion through the plate thickness instead of along the length. The complete layup was covered in a layer of plastic vacuum bagging film and sealed with synthetic rubber tape placed around the perimeter of the mold. The inlet and outlet were fitted with plastic tubing and sealed with rubber tape. The inlet was clamped closed, and vacuum was applied at the outlet tubing via a vacuum pump. Hexion RIMR 135/1366 resin was mixed for four minutes by a motorized spindle mixer. The mixed resin was introduced to the laminate by placing the inlet tubing into the

resin bucket and slowly unclamping the tubing allowing the vacuum to pull resin through the laminate. When the laminate was observed to be fully saturated ("wet-out"), the inlet was again clamped. The laminate was left cure on the mold at room temperature (~25˚C) for 24 hours. The entire layup was removed from the tool and placed in an oven set to 70˚C for 12 hours. This cure cycle concurs with the resin manufacturer's recommendations. Peel ply and vacuum bagging were removed from the laminate after curing.

GPP1 and GPP2 were manufactured simultaneously on a rectangular aluminum plate. The plate was coated with a wax-solvent releasing agent. The release plate was placed in an over set to 150 ˚C for 3 hours to burn off the releasing agent, leaving a clean mold. Non-porous Teflon peel ply was placed above and below the prepreg layup. Stitched fabric was cut into strips and placed between the peel ply around the layup without touching the prepreg to ensure vacuum. Plastic vacuum bagging covered the complete layup and was sealed with high temperature synthetic rubber tape. Vacuum was applied with a vacuum pump connected to brass tubing routed through the rubber tape. The tool was placed in an oven set to 121 ˚C for 6 hours. The prepreg spec sheet recommends that 345 kPa (50 psi) is applied to the part during curing. The method used here was only able to apply 80 kPa (11.6 psi), near atmospheric pressure at manufacturing elevation. During the curing process viscosity drops and the resin begins to flow. Under higher pressure more resin is squeezed out of the part. Lower pressure resulted in a lower fiber volume fractions and the possibility for some porosity.

All other material systems were acquired from various manufacturers. Therefore, the specifics of their manufacturing are not known. It is assumed from surface finish and

knowledge of the supplier that B13, B14, B15t, and B15 were cured in an autoclave according to the manufacturer's specifications. B15t is the same laminate at B15 cut in the transverse direction.

Matrix burn offs were performed on all material systems to determine fiber volume fractions, reported in Table 4. A sample of each material is cut, and mass and volume are measured. Samples were placed in an oven heated to 650 ˚C, where the matrix burns away. The remaining fiber mass is measured, and the volume is calculated with the known fiber density. Burn-offs were not conducted for carbon fiber laminates because there is no way to prevent carbon from the fibers burning off with the resin. Acid digestion is the standard way to measure fiber volume fractions in carbon laminates, but this method required the purchase and handling of dangerous chemicals, which would not have added justifiable value to the study.

Coupons of each system (except for 4108) were cut with a water lubricated diamond abrasion saw to nominal geometries of 200 x 25mm. Coupons of 4108 were acquired from another researcher, which had already been cut to geometries of 300x30mm and tabbed. Thickness and width measurements were made of each coupon with digital caliper and recorded. Theses dimensions were used in calculating modulus and stress after testing. For systems 4191, 4108, GPP1, GPP2, B13, and B15 tabs were adhered with an epoxy adessive to the gripping area at each end, leaving a total gage section of 90mm. 4115, 4113, B14, and B15t were left without tabs. Exemplary coupons are shown in Figure 35. Note that many of those coupons shown had already been tested. Damage present, especially in 4191-3 is not typical of a pristine coupon and was sustained during testing.

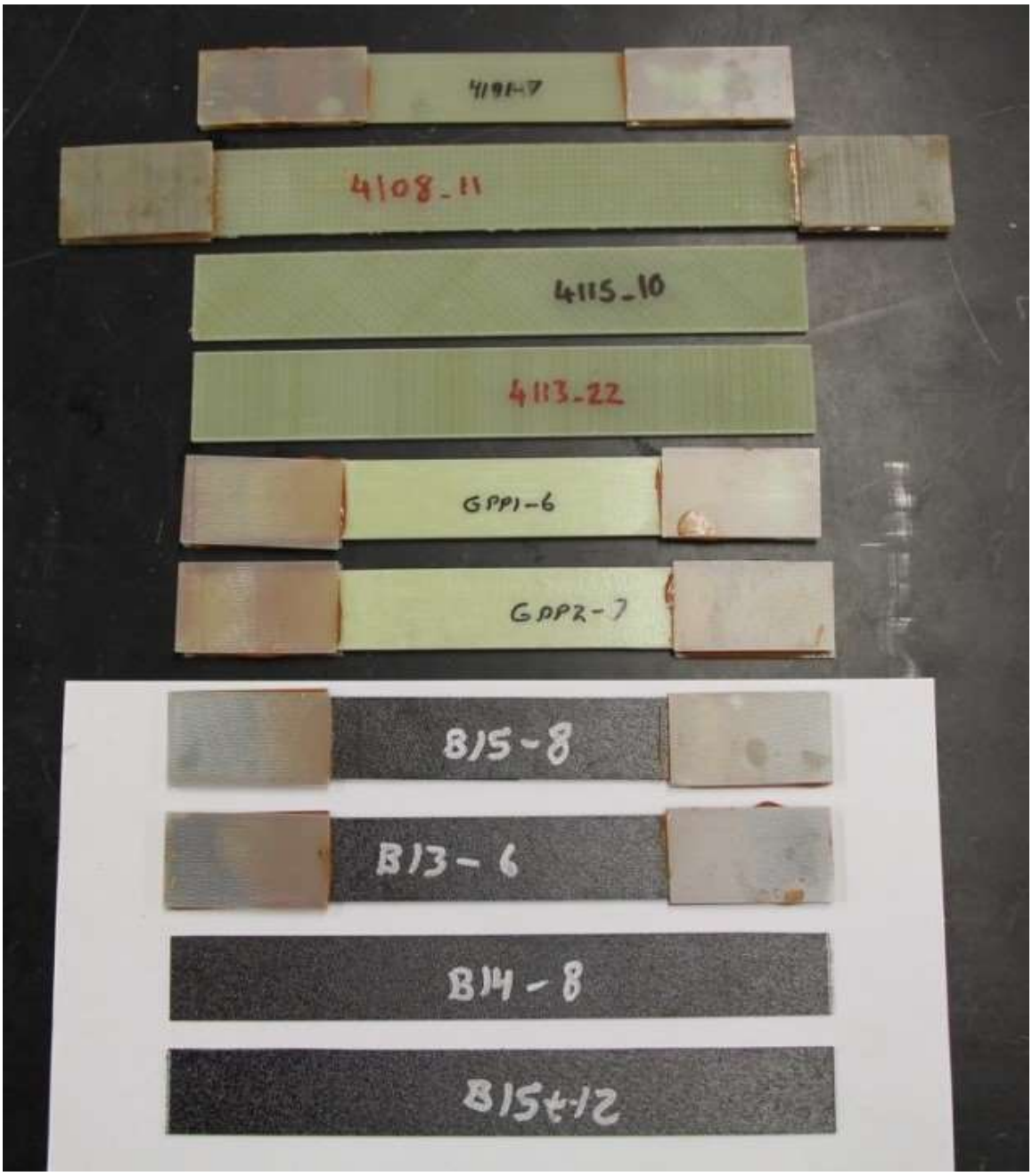

Figure 35: Examples of test coupons for DMS material study

Results

Samples were tested with the procedure outlined in the Acoustic Emission Methodology section.

Mechanical

Mechanical testing data result are summarized in the able below. Though a minimum of 5 coupons from each system were tested, not all tested were run to failure. Among failure tests, grip failures were common among some materials. These mechanical results are reported for relative comparison and to provide frame of reference for the reader.

Table 5. Diverse material set mechanical data summary

Label	Layup	Modulus (GPa)	Max Stress (MPa)	Failure Strain (%)
4191	[0]2	36.5	988.6	3.56
4108	[0/90]s	28.7	600.8	3.11
4115	[45/-45]s	11.2	83.6	5.06
4113	[90]4	15.3	112.5	2.15
GPP1	[0]8	35.8	810.0	2.78
GPP2	[0/90]2s	20.7	382.9	3.10
B15	[0]8	141	2026	1.44
B13	[0/90]2s	71.1	1174	1.44
B14	[45/-45]2s	14.0	168.8	2.53
B15t	[90]8	7.98	47.48	0.49

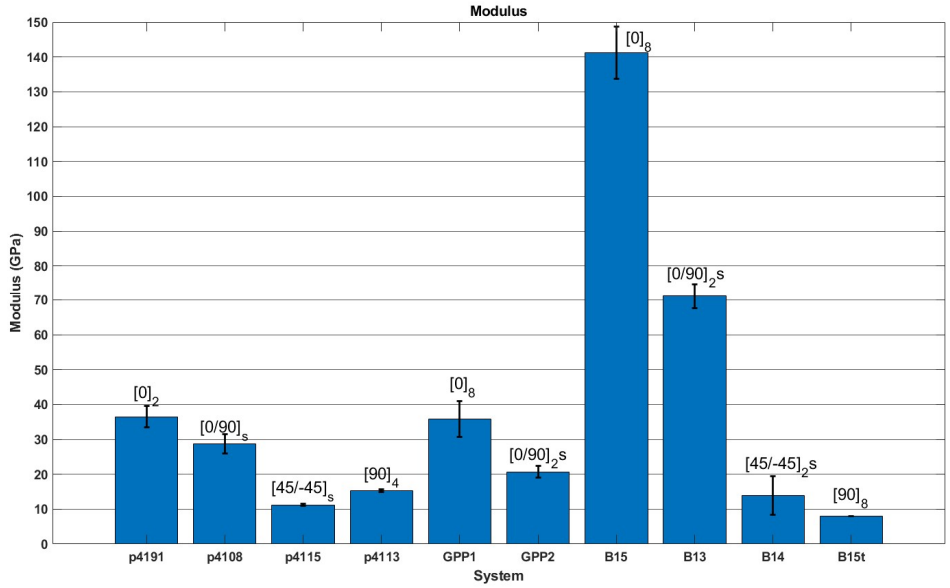

Figure 36: Diverse material set modulus bar graph

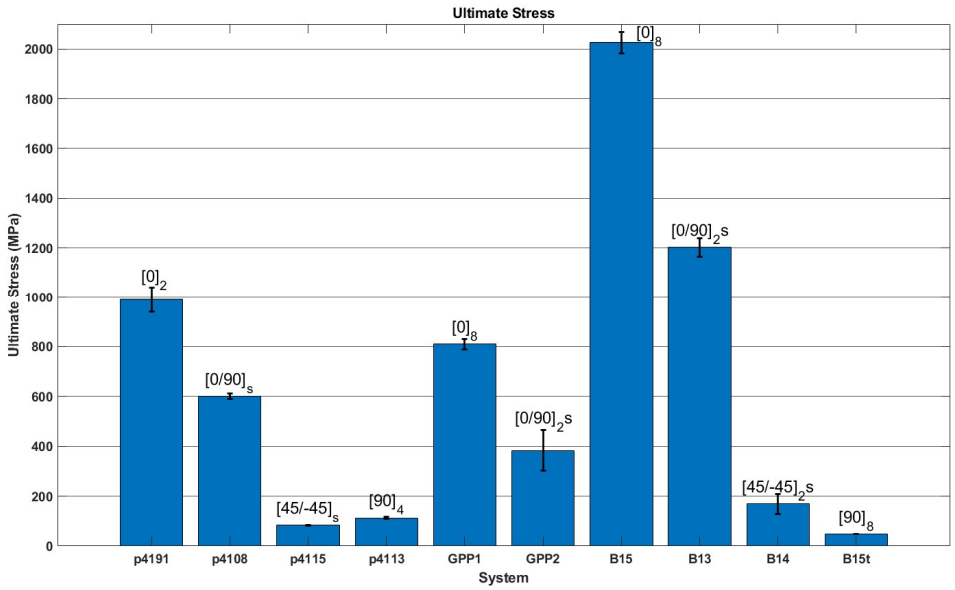

Figure 37: Diverse material set ultimate strength bar graph

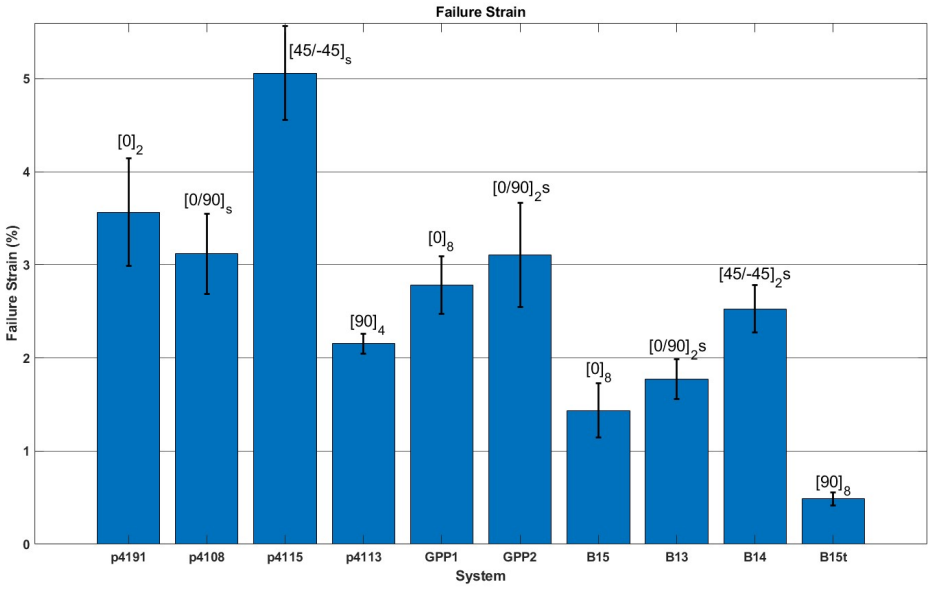

Figure 38: Diverse material set failure strain bar graph

With respect to modulus, carbon prepregs are the stiffest by nearly an order of magnitude, which is to be expected. Carbon fibers are much stiffer than glass (~70 GPa vs. ~250 GPa), and since these samples were manufactured in autoclave, it can be assumed that the fiber volume fraction is very high. The carbon laminates were also the strongest, which is also expected as carbon fibers are stronger than glass. The glass prepreg results were mixed and are discussed.

Failure strains are mostly consistent with material class and layup. Unidirectional 90-degree layups had the lowest failure strains. This is because it is a matrix dominated system. The first transverse matrix crack is ultimate failure. The order of unidirectional 0-

degree and cross-ply laminates will depend on layup, damage tolerance, and materials interactions and is therefore not consistent. Angle-ply laminates had the highest failure strains. As the coupon is pulled in tension matrix cracks appear and fibers slide relative to one another as they align with the load.

The prepregs (glass and carbon) experienced almost exclusively grip failures. This is the result of being thin and having high strength. Testing high strength coupons creates a challenge in load introduction. Because load is introduced via shear on the gripping surface, the gripping area is an inherent stress concentration. Because of the common grip failures it should be noted that the true strength of these prepreg systems is likely greater than those numbers presented here.

Another problem experienced with the prepreg systems were tab failures, where the tabbing epoxy experienced adhesive failure before the coupon. This is a result of inadequate bonding to the coupon surface. As a result of these frequent tab failures mechanical results for the prepreg systems reported here are based on few coupons (2-3). Despite these imperfect test executions, stiffness and strength are consistent with layups. That is, layups with more fibers oriented in the longitudinal direction are stiffer and stronger. Failure strains are also consistent with layup expectations.

Infused glass laminates were slightly stiffer than the glass prepreg laminates. This is likely the result of relatively higher volume fraction (50s vs. 40s). The prepreg laminates had low fiber volume fraction, especially for a prepreg system, which is a result of using only vacuum instead of autoclave. If the volume fractions were equal between infused and prepreg laminates, modulus of the prepreg coupons should measure higher because of the

transverse backing strands in the stitched infused fabric. Infused laminates also had significantly higher strengths than the prepregs, which could be an effect of backing strands preventing crack propagation but is more likely due to gripping effects.

Among the infused laminates, stiffnesses and strengths concur with expectations consistent with layups, except for the unidirectional transverse laminate 4113, which had higher stiffness and strength than the [45/-45] laminate 4115. This is due to the backing strands in the fabric. These backing strands are aligned longitudinally and provide significant support. Failure strains also concur with layup predictions.

Acoustic Emission

Because of the heavy emphasis in previous literature on frequency content of acoustic emission, a gross over view of peak spectral frequency in the different material classes is presented first. Referring to Figure 39, Figure 40, Figure 41, and Figure 42, there are differences to call attention to, but first the figures shall be explained.

The top plot of each figure is a scatter plot of peak spectral frequency versus strain for 5 coupon tests of each material system shown in the legend. In the bottom plot, the number of events for each material system are summed by frequency and plotted in a stacked histogram. Sensitivity curves for the sensors used to collect the data are plotted over the histogram for unidirectional 0-degree laminates to compare to frequency content.

There is correlation between sensitivity peaks and number of events, which is most pronounced 200-300 kHz. Greater numbers of events are detected where sensors have peaks in sensitivity. However, there are also great number of events at 500-600 kHz where there is no peak in sensitivity. It is the opinion of the author that underlying frequency

content is related to damage modes in composites that are filtered and accentuated by different sensors used in different studies. Most AE studies report frequency bands like those shown here, but the 'true' frequency of a damage mode can be skewed by the sensor and the related damage mode can vary with interpretation by the analyst.

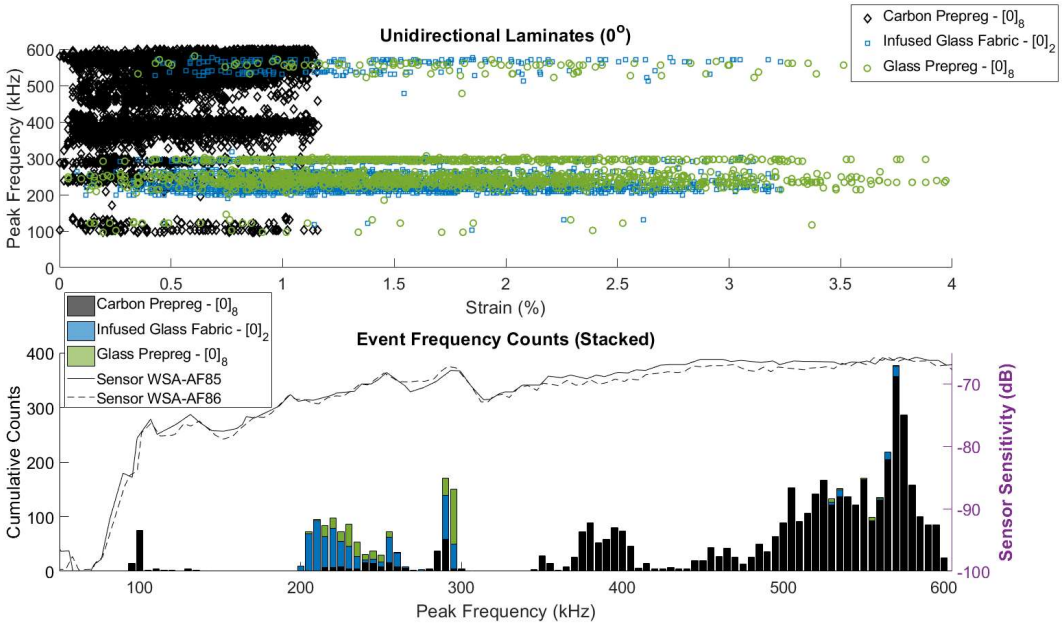

Figure 39: Peak spectral frequency versus strain (top) and total events per frequency with sensor sensitivity curves (bottom) - unidirectional 0-degree laminates

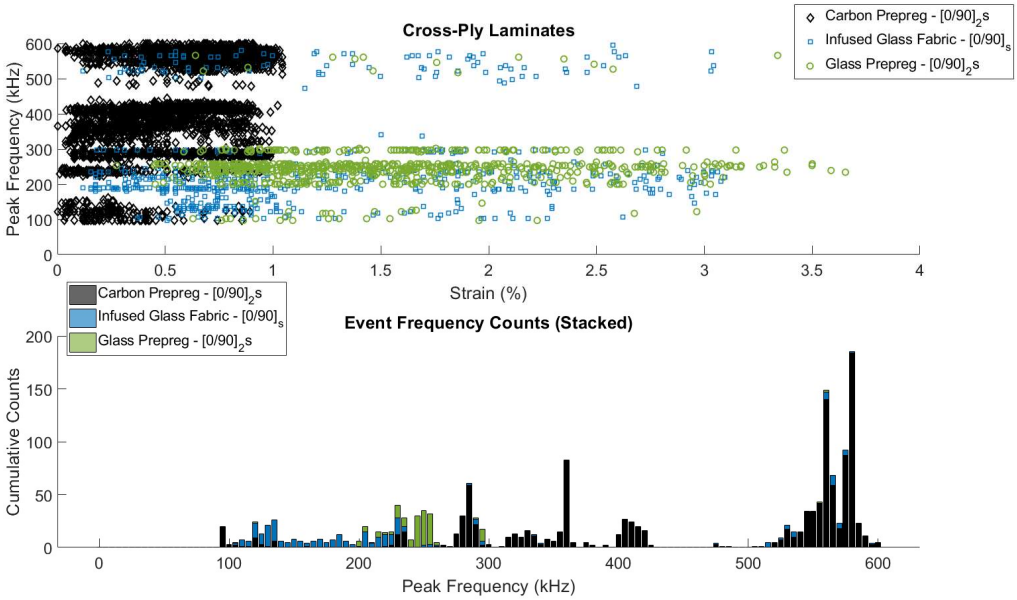

Figure 40: Peak spectral frequency versus strain (top) and total events per frequency with (bottom) – cross-ply Laminates

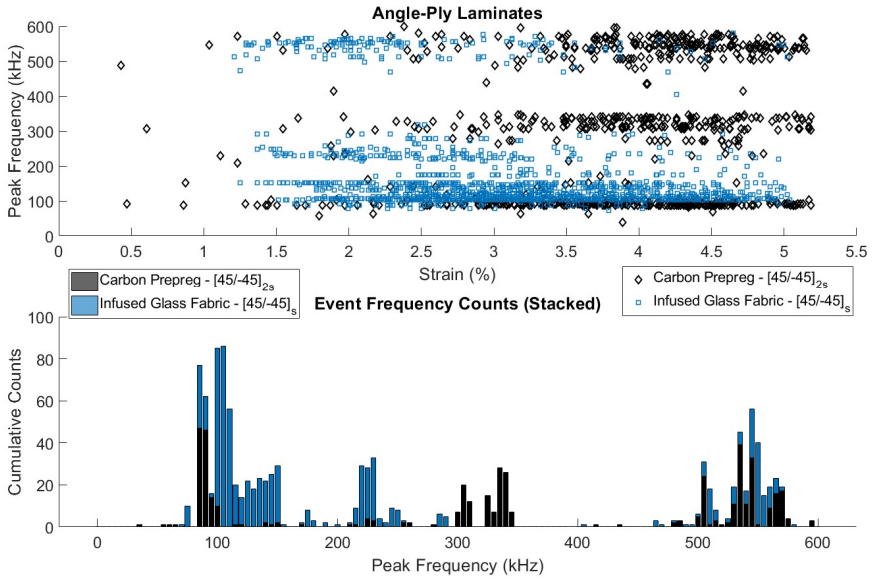

Figure 41: Peak spectral frequency versus strain (top) and total events per frequency (bottom) – angle-ply laminates

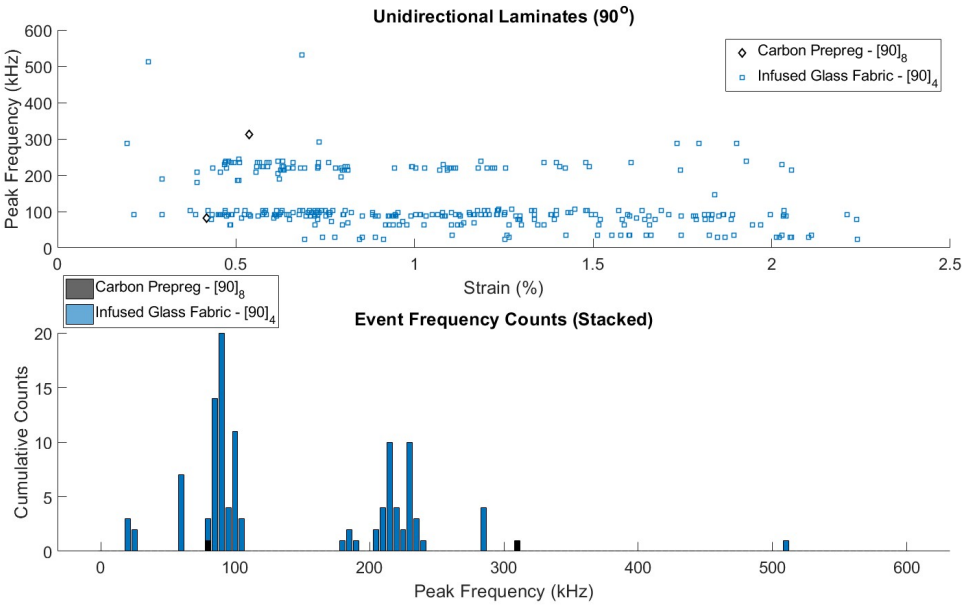

Figure 42: Peak spectral frequency versus strain (top) and total events per frequency (bottom) – unidirectional 90-degree laminates

The frequency bands that are correlated with damage modes are dependent on layup and are well correlated with expected damage progression. The unidirectional and cross-ply laminates exhibit all damage type frequency bands. There are far more high frequency fiber failure events (500-600 kHz) in the unidirectional layups, which is to be expected. This band is almost non-existent in the transverse layups. However, it is surprising to see the high level of high frequency activity in the angle ply layups. There is no clear cause for this activity, but fiber failures may occur in shear. This hypothesis may be confirmed optically through SEM. In the angle-ply and transverse layups on a proportional basis there

are a greater number of low frequency matrix cracking events (~100 kHz), though this frequency range is present in all layups.

The mid-range frequency bands (150-325 kHz) are less determinate. This range is broken into sub-bands which are seen to be present in some layups and materials while not in others. Through comparison of layups bands are found to indicate type of failure. A high number of events clustered around 250 kHz is present in the 90-degree laminates and the angle-ply laminates, which are expected to experience mainly interphase failure in tension. This frequency band is also present in the other laminates but is most isolated and prevalent in those that are off-axis.

The upper portion of the mid-range frequency range takes a more defined line about 300 kHz, which is suspected to be fiber pullout as it is most pronounced in the 0-degree and cross-ply laminates. It is still present in the 90-degree laminates but far less prevalent, which is representative of the very few fibers oriented longitudinally. It is important to mention the activity in this frequency band of the angle-ply layups because it is uncharacteristic of the layup. No fibers are oriented longitudinally. However, this suspected pullout type damage combined with the high frequency fiber breakage activity mentioned before indicates that off-axis fiber loading may still produce these damage types via shear.

Material-based frequency content differences are evident. The most obvious difference is the high number of events at 315-430 kHz in the carbon prepreg laminates, which is absent in all other materials tested in this work and that produced by MSU [13], [37], [46], [54], [55], though none of these studies incorporated carbon prepreg or high volume fraction laminate. Searching the literature was of limited success as very few of the

publications considering AE in carbon laminates reported peak spectral frequency as an isolated variable. Many modern papers employ clustering techniques with incorporate peak frequency instead of a single parameter. Woo et al. report peak frequency which has events in this frequency range, but the frequency banding present in all other AE data does not appear. Frequencies in their data exist in a continuum [56]. Fu et al. report peak frequency in this range for carbon laminates in 3 point bending, but the band is very localized at 400 kHz unlike the data found here [57]. The oft-cited de Groot publication tested unidirectional uncured prepreg in tension. Their results do show frequency activity near that found in this study, but the center of the band is shifted significantly higher than the data presented here [25].

Greater stiffness and strength in the prepreg laminates may create an upward shift in damage mode frequency as the mid-range interphase band has been seen to shift between different material combinations. With this consideration, upper mid (400 kHz) would be pullout and low mid (<350 kHz) would be interphase failure. Comparing by layup, supports this hypothesis. Both are present in the 0-degree and cross-ply layups, and there is a greatly reduced activity in the pullout frequency band in the angle-ply layup. The proportional activity of interphase versus pullout damage types are similar between glass and carbon angle-ply samples. A material influence would should not justify an upward shift in the de Groot data as they were testing uncured prepreg, which will be softer, weaker, and less securely bonded between fiber and matrix.

Material influence on frequency content is still dubious because that would create a continuum in correlation between mechanical properties and frequency content of

materials. That is stiffness and strength of a laminate would be directly correlated with the frequencies produced. This is not case. Therefore, the source of this frequency content is ultimately unknown though carbon fiber pullout is strongly suspected because of layup comparisons and considering expected damage types.

This new frequency content found in high volume fraction carbon materials requires further experimental investigation. As the difference between these materials and those tested previously at MSU bare no drastic difference in resin chemistry or fiber type (IM7 carbon in epoxy), discrepancy in outcome could stem from volume fraction.

Associating damage types with universal frequency bands across layups also seems problematic as slight frequency shift is observed between layups of the same material system in a manner that does not just reflect changes in damage types. The activity shifts between bands to correspond with preferred damage types, but the ultimate band center for each damage mode is found to shift between layups. This effect is most readily seen in comparing bands between the 0-degree and angle-ply carbon prepreg in Figure 43, but is present in other materials. The mid-range activity in the angle-ply layup is most likely interphase activity, but it overlaps two frequency bands shown in the 0-degree layup. The upper is suggested here to be pullout, and the lower is suggested to be interphase activity. This interphase activity would indicate an upward shift in frequency in the angle-ply layup. This shift is counter to the material influence theory, but there is no guarantee that this is a material influence, as it was found that the tabbing of a coupon can affect frequency content.

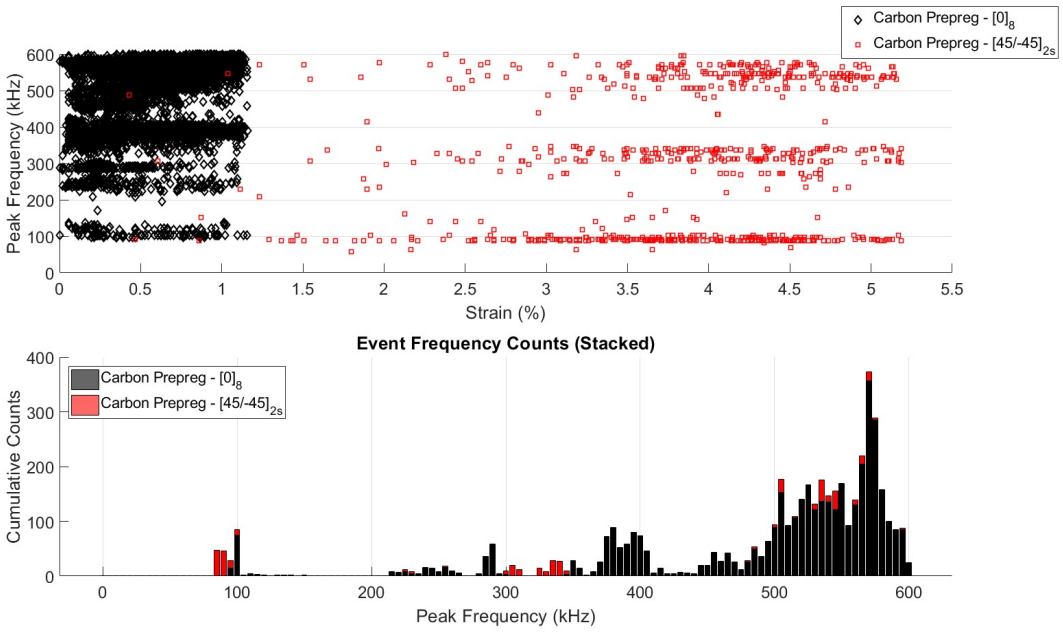

Figure 43: Frequency Content Comparison Between B15 and B14 Laminates

Looking to other material-basis differences, there are proportional changes in types of damage events between glass materials. Referring to the 0-degree and cross-ply laminates (Figure 39 and Figure 40) and considering the frequency range 100-300 kHz, interphase strength may have an influence on frequency. This effect was also found in materials of the MHK study presented earlier in this work.

Based on the frequency comparisons made between layups a different break-down of frequency ranges has been put forth in Table 6. Rigid application of these band bounds is only made to data collected in this study for materials with glass reinforcement. General locations and band widths should be loosely applicable to other studies. This distinction is made because a myriad of factors is found to affect frequency content resulting in the need to delineate between damage modes on a case-by-case basis. Frequency bands compared

between material systems and layups are similar but ultimately different in distribution centers and how tightly the event clusters are collected (band widths). As mentioned before carbon prepreg material systems are found to exhibit previously unseen frequency content, and the source is ultimately unknown. Further investigation into this material set is required to make an educated assertion on those frequency band ranges. By utilizing damage mode isolation test methods it may be possible to determine what type(s) of damage mechanisms are creating this previously unseen frequency content.

Table 6. Peak Frequency Damage Mode Association Newhouse vs. Schuster

	Frequency Range (kHz)		
Damage Mode	**Newhouse**	**Schuster**	**de Groot**
Matrix Cracking	50 – 150	50 – 120	80 – 180
Fiber-Matrix De-bond	175 - 275	200 – 300	240 – 300
Fiber Pullout	275-430	120 – 200	180 – 240
Fiber Breakage	> 430	> 300	> 300

The most significant difference between the frequency ranges defined previously and those presented here is the ordering of fiber-matrix de-bond and fiber pullout. Traditionally, fiber pullout has been classified as producing lower frequencies than de-bond. This paradigm is contested on the grounds that the fiber relaxation time is the dominant factor in the frequency of a pullout event. A pullout event will depend on the relaxation time of the fiber and the matrix. It is assumed that before failure the fiber will contain more energy. The resulting energy release from the fiber will be a higher amplitude

than the matrix and the peak frequency from this higher amplitude will be the dominating feature in the FFT if the resulting waveform.

From a layup comparison perspective, it is surprising that de Groot assigned the range 180-240 kHz to fiber pullout, when his own data shows nearly complete absence of activity in this frequency range. The only layup in his data set with activity in this range is the unidirectional 0-degree uncured carbon prepreg, which has far more activity just below 300 kHz. He labeled this activity de-bond, but fiber pullout concurs more with our understanding of damage progression in unidirectional 0-degree laminates.

The other main difference in the frequency bands put forth here is the fiber breakage range. Schuster and de Groot both categorize anything greater than 300 kHz as fiber breakage where this work draws the line at approximately 430 kHz. Given the capabilities of the AE data acquisition system used by Schuster, which was limited to 400 kHz, it is not surprising that he assigned a cutoff of 300 kHz. de Groot however, was able to capture a maximum frequency of 562.5 kHz and much of the high frequency activity occurred about 400 kHz.

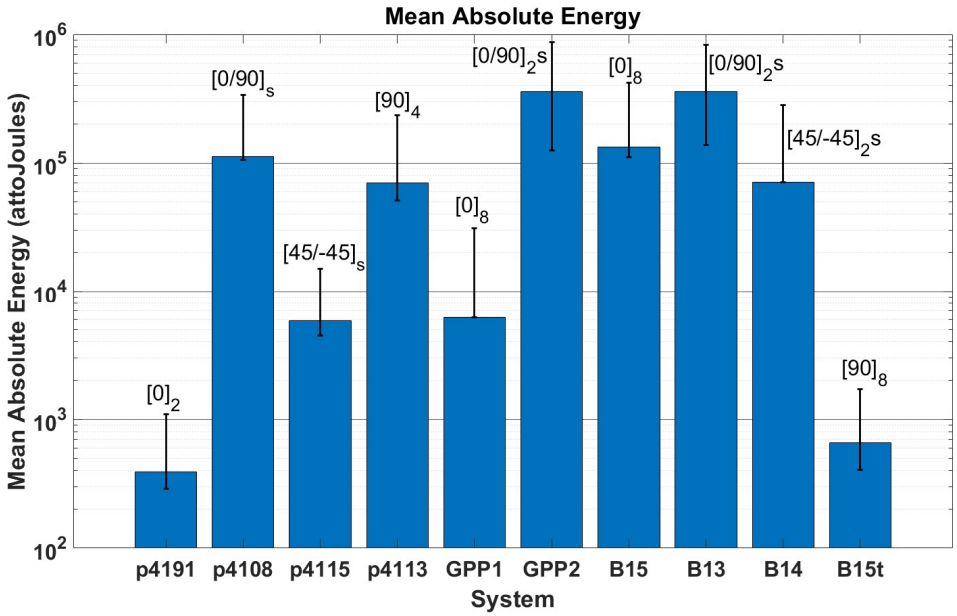

Figure 44: Mean Absolute Energy Per event for DMS Study Materials

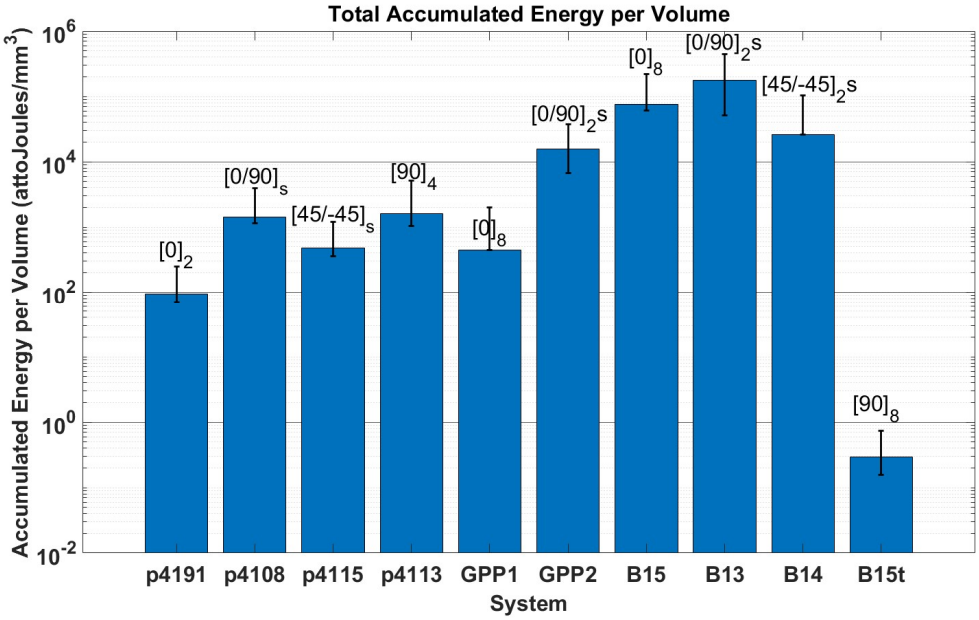

Figure 45: Mean Accumulated Energy for DMS Study Materials

Absolute energy is the other common single parameter analysis method and is also considered here. Energy of a damage event is independent of material type. This is interesting as different fibers and matrices have vastly different stiffnesses and strengths. Energy release is highly dependent on layup. Unidirectional laminates are found to produce more events than cross-ply laminates. Yet, cross-ply laminates yield higher energy events, see Figure 44, which also results in higher yield is accumulated energy, see Figure 45. That is, the energy yield from GPP2 is greater than GPP1, B13 is greater than B15, and 4108 is greater than 4149. This concurs with our understanding of the damage progression in these layups. AE was not collected at final failure for all these materials. Data is only compared for the damage regime before failure. Large damage events like transverse matrix cracking, interphase failure, debonding, and delamination will occur readily in a cross-ply layup well before failure. Whereas, very little damage should be present a unidirectional layup until just before final failure. No laminate is without imperfections for damage nucleation, therefore a great number of smaller damage events are still detected in the unidirectional samples. This reasoning is the same for the greater energy release from the infused 90-degree layup (4113). Large transverse cracks will yield high energies, and backing strand failures will contribute to the energy release. Energy release for the carbon 90-degree layup is very low. These coupons only yielded a single very high energy event at failure.

Modulus Degradation & Absolute Energy Accumulation

There is very good correlation between acoustic emission activity and softening of a material during a static tensile test (Figure 46). Events are detected just around a ‘knee’ in the stress strain curve. This effect of event clustering corresponding with modulus

degradation is variable between different material systems and layups. Energy accumulation is more consistently correlated with softening (Figure 47), where tangent modulus is plotted versus strain along with accumulated absolute energy. Finding this repeated trend in the data is an exciting development and is relevant to the field of structural health monitoring because structure modulus is a critical element in wind turbine and MHK design.

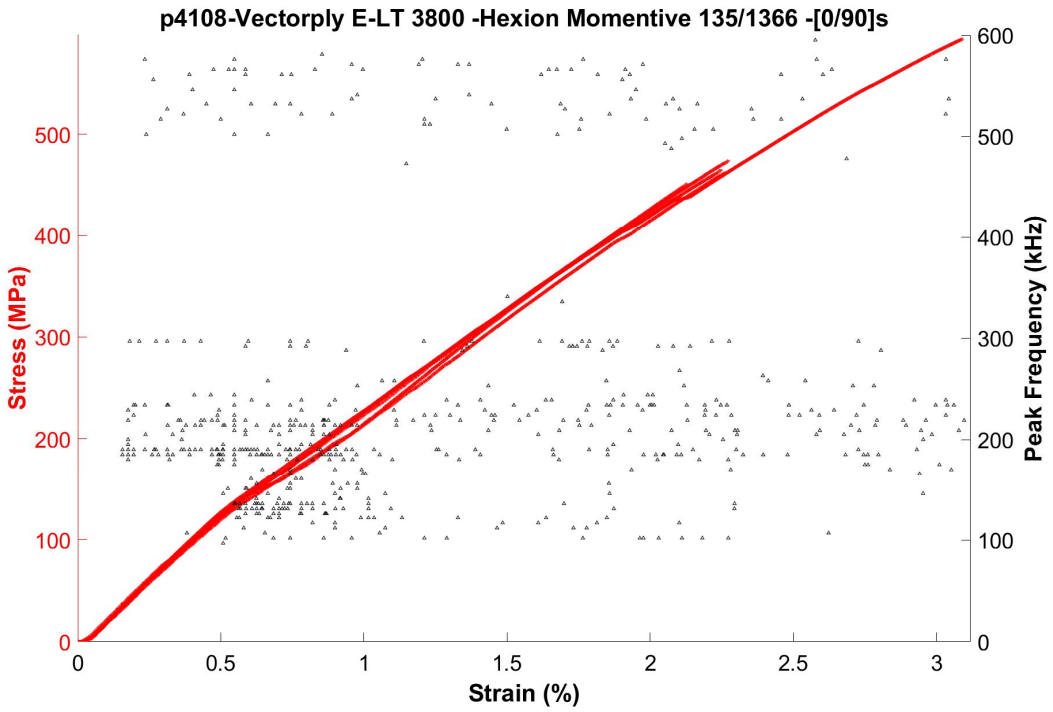

Figure 46: Stress versus strain plotted with peak spectral frequency

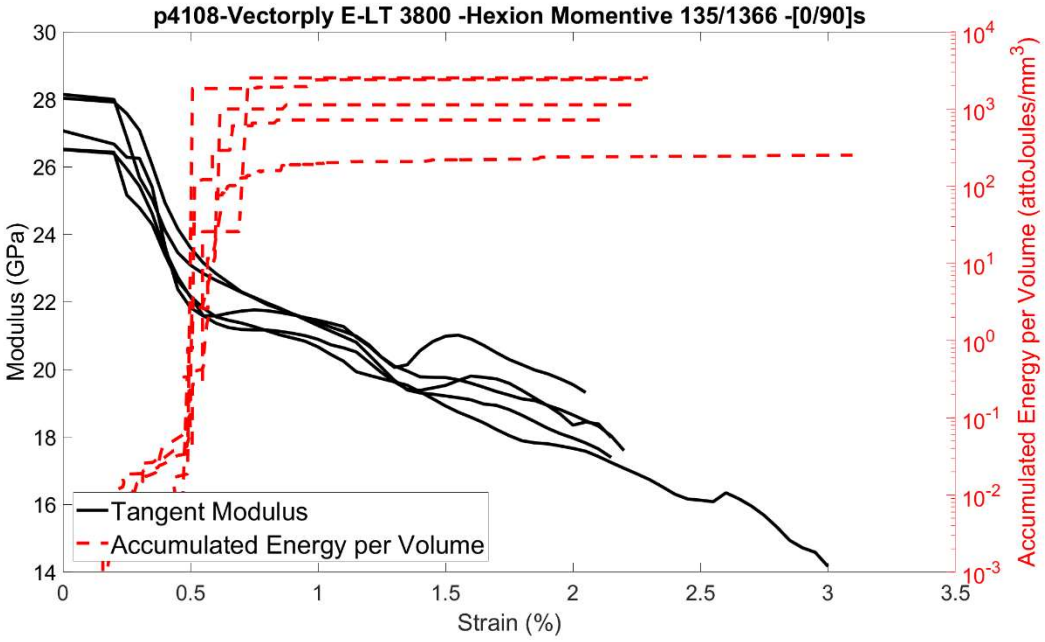

Figure 47: Accumulated energy per volume correlated with drop in tangent modulus

To affectively assess correlation, tangent modulus was transformed into percent degradation via equation 9, ϕ where is percent modulus degradation, E_{Tan} is tangent modulus, and E_o is starting modulus. This data was then normalized to one along with Accumulated absolute energy. An example of this data transformation is shown in Figure 48. Finally, coefficients of correlation were calculated for each coupon test and averaged within each laminate. These values are reported in Table 7. Results are varied. The thermoplastic laminates (P series) show very good correlation; while others do not.

$$\phi = 1 - \frac{E_{Tan}}{E_o} \tag{9}$$

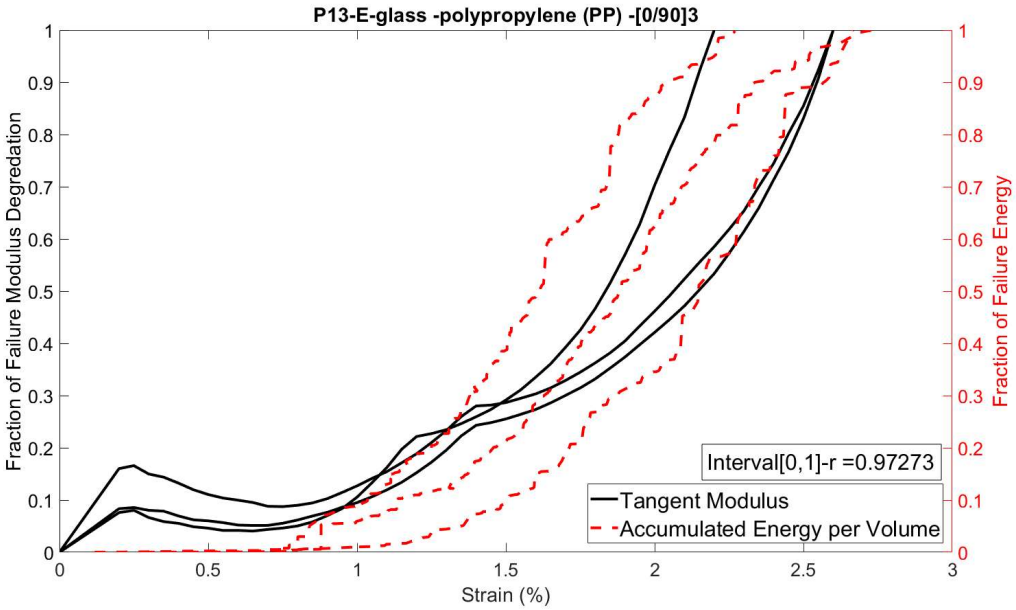

Figure 48: Percent tangent modulus loss versus accumulated energy per volume normalized correlation

Table 7. R values for accumulated energy release predicting tangent modulus degradation

System	Layup	R Value
J1	[0/45/90/-45]4	0.73
J2	[0/45/90/-45]4	0.93
J3	[0/45/90/-45]4	0.81
J4	[0/90/45/-45]4	0.87
J5	[0/90/45/-45]4	0.87
J6	[0/90/45/-45]4	0.63
J7	[0/45/90/-45]4	0.89
J8	[0/45/90/-45]4	0.79
CE1	[45/-45g/0/0c/45/-45g]	0.71
CE2	[45/-45g/0/0c/45/-45g]	0.45
CE3	[45/-45g/0/0c/45/-45g]	0.77
CE4	[45/-45g/0/0c/45/-45g]	0.41
CE5	[45/-45g/0/0c/45/-45g]	0.51
CE6	[0/45/-45/0]	0.80
N1	[0b 0b]s	0.43
P1	[0/90]3	0.93
P4	[0/90]3	0.87
P5	[0/90]3	0.57

Table 7 Continued

P6	[0/90]3	0.91
P9	[0/90]3	0.92
P11	[0/90]3	0.93
P13	[0/90]3	0.97
p4191	[0b]s	0.87
p4108	[0/90]s	0.54
p4115	[45/-45]s	0.59
p4113	[90]4	0.55
GPP1	[0]8	0.59
GPP2	[0/90/0/90]s	0.79
B15	[0]8	0.21
B14	[45/-45/45/-45]s	0.43
B13	[0/90/0/90]s	-0.04

Instead if continuous correlation between energy release and tangent modulus an alternative method of prediction is presented. Further statistical analysis was conducted to determine variability in the data. Consistency and low variability in the data is necessary to create a standard by which to determine modulus degradation based on AE energy release. Mean, standard deviation, and coefficient of variation were calculated for maximum accumulated energy per volume for each material system. An energy threshold was selected as an arbitrary proportion of the max energy. The amount of modulus degradation is determined at the energy threshold. It is found that max accumulated energy per volume is a consistent value within almost any given layup, but a few systems show variable results. The level of modulus degradation at any energy threshold varies between laminates, but at a given threshold the data is consistent for a laminate (table 7.) In general, a CV less than one is considered low variability. That is the distribution is tightly grouped around the mean. Therefore, it is possible to determine the energy threshold at which

modulus has dropped below an acceptable level. Such an energy threshold would be a valuable tool in structural health monitoring.

Table 8. Statistical analysis of accumulated energy and tangent modulus degradation correlation

		Max Energy per Volume (attoJoules/mm^3)			Percent Modulus Loss at 50% Max Energy		
System	**Layup**	μ	σ	CV	μ	σ	CV
J1	[0/45/90/-45]4	195	133	0.68	27	0.045	0.06
J2	[0/45/90/-45]4	1225	636	0.52	42	0.044	0.08
J3	[0/45/90/-45]4	2857	1701	0.60	18	0.076	0.09
J4	[0/90/45/-45]4	2719	1246	0.46	18	0.087	0.11
J5	[0/90/45/-45]4	364	322	0.88	21	0.133	0.17
J6	[0/90/45/-45]4	2069	2911	1.41	15	0.238	0.28
J7	[0/45/90/-45]4	96	79	0.83	22	0.012	0.02
J8	[0/45/90/-45]4	2	1	0.27	38	0.022	0.04
CE1	[45/-45g/0/0c/45/-45g]	23	25	1.10	8	0.040	0.04
CE2	[45/-45g/0/0c/45/-45g]	8	3	0.40	6	0.009	0.01
CE3	[45/-45g/0/0c/45/-45g]	3	0.5	0.18	5	0.026	0.03
CE4	[45/-45g/0/0c/45/-45g]	77	118	1.54	7	0.009	0.01
CE5	[45/-45g/0/0c/45/-45g]	2	0.4	0.23	7	0.016	0.02
CE6	[0/45/-45/0]	13387	8881	0.66	8	0.039	0.04
N1	[0b 0b]s	85499	105857	1.24	6	0.034	0.04
P1	[0/90]3	5179	2554	0.49	12	0.031	0.04
P4	[0/90]3	9026	6176	0.68	19	0.035	0.04
P5	[0/90]3	599	573	0.96	8	0.041	0.04
P6	[0/90]3	5322	1798	0.34	25	0.039	0.05
P9	[0/90]3	2845	1228	0.43	25	0.036	0.05
P11	[0/90]3	86	30	0.35	19	0.042	0.05
P13	[0/90]3	1313	570	0.43	21	0.078	0.10
p4191	[0b]s	94	56	0.60	35	0.214	0.33
p4108	[0/90]s	1408	1018	0.72	19	0.017	0.02
p4115	[45/-45]s	483	316	0.65	98	0.019	0.84
p4113	[90]4	1590	1672	1.05	61	0.019	0.05
GPP1	[0]8	443	638	1.44	20	0.113	0.14
GPP2	[0/90/0/90]s	15675	5277	0.34	35	0.106	0.16
B15	[0]8	75138	57496	0.77	7	0.044	0.05
B14	[45/-45/45/-45]s	26335	45201	1.72	73	0.305	1.15
B13	[0/90/0/90]s	176664	54448	0.31	8	0.031	0.03

μ – Mean σ – Standard Deviation CV – Coefficient of Variation

Implementation of this monitoring technique necessitates prior study of the material implemented in the structure. Unsurprisingly, layup is the largest influencing factor in severity of modulus degradation. Layups with more off-axis fibers show higher levels of modulus loss than those with more longitudinal fibers. This is because laminates with more off-axis plies will load the matrix and interphase more than the fibers, creating more severe damage. This increased damage severity contributes to softening but does not always contribute to a greater amount of energy release. That is the mean maximum accumulated energy release for primarily off-axis layups is not always higher than a layup of mostly zeros.

Comparing layups within a material system does not yield a consistent trend with varying layup. Therefore, laminates should be judged on a case-by-case basis. A laminate with representative materials and layup (proportion of each ply orientation) should be tested in the same loading type (axial, bending, etc.) and regime (static or fatigue) expected on the structure while monitoring acoustic emission in addition to stress and strain. Accumulated absolute energy should be calculated and normalized to the volume of the monitored mass and correlated with percent modulus loss (tangent or secant). Enough samples should be tested to create a confident correlation curve. With this method it should be possible to judge modulus degradation via AE monitoring.

CONCLUSIONS

Conclusions and Impacts

Conducting frequency analysis of a diverse material set has provided valuable insight into the damage progression the differences in AE signals. Frequency shifts are observed to be a function of material, via interphase strength, layup, sensor sensitivity, AE timing parameters, and AE data acquisition system. It is also suspected that additional influences on frequency content originate in volume fraction, coupon geometry, and even coupon tabbing.

With these considerations, new frequency ranges were put forth to be associated with damage mechanisms. These frequency band centers and band widths have significant differences from commonly referenced publications in this field as well as previous researchers at MSU. The first is re-defining fiber pullout events to have higher frequency than fiber de-bond based on AE activity between layups as well as the relationship between relaxation time material parameter and frequency. New frequency ranges were applied strictly to glass reinforcement material systems of this study. The ranges still generally apply to carbon reinforcement material systems, but new frequency content from carbon prepreg samples prohibit warrant further investigation. Ordering and ranges apply loosely to materials tested in other studies, but influences from AE data acquisition system, sensors, coupon geometry, and other factors make direct comparison impractical and inaccurate.

Mechanical properties of material types and layups yielded expected results. Reinforcement type, matrix material, and volume fraction are significant factors in stiffness and strength. Carbon fiber laminates are stiffer and stronger than glass laminates and

exhibit lower strains to failure. Epoxy and other thermoset matrix materials will produce a stiffer and stronger laminates of comparable layups. Low fiber volume fraction will reduce mechanical performance, and layups with more fibers aligned along the coupons testing axis will perform higher. Laminate quality is also found to be a major contributor to all mechanical performance. Fiber alignment, wetting out, and other good manufacturing practices are imperative to creating a high-quality laminate.

Accumulated absolute energy was found to correlate well with drop in tangent modulus. Direct continuous correlation of energy accumulation and modulus drop may not be practical. The rate of degradation and energy release for each laminate were found be consistent within each laminate but significantly different between material systems and layups. This data also was not easily reducible to a governing trend or 'rule of thumb.' However, this trend in the data is relevant to the field of structural health monitoring and could be a valuable tool to detect modulus drop via establishing an appropriate accumulated energy threshold.

For those laminates included in the hygrothermal conditioning study, moduli across all systems was not significantly affected by conditioning. There is a significant downward trend of strength and strain to failure with conditioning, which is most accentuated in the thermoplastic systems. This concurs with previous research. Poor quality laminates were less effected by conditioning indicating that swelling stresses or micro damage induced by moisture uptake are less detrimental than issues created by poor manufacturing methodology.

Lastly considering moisture absorption, results are consistent with previous literature. Thermoplastic laminates absorb more water and at a greater rate than laminates made with thermoset matrix material. There are no further confidently discernable differences between plastics with respect to rate of moisture uptake nor free volume for absorption.

Future Work

Acoustic emission is a powerful research technology. In trying to identify damage modes there is application in structural health monitoring to judge damage severity, but the application for the data produced in this work is in evaluating constitutive models. It is suggested that a strain-energy based failure model could be easily validated with the data presented in this thesis by comparing to strain of softening and failure. Additionally, if damage mode information could be extracted from the model, it could be compared to preferred frequency modes at different strain levels. A model based on strain could also easily incorporate swelling stresses from moisture absorption, but incorporating chemical effects would be more challenging.

With the goal of damage mode identification, it is suggested that techniques of damage mode isolation are adopted to fully prove the damage mode peak frequency correlation hypothesis. Among these damage mode isolating techniques are single fiber fragmentation, transverse tension, fiber push-in, fiber pull-out, cruciform single fiber test, short beam shear, and micro-droplet test.

To implement the modulus degradation detection technique presented in this work, it is necessary to verify that the correlation remains consistent under fatigue loading.

Additionally, further investigation should be made into 2D and 3D sub-structure elements to ensure that his trend is still valid.

The other general area of acoustic emission research is more tailored to structural health monitoring where artificial neural networks, statistical models, clustering, or other processing techniques are implemented to sidestep stochastic elements of AE signals to deduce relevant information about flaw sizes, remaining life, or gross mechanical properties. To further this area of research it is suggested to combine guided ultrasonic wave testing with acoustic emission monitoring in a manner similar to the work done by Murdy predicting modulus degradation [37]. This methodology should be applied to failure prediction.

With respect to specific material research, the new frequency content produced by carbon prepreg in this study is puzzling and warrants further investigation. Other carbon laminates have been tested at this institution in the past, but the only major difference in material is volume fraction and matrix material. An AE study focused on the acoustic emission of carbon laminates in different matrix materials at varying volume fractions may illuminate the source of this new frequency content.

With respect to moisture absorption, the effect of moisture on fiber sizing is not well defined. Investigating the mechanical performance of laminates made from fiber which have had their sizing “washed off” could yield valuable insight into this interaction. Additionally, a diverse set of fiber-matrix combinations soaked to full saturation and tested after desorbing could also be a fruitful investigation. The effect of any possible micro-damage from swelling would have to be sought out and considered.

REFERENCES CITED

[1] U. S. E. I. Administration, “Annual Energy Outlook 2018 with projections to 2050,” *J. Phys. A Math. Theor.*, vol. 44, no. 8, pp. 1–64, 2018.

[2] B. Bose, “Global Warming: Energy, Environmental Pollution, and the Impact of Power Electronics,” *IEEE Ind. Electron. Mag.*, vol. 4, no. 1, pp. 6–17, 2010.

[3] H. Reichle *et al.*, “References 5.,” vol. 302, no. December, pp. 1719–1723, 2003.

[4] “U.S. Energy Facts - Energy Explained, Your Guide To Understanding Energy - Energy Information Administration.” [Online]. Available: https://www.eia.gov/energyexplained/?page=us_energy_home. [Accessed: 10-Sep-2018].

[5] “Marine and Hydrokinetic Resource Assessment and Characterization | Department of Energy.” [Online]. Available: https://www.energy.gov/eere/water/marine-and-hydrokinetic-resource-assessment-and-characterization. [Accessed: 07-Sep-2018].

[6] P. Beiter *et al.*, “A Spatial-Economic Cost- Reduction Pathway Analysis for U.S. Offshore Wind Energy Development from 2015–2030,” no. September, 2016.

[7] [DOE] U.S. Department of Energy, “Offshore Wind Initiatives at the U.S . Department of Energy,” *Doe/Ee-1486*, p. 4, 2017.

[8] D. S. Jenne, Y. Yu, and V. Neary, “Levelized Cost of Energy Analysis of Marine and Hydrokinetic Reference Models Preprint,” no. April, 2015.

[9] EIA, “Levelized Cost and Levelized Avoided Cost of New Generation Resources in the Annual Energy Outlook 2018,” no. March, pp. 1–20, 2018.

[10] E. J. Barbero, *Introduction to Composite Materials Design*. 2015.

[11] Z. Chen, X. Zhou, X. Wang, L. Dong, and Y. Qian, “Deployment of a smart structural health monitoring system for long-span arch bridges: A review and a case study,” *Sensors (Switzerland)*, vol. 17, no. 9, 2017.

[12] W. A. Altabey and M. Noori, “An Extensive Overview of Lamb Wave Technique for Detecting Fatigue An Extensive Overview of Lamb Wave Technique for Detecting Fatigue Damage in Composite Structures,” *Ind. Syst. Eng.*, vol. 2, no. 6, pp. 1–20, 2017.

[13] M. F. Schuster, “CHARACTERIZATION AND ENERGY ANALYSIS OF FIBER REINFORCED POLYMER COMPOSITES BY ACOUSTIC EMISIION ANALYSIS,” 2014.

[14] K. L. Reifsnider, *Fatigue of Composite Materials*. 1991.

[15] G. Camino, A. Y. Polishchuk, M. P. Luda, M. Revellino, R. Blancon, and J. J. Martinez-Vega, "Water ageing of SMC composite materials: A tool for material characterisation," *Polym. Degrad. Stab.*, vol. 61, no. 1, pp. 53–63, 1998.

[16] "66 Weatheirng study of glass-fiber reinforced polyester sheets by scanning electron microscopy - 10.1002@pen.760120109.pdf," pp. 53–58.

[17] L. Prian and A. Barkatt, "Degradation mechanism of fiber-reinforced plastics and its implications to prediction of long-term behavior," *J. Mater. Sci.*, vol. 34, no. 16, pp. 3977–3989, 1999.

[18] C.-H. Shen and G. S. Springer, "Moisture absorption and desorption of composite materials," *Compos. Mater.*, vol. 10, pp. 2–20, 1976.

[19] G. C. Papanicolaou, T. V. Kosmidou, A. S. Vatalis, and C. G. Delides, "Water absorption mechanism and some anomalous effects on the mechanical and viscoelastic behavior of an epoxy system," *J. Appl. Polym. Sci.*, vol. 99, no. 4, pp. 1328–1339, 2006.

[20] P. Nogueira *et al.*, "Effect of water sorption on the structure and mechanical properties of an epoxy resin system," *J. Appl. Polym. Sci.*, vol. 80, no. 1, pp. 71–80, 2001.

[21] H. N. Narasimha Murthy, M. Sreejith, M. Krishna, S. C. Sharma, and T. S. Sheshadri, "Seawater durability of epoxy/vinyl ester reinforced with glass/carbon composites," *J. Reinf. Plast. Compos.*, vol. 29, no. 10, pp. 1491–1499, 2010.

[22] M. R. Gorman, "Plate wave acoustic emission," *J. Acoust. Soc. Am.*, vol. 90, no. 1, pp. 358–364, 1991.

[23] G. N. Morscher, "Modal acoustic emission of damage accumulation in a woven SiC / SiC composite," *Compos. Sci. Technol.*, vol. 59, no. 5, pp. 687–697, 1999.

[24] N. R. Center, "AE Signal Features." [Online]. Available: https://www.nde-ed.org/EducationResources/CommunityCollege/Other Methods/AE/AE_Signal Features.php.

[25] P. J. de Groot, P. A. M. Wijnen, and R. B. F. Janssen, "Real-time frequency determination of acoustic emission for different fracture mechanisms in carbon/epoxy composites," *Compos. Sci. Technol.*, vol. 55, no. 4, pp. 405–412, 1995.

[26] A. R. Oskouei, M. Ahmadi, and M. Hajikhani, "Wavelet-based acoustic emission characterization of damage mechanism in composite materials under mode I delamination at different interfaces," *Express Polym. Lett.*, vol. 3, no. 12, pp. 804–813, 2009.

[27] M. G. R. Sause, A. Gribov, A. R. Unwin, and S. Horn, “Pattern recognition approach to identify natural clusters of acoustic emission signals,” *Pattern Recognit. Lett.*, vol. 33, no. 1, pp. 17–23, 2012.

[28] J. Martínez-Jequier, A. Gallego, E. Suárez, F. J. Juanes, and Á. Valea, “Real-time damage mechanisms assessment in CFRP samples via acoustic emission Lamb wave modal analysis,” *Compos. Part B Eng.*, vol. 68, pp. 317–326, 2015.

[29] J. Bohse, “Acoustic emission characteristics of micro-failure processes in polymer blends and composites,” *Compos. Sci. Technol.*, vol. 60, pp. 1213–1226, 2000.

[30] W. Haselbach and B. Lauke, “Acoustic emission of debonding between fibre and matrix to evaluate local adhesion,” *Compos. Sci. Technol.*, vol. 63, no. 15, pp. 2155–2162, 2003.

[31] C. R. Ramirez-Jimenez, N. Papadakis, N. Reynolds, T. H. Gan, P. Purnell, and M. Pharaoh, “Identification of failure modes in glass/polypropylene composites by means of the primary frequency content of the acoustic emission event,” *Compos. Sci. Technol.*, vol. 64, no. 12, pp. 1819–1827, 2004.

[32] A. Marec, J. H. Thomas, and R. El Guerjouma, “Damage characterization of polymer-based composite materials: Multivariable analysis and wavelet transform for clustering acoustic emission data,” *Mech. Syst. Signal Process.*, vol. 22, no. 6, pp. 1441–1464, 2008.

[33] S. Barr and M. L. Benzeggagh, “ON THE USE OF A C O U S T I C EMISSION TO I N V E S T I G A T E D A M A G E M E C H A N I S M S IN G L A S S - F I B R E - R E I N F O R C E D POLYPROPYLENE,” vol. 3538, no. 94, pp. 369–376, 1994.

[34] M. G. R. Sause, T. Müller, A. Horoschenkoff, and S. Horn, “Quantification of failure mechanisms in mode-I loading of fiber reinforced plastics utilizing acoustic emission analysis,” *Compos. Sci. Technol.*, vol. 72, no. 2, pp. 167–174, 2012.

[35] N. Godin, S. Huguet, and R. Gaertner, “Integration of the Kohonen’s self-organising map and k-means algorithm for the segmentation of the AE data collected during tensile tests on cross-ply composites,” *NDT E Int.*, vol. 38, no. 4, pp. 299–309, 2005.

[36] C. Suresh Kumar, V. Arumugam, R. Sengottuvelusamy, S. Srinivasan, and H. N. Dhakal, “Failure strength prediction of glass/epoxy composite laminates from acoustic emission parameters using artificial neural network,” *Appl. Acoust.*, vol. 115, pp. 32–41, 2017.

[37] P. Murdy, “Combining Acoustic Emission and Guided Ultrasonic Waves for Global Property Prediction and Structural Health Monitoring of Glass Fiber Composites,”

2018.

[38] Q. Q. Ni and M. Iwamoto, “Wavelet transform of acoustic emission signals in failure of model composites,” *Eng. Fract. Mech.*, vol. 69, no. 6, pp. 717–728, 2002.

[39] M. M. Voth, D. A. Miller, J. D. Nunemaker, P. Murdy, D. D. Samborsky, and D. S. Cairns, “Exploring Frequency Based Analysis Methods for Damage Identification in Fiberglass-Epoxy Composite Systems .,” 2017.

[40] M. A. Hamstad, “Local Characterization of Fiber Composites by Acoustic Emission,” *J. Acoust. Soc. Am.*, vol. 73, no. 6, pp. 2230–2230, 1983.

[41] A. Garg and O. Ishai, “Hygrothermal influence on delamination behavior of graphite/epoxy laminates,” *Eng. Fract. Mech.*, vol. 22, no. 3, pp. 413–427, 1985.

[42] A. C. Garg, “Intralaminar and Interlaminar Fracture in Graphite.Epoxy Laminates,” vol. 23, no. 4, pp. 719–733, 1986.

[43] K. Komai, K. Minoshima, and T. Shibutani, “Intestigations of the Fracure Mechanism of Carbon/Epoxy Composites by AE Signal Analysis,” *JSME Int. J.*, vol. 34, 1991.

[44] T. Czigány, Z. A. Mohd Ishak, and J. Karger-Kocsis, “On the failure mode in dry and hygrothermally aged short fiber-reinforced injection-molded polyarylamide composites by acoustic emission,” *Appl. Compos. Mater. An Int. J. Sci. Appl. Compos. Mater.*, vol. 2, no. 5, pp. 313–326, 1995.

[45] N. Ning *et al.*, “Realizing the enhancement of interfacial interaction in semicrystalline polymer/filler composites via interfacial crystallization,” *Prog. Polym. Sci.*, vol. 37, no. 10, pp. 1425–1455, 2012.

[46] M. M. Voth, “CHARACTERIZATION OF THE EFFECTS OF HYGROTHERMAL-AGING ON MECHANICAL PERFORMANCE AND DAMAGE PROGRESSION OF FIBERGLASS EPOXY COMPOSITE,” no. April, 2018.

[47] EVAL; KURARAY, “Technical Bulletin No . 110 GAS BARRIER PROPERTIES OF The most outstanding property of EVAL ® resins is their ability to provide a barrier to gases such as oxygen , nitrogen , carbon dioxide and helium . This property is especially important when consider,” no. 110, pp. 1–12.

[48] J. D. Nunemaker, M. M. Voth, D. A. Miller, D. D. Samborsky, P. Murdy, and D. S. Cairns, “Effects of moisture absorption on damage progression and strength of unidirectional and cross-ply fiberglass – epoxy composites,” pp. 427–438, 2018.

[49] David Miller; John F. Mandell; Daniel D. Samborsky; Bernadette A. Hernandez-Sanchez; D. Todd Griffith, “Performance of Composite Materials Subjected to Salt Water Environments,” *2012 AIAA SDM Wind Energy Sess.*, 2012.

[50] J. F. Mandell, D. D. Samborsky, and D. S. Cairns, “SANDIA CONTRACTORS REPORT FATIGUE OF COMPOSITE MATERIALS AND by,” *Mont. Mag. West. Hist.*

[51] V. M. Karbhari and G. Xian, “Hygrothermal effects on high VFpultruded unidirectional carbon/epoxy composites: Moisture uptake,” *Compos. Part B Eng.*, vol. 40, no. 1, pp. 41–49, 2009.

[52] K. Liao, C. R. Schultheisz, and D. L. Hunston, “Effects of environmental aging on the properties of pultruded GFRP,” *Compos. Part B Eng.*, vol. 30, no. 5, pp. 485–493, 1999.

[53] M. W. Keller, B. D. Jellison, and T. Ellison, “Composites : Part B Moisture effects on the thermal and creep performance of carbon fiber / epoxy composites for structural pipeline repair,” *Compos. Part B*, vol. 45, no. 1, pp. 1173–1180, 2013.

[54] J. D. Nunemaker, “EXPLORING THE EFFECTS OF FIBER ANGLE AND STACKING SEQUENCE,” no. January, 2017.

[55] A. J. Lolatte, “Influence of Fabric Architecture on Damage Progression as Evidenced by Acoustic Emission,” no. July, 2016.

[56] S. C. Woo and N. S. Goo, “Analysis of the bending fracture process for piezoelectric composite actuators using dominant frequency bands by acoustic emission,” *Compos. Sci. Technol.*, vol. 67, no. 7–8, pp. 1499–1508, 2007.

[57] T. Fu, Y. Liu, Q. Li, and J. Leng, “Fiber optic acoustic emission sensor and its applications in the structural health monitoring of CFRP materials,” *Optics and Lasers in Engineering*, vol. 47, no. 10. pp. 1056–1062, 2009.

APPENDICES

APPENDIX A

APPENDIX A: MATERIALS FROM IN-HOUSE MANUFACTURING

VECTORPLY
Performance Composite Reinforcements

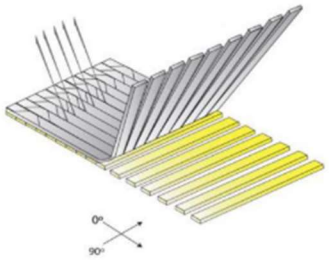

E-LT 3800-10

Fiber Type: E-Glass
Architecture: 0º/90º Biaxial

Total Weight: 37.26 oz/sq.yd / 1263 g/sq.m

Roll Specifications			Fiber Architecture Data	
Roll Width:	Roll Weight:	Roll Length:	0 ° :	33.55 oz/sq.yd / 1138 g/sq.m
50 in. / 1270 mm	220 lbs / 100 kg	68 yd / 62 m	90 ° :	3.36 oz/sq.yd / 114 g/sq.m
			Chopped Mat:	N/A
			Polyester Stitching:	0.35 oz/sq.yd / 12 g/sq.m

* Packaging: Bag

Vectorply Corporation
3500 Lakewood Drive Phenix City, AL 36867
tel. 334-291-7704 fax. 334-291-7743

REV: 3/13/2015

HEXION
Responsible Chemistry

Technical Data Sheet

EPIKOTE™ Resin MGS LR 135 and EPIKURE™ Curing Agent MGS LH 133-138

Application

EPIKOTE™ Resin MGS™ LR135 laminating resin system approved by the German Lloyd. It contains no solvents and fillers and is available for different pot lives. The system is used for processing of glass, carbon and aramide fibres, featuring high static and dynamic loadability. This system has very good adhesive properties with wood and other materials.

The range of pot lives is between approx. 10 min. and more than 6 hours. This enables a selection of the optimum system for all processing methods. After precuring at room temperature, the manufactured components are workable and demouldable. The final properties, however, will only be obtained after postcuring at temperatures of more than 40°C. At room temperature, the fast curing agents LH 133 - 135 are processable and demouldable after 6 - 12 hours, while the very slow curing agents LH 136 - 138 have curing periods of 2 - 4 days at room temperature.

Laminates produced with this system result in high-gloss and non-tacky surfaces, even with unfavourable curing conditions, e. g. lower temperatures and/or high humidities. The mixing viscosity guarantees a fast and complete impregnation of the reinforcement fibres, however, the resin will not drain out of the fabrics on vertical surfaces.

Due to the chemical characteristics of this system we do not expect any problems concerning compatibility (e.g. blisters, tearing or changes in colour), when it is processed with gelcoats. However, comprehensive tests are indispensable.

Epoxy resins are super cooled liquids, therefore crystallisation is immanently possible. In an early stage, crystallisation is visible as a clouding, and can progress to a stage, where the resin becomes a wax-like solid. Crystallisation can be reversed by slow heating of the product to approx. 40°C - 60°C. This physical phenomenon is reversible and is no restriction to quality. In fact a high purity of material will increase a tendency for crystallisation.

Although LR135 is unlikely to crystallize at low temperatures, storage conditions of 15 - 30°C and low humidity are recommended. After dispensing material, the containers must again be closed carefully, to avoid contamination or absorption of water. All amine hardeners show a chemical reaction when exposed to air, known as „blushing". This reaction is visible as white carbamide crystals, which could make the materials unusable.

The materials have a shelf life of minimum 2 years, when stored in their originally sealed containers.

Due to selected raw materials, we expect only minor problems concerning skin irritation and allergies during processing.

The relevant industrial safety regulations for the handling of epoxy resins and hardeners and our instructions for safe processing are to be observed.

Specifications

		Laminating resin LR135
Density [1)]	[g/cm³]	1,13 – 1,18
Viscosity [1)]	[mPa⋅s]	2.300 – 3.000

Refractory index [1]		1,558 – 1,562

		Curing agent		
		LH133	LH134	LH135
Density [1]	[g/cm³]	1,04 – 1,08	1,03 – 1,09	0,99 – 1,03
Viscosity [1]	[mPa·s]	400 – 700	200 – 350	50 – 150
Refractory index [1]		1,554 – 1,562	1,561 – 1,570	1,508 – 1,513
Potlife [2]	[min]	app. 10 min.	app. 10 min.	app. 20 min.
Tg_{pot}	[°C]	80 – 90 °C unconditioned 65 – 75°C conditioned [3]		

		Curing agent			
		LH136	LH1364	LH137	LH138
Density [1]	[g/cm³]	0,96 – 1,00	0,94 – 0,98	0,94 – 0,98	0,93 – 0,96
Viscosity [1]	[mPa·s]	10 – 80	5 – 50	5 – 50	5 – 50
Refractory index [1]		1,472 – 1,480	1,460 – 1,468	1,452 – 1,462	1,450 – 1,460
Potlife [2]	[min]	app. 1 h	app. 2,5 h	app. 4 h	app. 6 h
Tg_{pot}	[°C]	80 – 90 °C unconditioned 65 – 75°C conditioned [3]			

Measuring conditions:

1) measured at 25°C

2) 100g sample in water bath at 30°C

3) conditioned at 40 °C / 90% r.H.

Characteristics

Approval	DNV-GL SE (Germanischer Lloyd)
Application	Rotor blades for wind turbines, boatbuilding, as laminating and adhesive resins (wood-epoxy construction), sporting goods, moulds, tools and other devices
Operational temperature	-60 °C up to +50 °C without heat treatment -60 °C up to +80 °C after heat treatment
Processing	Generally at temperatures between 15°C and 50°C, all common processing methods
Features	Pot life from approx. 10 min to 6hrs Limited irritation potential
Special modifications	LR 135 LV: low viscosity LR 135 T: thixotropic
Storage	Shelf life of 24 months in originally sealed containers

Temperature Development

Measuring conditions: 100g sample in water bath at 30°C

Optimum processing temperature is in the range of 20°C to 35°C. Higher temperatures are possible, but will shorten pot life. A temperature increase of 10°C will halve the pot life. Water (e.g. high humidity or contained in additional fillers) causes an acceleration of the resin/ curing agent reaction. Different temperatures during processing are not known to have significant impact on the mechanical properties of the cured product.

Do not mix large quantities – particularly of highly reactive systems – at elevated processing temperatures. As the heat dissipation in the mixing container is very slow, the contents will be heated up by the reaction heat (exothermic resin-curing agent reaction) rapidly. This can result in temperatures of more than 200°C in the mixing container, which may cause smoke-intensive burning of the resin mass.

TG DEVELOPMENT

Measuring conditions for all Tg measurements: DSC, DIN EN ISO 11357

MIXING RATIOS

	LR135 : All curing agents
Parts by weight	100 : 35 ± 2
Parts by volume	100 : 41 ± 2

The mixing ratio stated must be observed very carefully. Adding more or less curing agent will not result in a faster or slower reaction – but in incomplete curing which cannot be corrected in any way. Resin and curing agent must be mixed very thoroughly. Mix until no clouding is visible in the mixing container. Pay special attention to the walls and bottom of the mixing container.

All curing agents have blue colour to distinguish between resin and curing agents, and for easier identification of a correct mixing process. Although unlikely, deviations in colour are possible (e.g. due to UV radiation after longer exposure to sun light), but however have no effect on the processing and final properties of the material

GEL TIME

	Curing agent		
	LH133	LH134	LH135
20 – 25°C	app. 1 – 2 hours	app. 2 – 3 hours	app. 4 – 5 hours
40 – 45°C	app. 30 min.	app. 40 min.	app. 50 min.

	Curing agent		
	LH136	LH137	LH138
20 – 25°C	app. 6 – 7 hours	app. 10 – 12 hours	app. 15 – 20 hours
40 – 45°C	app. 1 – 2 hours	app. 3 – 4 hours	app. 6 – 7 hours

Measuring conditions: Film thickness 1 mm at different temperatures

MECHANICAL DATA OF NEAT RESIN

Mechanical data		
Density DIN EN ISO 1183-1	[g/cm³]	1,10 – 1,20
Flexural strength DIN EN ISO 178	[MPa]	100 – 120
Modulus of elasticity DIN EN ISO 178	[GPa]	2,8 – 3,2
Tensile strength DIN EN ISO 527-2	[MPa]	65 – 75
Compressive strength DIN EN ISO 604	[MPa]	80 – 100
Elongation at break DIN EN ISO 527-2	[%]	7,0 – 10,0
Impact strength ISO 179-1	[kJ/m²]	60 – 80
Water absorption at 23°C DIN EN ISO 175	24h [%] 7d [%]	0,10 – 0,50 0,20 – 0,80
Curing: 8h at 70°C		

Advice:

Mechanical data are typical for the combination of laminating resin LR135 with curing agent LH135. Data can differ in other applications.

VISCOSITY OF MIXTURE

301

NEWPORT HIGH PERFORMANCE MATERIALS

250-300°F (121-149°C) Cure Epoxy Resin System

Typical applications
Sporting goods
Marine
Medical
Industrial manufacturing

Out life
30 days at 70°F (21°C)

Shelf life
6 months at 40°F (4°C)
12 months at 0°F (-18°C)

Description
301 is a 250°F (121°C) to 300°F (149°C) cure, toughened, controlled flow epoxy resin system that has been the industry standard for over 25 years. Versatile processing, excellent mechanical properties, and long out time make 301 suitable for a variety of applications, including large scale structures where layup requirements can take days or weeks.

Benefits/features
- Excellent mechanical properties
- Moderate tack
- Good toughness
- Controlled flow
- Flexible processing

Variants
- 301-1: Increased tack
- 301-D: Decreased tack
- 301-5: Snap cure (3 min. at 300°F, 10 min. at 275°F)
- 301-T: Clearer aesthetics

Application
301 can be supplied with most commercially available fibers (carbon, quartz, aramid, S-glass, E-glass, etc.) in both woven form (designated as NB) as well as unidirectional tape (designated as NCT).

Woven fabrics are available in standard commercial widths up to 60 inches (1.5 m). Unitape widths up to 39 inches (1 m) are available in standard fiber weights ranging from 70 – 300 gsm (0.014 – 0.060 psf).

Recommended processing conditions
301 is typically cured at 250°F - 300°F (121°C - 149°C) depending on part size and complexity. With extended cure times, larger scale structures can be cured as low as 195°F-220°F (90°C-104°C). Low, medium and high pressure molding techniques may be used for curing. Recommended cure cycle is 50 psi (345 kPa); 3°F (1.7°C)/min ramp to 275°F (135°C); hold for 60 minutes, cool to <140°F (60°C).

MITSUBISHI CHEMICAL CARBON FIBER AND COMPOSITES

Technical Data Sheet

Uni E-glass, 300gsm, 36%RC, autoclave cured, 60psi, 90 minutes at 275°F, normalized to 60%FV

Property	Test method	RT
0° Tensile strength, ksi (MPa)	ASTM D3039	179 (1230)
0° Tensile modulus, Msi (GPa)		7.2 (49.6)
0° Compressive strength, ksi (MPa)	ASTM D695mod	234 (1610)
0° Compressive modulus, Msi (GPa)		7.4 (51.0)
0° Flexural strength, ksi (MPa)	ASTM D790	196 (1350)
0° Flexural modulus, Msi (GPa)		7.1 (49.0)
Short beam shear strength, ksi (MPa)	ASTM D2344	13.3 (92)

Viscosity profile

TA - AR2000 parallel plate rheometer

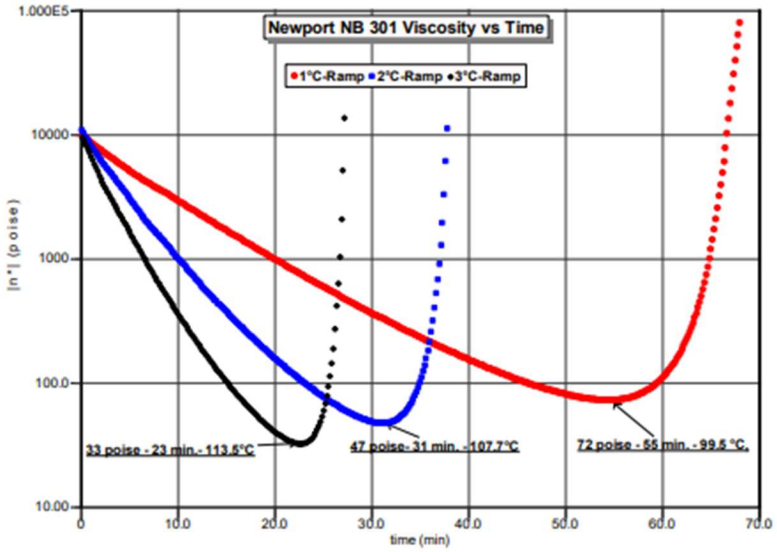

Gel curve

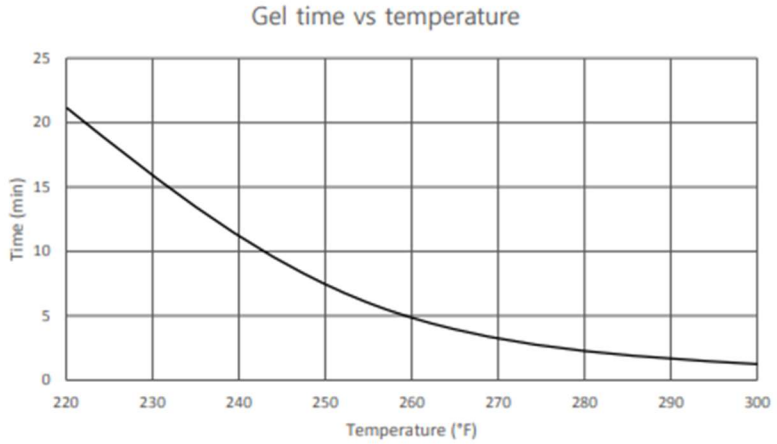

Innegra™S is a trademark of Innegra Technologies, LLC

CORPORATE OFFICE
Composite Materials Div.
1822 Reynolds Ave.
Irvine, CA 92614

Tel: (949) 253-5680
Fax: (949) 253-5692
http://www.mrcfac.com
compositesales@mrcfac.com

THE KAITEKI COMPANY
Mitsubishi Chemical Holdings Group

MITSUBISHI CHEMICAL CARBON FIBER AND COMPOSITES

Technical Data Sheet

PL-301 - 052016

APPENDIX B

APPENDIX B: ACOUSTIC EMISSION SYSTEM INFORMATION

MISTRAS
A World of NDT Solutions | Products & Systems Division

Product Bulletin

USB Acoustic Emission (AE) Node

Easy Laptop & PC Connection and Low Cost Acoustic Emission System

USB AE Node

The USB AE Node is a single channel Acoustic Emission (AE) Digital Signal Processor with full AE hit and time based features, including waveforms. Through the USB Connector, the AE Node is easily interfaced to a Notebook or PC running Windows XP™ or Vista™ and Physical Acoustics Corporation (PAC) well known AEwin™ or AEwin Lite™. Up to 4 AE Nodes can be controlled by one Notebook or PC.

The AE Node can accept single ended or differential sensors amplified by an internal low noise preamplifier. Additionally, PK Series low power integral preamp sensors can be used for long distance connections.

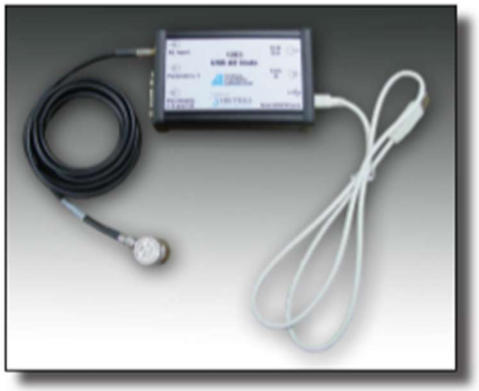

"AEwin for USB" AE NODE Software

Extracted Hit Features:
Time of 1st Threshold Crossing
Time to Peak, Peak Amplitude, Envelope Strength,
Duration Rise Time, Counts, True Energy
RMS, ASL
Parametrics (1-2)

Time Based Features
ASL, RMS, Parametrics (1-4)
Peak Amplitude, Crest Factor, Energy rate

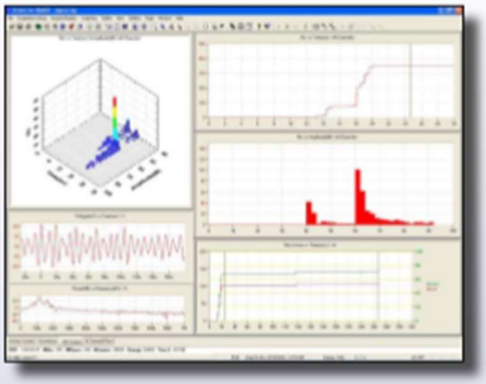

Features & Benefits

- Powered and operated through USB Port
- Rugged surface mount (SMT) construction
- High performance AE at a low cost
- 1kHz to 1MHz bandwidth
- Selectable analog filters and programmable digital filter
- Waveform and Location Options

Specifications

AE Input:	1 Channel per USB node (4 nodes per system)
Frequency Response:	1.0 kHz to 1.0 MHz
AE Digitizing:	16 bit, 20 MSPS ADCs
Parametric Inputs:	CH 1, +/- 10V, 16 bits CH 2-4, 0-10V, 16 bits
OS:	Windows XP or Vista
Case Size:	L5.25" x W3.25" x H1.25" (133 x 83 x 32mm)
Weight:	0.5 lbs. (0.23kg)
Power Requirements:	USB Powered (5V) < 100 mA when running
Power Consumption:	< 0.5 watt

For additional information, please contact:
Physical Acoustics at 609-716-4000 or
email: sales.systems@mistrasgroup.com

195 Clarksville Road, Princeton Junction, NJ 08550 USA
Phone: (609) 716-4000 • Fax: (609) 716-0706
Email: sales.systems@mistrasgroup.com • www.mistrasgroup.com

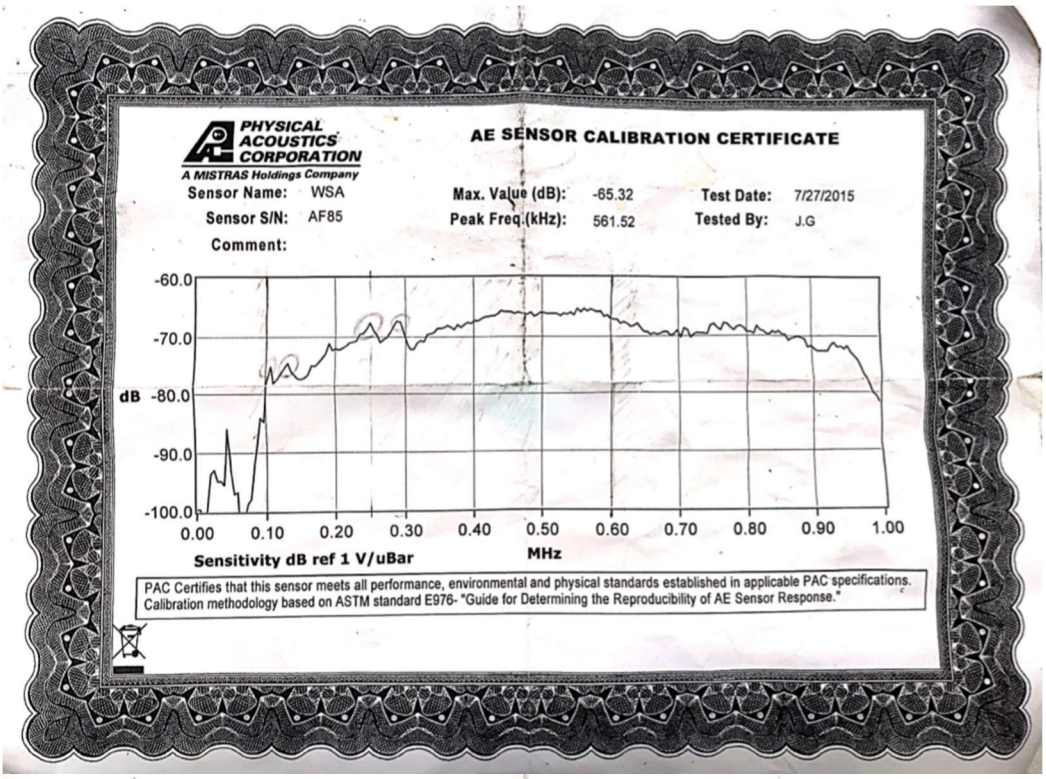

PHYSICAL ACOUSTICS CORPORATION
A MISTRAS Holdings Company

AE SENSOR CALIBRATION CERTIFICATE

Sensor Name: WSA
Sensor S/N: AF85
Comment:

Max. Value (dB): -65.32
Peak Freq.(kHz): 561.52
Test Date: 7/27/2015
Tested By: J.G

Sensitivity dB ref 1 V/uBar

PAC Certifies that this sensor meets all performance, environmental and physical standards established in applicable PAC specifications. Calibration methodology based on ASTM standard E976- "Guide for Determining the Reproducibility of AE Sensor Response."

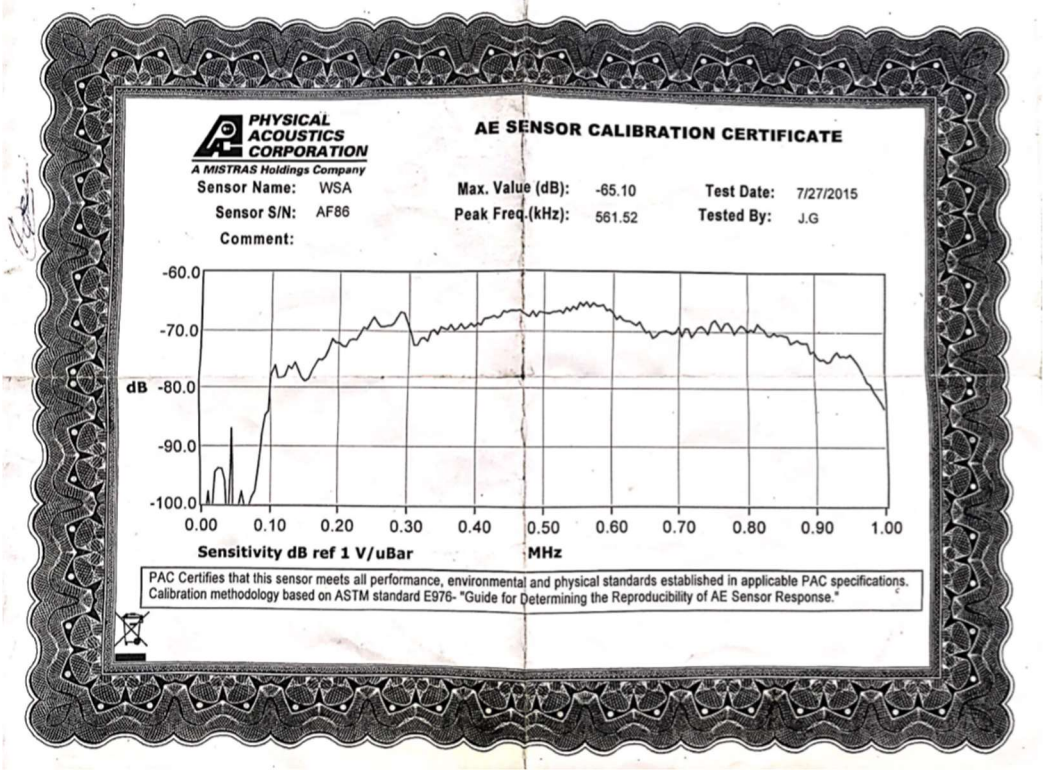

PHYSICAL ACOUSTICS CORPORATION
A MISTRAS Holdings Company

AE SENSOR CALIBRATION CERTIFICATE

Sensor Name: WSA
Sensor S/N: AF86
Comment:

Max. Value (dB): -65.10
Peak Freq.(kHz): 561.52
Test Date: 7/27/2015
Tested By: J.G

Sensitivity dB ref 1 V/uBar

PAC Certifies that this sensor meets all performance, environmental and physical standards established in applicable PAC specifications. Calibration methodology based on ASTM standard E976- "Guide for Determining the Reproducibility of AE Sensor Response."

PHYSICAL ACOUSTICS CORPORATION
A MISTRAS Holdings Company

AE SENSOR CHARACTERIZATION CERTIFICATE

Sensor Name: WSA
Sensor S/N: AJ03
Comment:

Max. Value (dB): -66.95
Peak Freq.(kHz): 551.76
Test Date: 9/20/2018
Tested By: M.E.

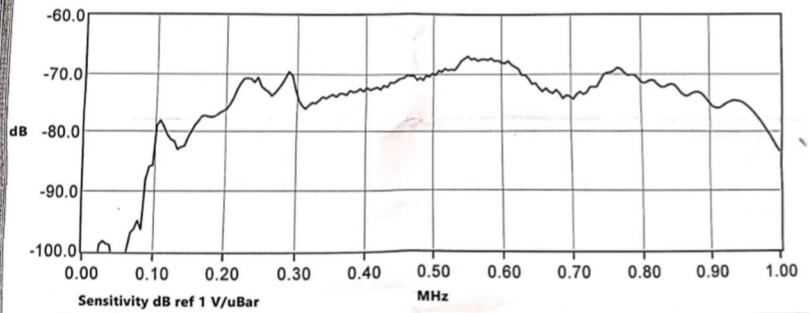

Sensitivity dB ref 1 V/uBar

PAC Certifies that this sensor meets all performance, environmental and physical standards established in applicable PAC specifications. Characterization methodology based on ASTM standard E976 sec. 4.3.1.2.

A World of NDT Solutions — MISTRAS GROUP INC.

PHYSICAL ACOUSTICS CORPORATION
A MISTRAS Holdings Company

AE SENSOR CHARACTERIZATION CERTIFICATE

Sensor Name: WSA
Sensor S/N: AJ04
Comment:

Max. Value (dB): -66.09
Peak Freq.(kHz): 561.52
Test Date: 9/20/2018
Tested By: M.E.

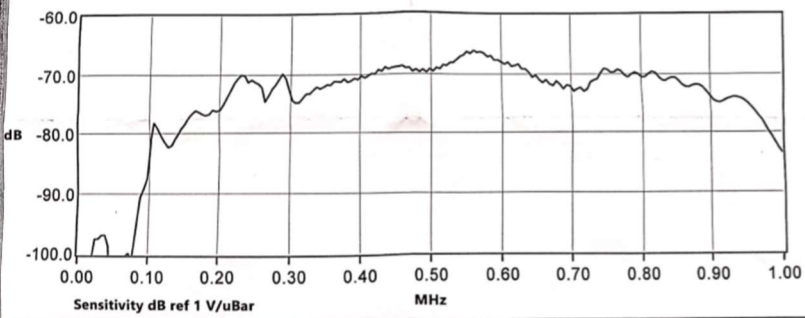

Sensitivity dB ref 1 V/uBar

PAC Certifies that this sensor meets all performance, environmental and physical standards established in applicable PAC specifications. Characterization methodology based on ASTM standard E976 sec. 4.3.1.2.

A World of NDT Solutions — MISTRAS GROUP INC.

PHYSICAL ACOUSTICS CORPORATION
A MISTRAS Holdings Company

AE SENSOR CHARACTERIZATION CERTIFICATE

Sensor Name: WD
Sensor S/N: FY18
Comment: 1 METER CABLE

Max. Value (dB): -64.37
Peak Freq.(kHz): 541.99

Test Date: 12/13/2016
Tested By: N.M.

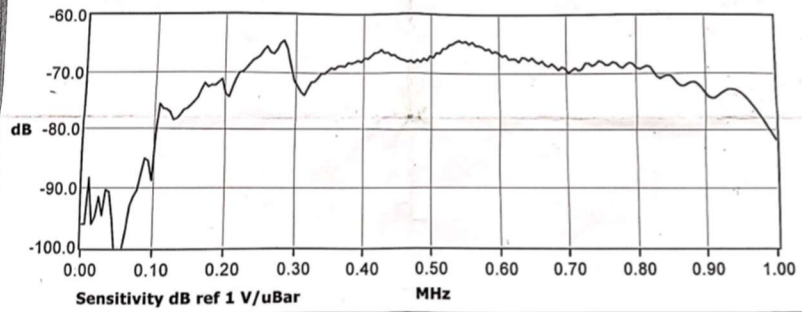

PAC Certifies that this sensor meets all performance, environmental and physical standards established in applicable PAC specifications. Characterization methodology based on ASTM standard E976 sec. 4.3.1.2.

A World of NDT Solutions — MISTRAS GROUP INC.

PHYSICAL ACOUSTICS CORPORATION
A MISTRAS Holdings Company

AE SENSOR CHARACTERIZATION CERTIFICATE

Sensor Name: WD
Sensor S/N: FY19
Comment: 1 METER CABLE

Max. Value (dB): -64.13
Peak Freq.(kHz): 551.76

Test Date: 12/13/2016
Tested By: N.M.

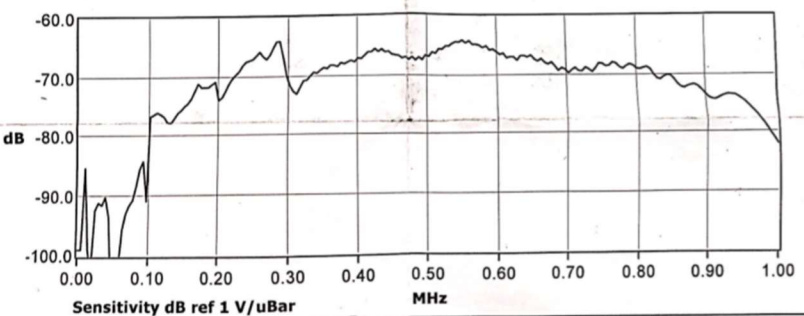

PAC Certifies that this sensor meets all performance, environmental and physical standards established in applicable PAC specifications. Characterization methodology based on ASTM standard E976 sec. 4.3.1.2.

A World of NDT Solutions — MISTRAS GROUP INC.

APPENDIX C

APPENDIX C: SUPPLEMENTAL ACOUSTIC EMISSION PLOTS

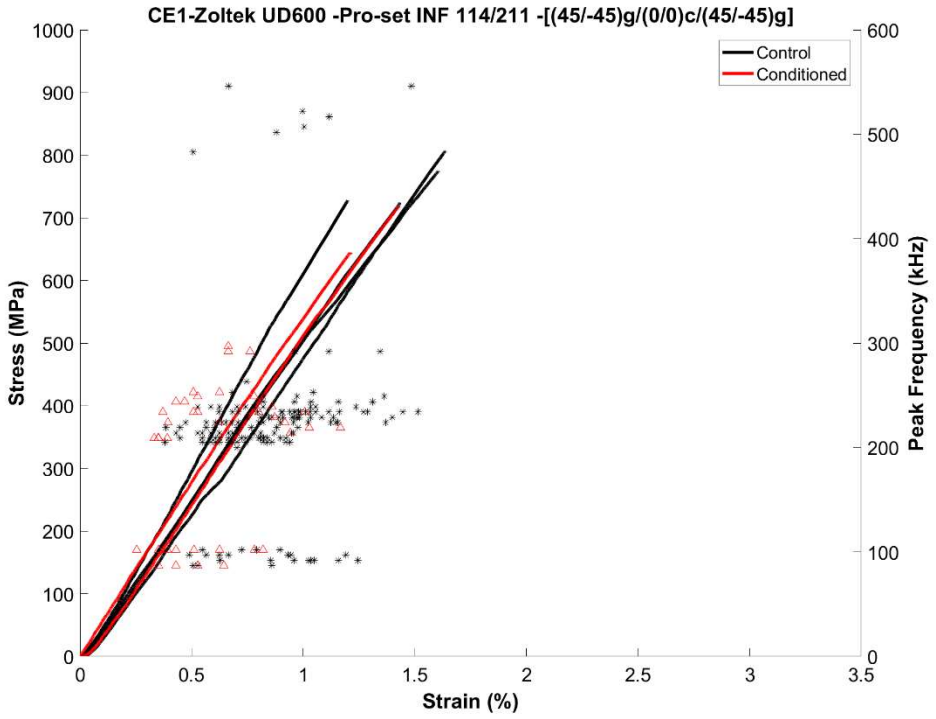
CE1-Zoltek UD600 -Pro-set INF 114/211 -[(45/-45)g/(0/0)c/(45/-45)g]
Control
Conditioned
Stress (MPa)
Peak Frequency (kHz)
Strain (%)
0
100
200
300
400
500
600
700
800
900
1000
0.5
1
1.5
2
2.5
3
3.5

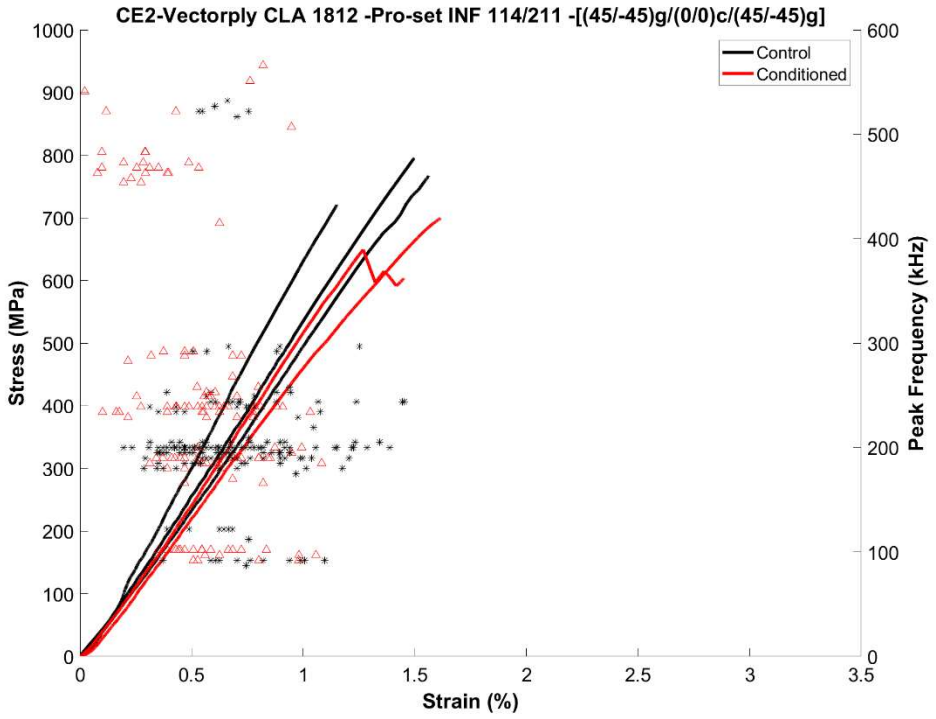
CE2-Vectorply CLA 1812 -Pro-set INF 114/211 -[(45/-45)g/(0/0)c/(45/-45)g]
Control
Conditioned
Stress (MPa)
Peak Frequency (kHz)
Strain (%)
0
100
200
300
400
500
600
700
800
900
1000
0.5
1
1.5
2
2.5
3
3.5

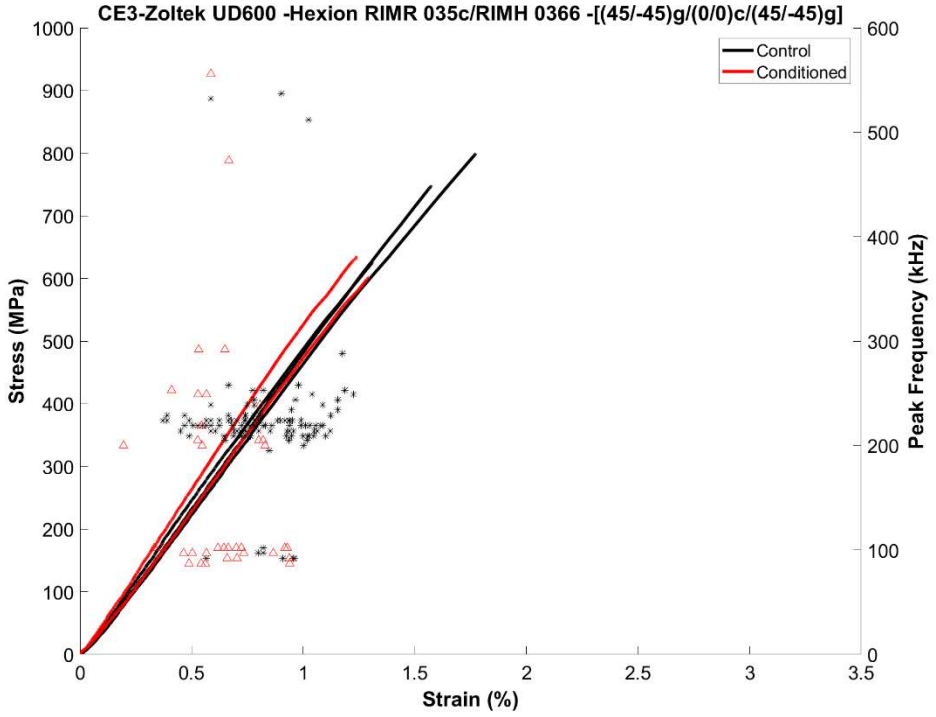
CE3-Zoltek UD600 -Hexion RIMR 035c/RIMH 0366 -[(45/-45)g/(0/0)c/(45/-45)g]
Control
Conditioned
Stress (MPa)
Peak Frequency (kHz)
Strain (%)
0
100
200
300
400
500
600
700
800
900
1000
0.5
1
1.5
2
2.5
3
3.5

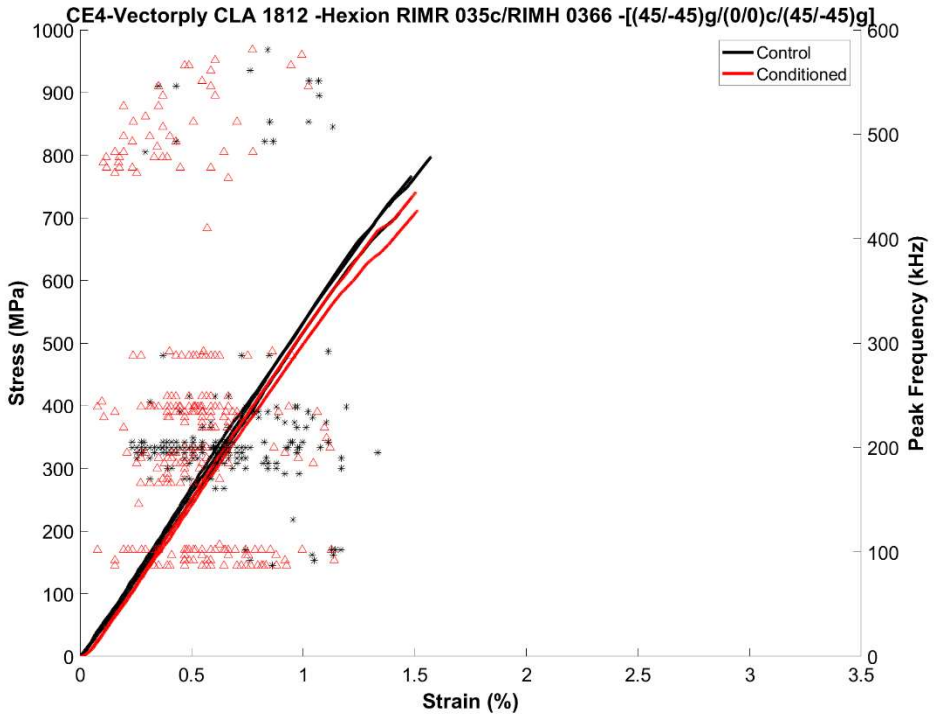
CE4-Vectorply CLA 1812 -Hexion RIMR 035c/RIMH 0366 -[(45/-45)g/(0/0)c/(45/-45)g]
Control
Conditioned
Stress (MPa)
Peak Frequency (kHz)
Strain (%)
0
100
200
300
400
500
600
700
800
900
1000
0.5
1
1.5
2
2.5
3
3.5

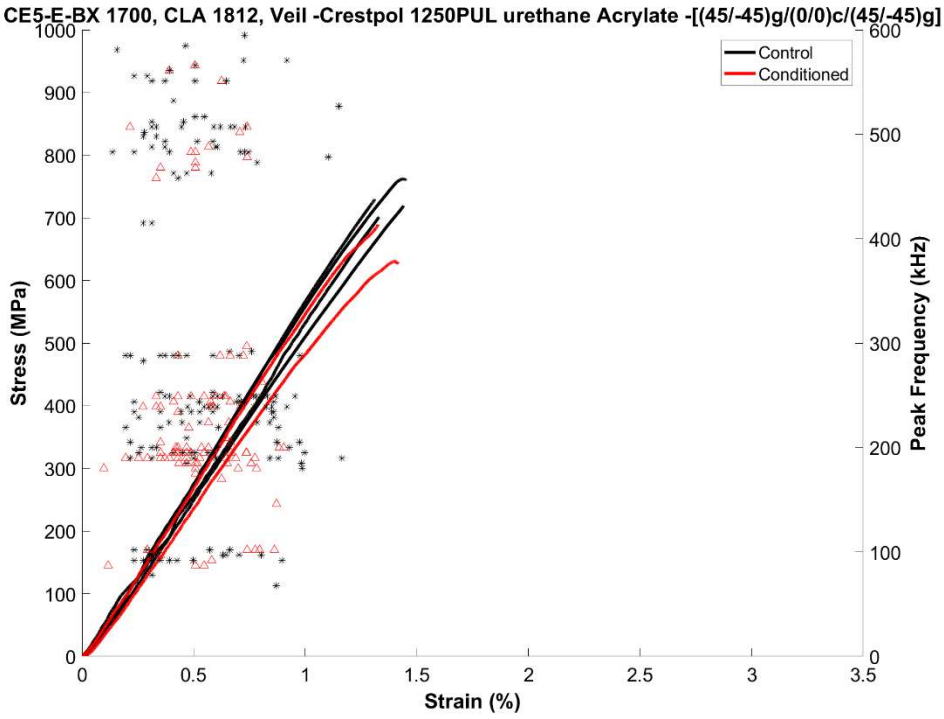
CE5-E-BX 1700, CLA 1812, Veil -Crestpol 1250PUL urethane Acrylate -[(45/-45)g/(0/0)c/(45/-45)g]
Control
Conditioned
Stress (MPa)
Peak Frequency (kHz)
Strain (%)
0
100
200
300
400
500
600
700
800
900
1000
0.5
1
1.5
2
2.5
3
3.5

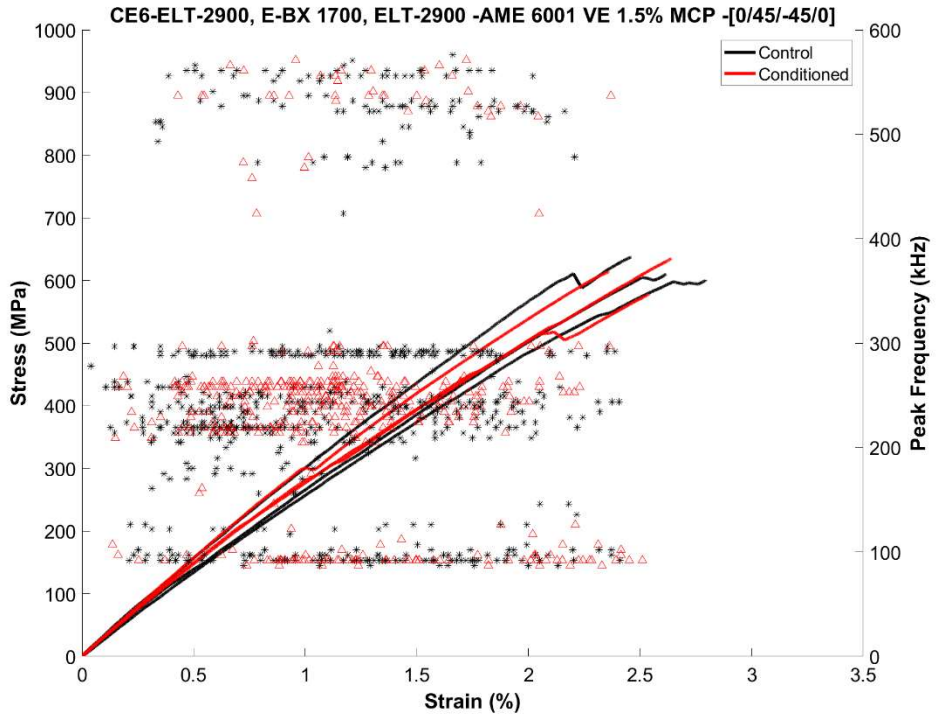
CE6-ELT-2900, E-BX 1700, ELT-2900 -AME 6001 VE 1.5% MCP -[0/45/-45/0]
Control
Conditioned
Stress (MPa)
Peak Frequency (kHz)
Strain (%)
0
100
200
300
400
500
600
700
800
900
1000
0.5
1
1.5
2
2.5
3
3.5

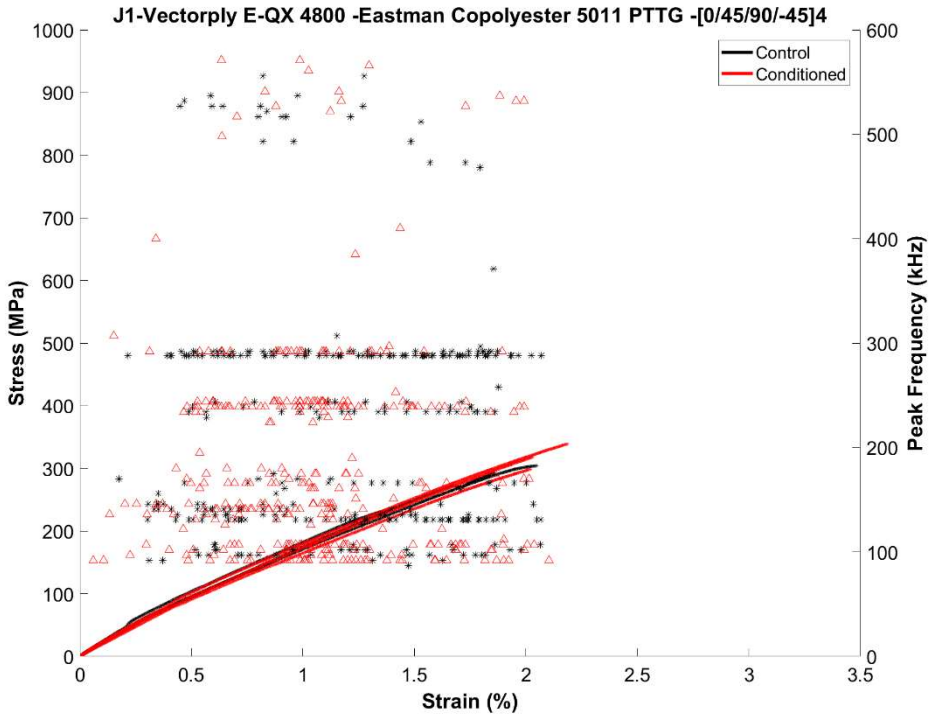
J1-Vectorply E-QX 4800 -Eastman Copolyester 5011 PTTG -[0/45/90/-45]4
Control
Conditioned
Stress (MPa)
Peak Frequency (kHz)
Strain (%)
0
100
200
300
400
500
600
700
800
900
1000
0.5
1
1.5
2
2.5
3
3.5

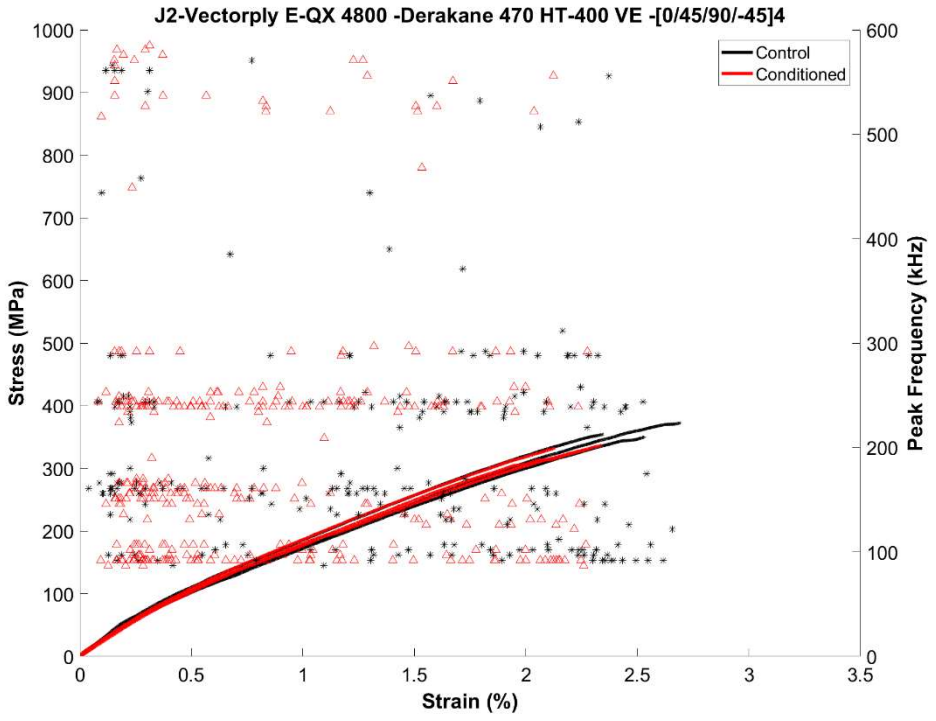
J2-Vectorply E-QX 4800 -Derakane 470 HT-400 VE -[0/45/90/-45]4
Control
Conditioned
Stress (MPa)
Peak Frequency (kHz)
Strain (%)
0
100
200
300
400
500
600
700
800
900
1000
0.5
1
1.5
2
2.5
3
3.5

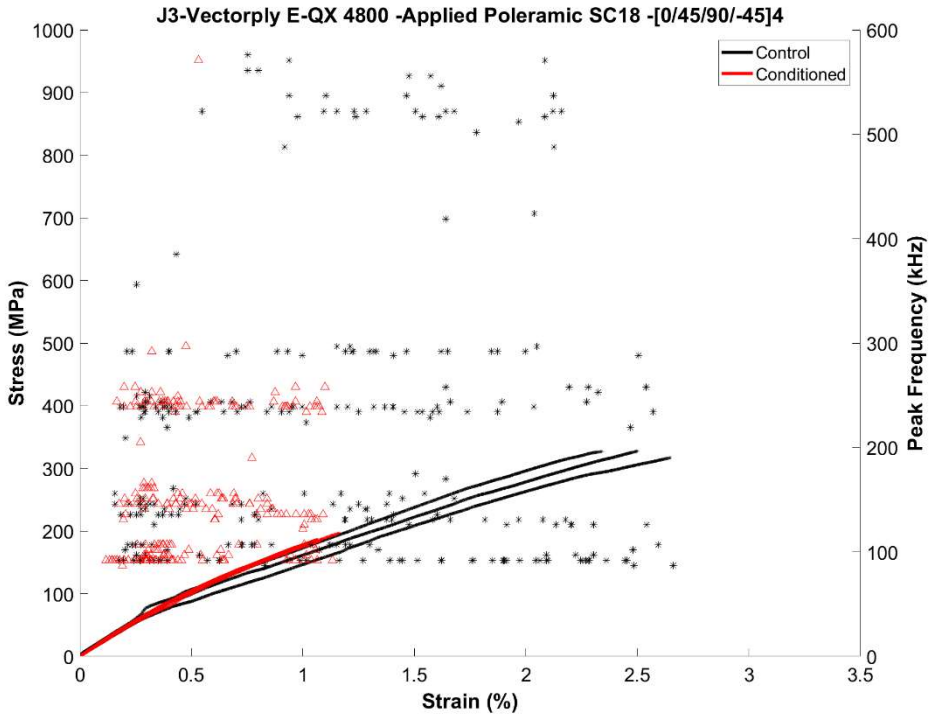
J3-Vectorply E-QX 4800 -Applied Poleramic SC18 -[0/45/90/-45]4
Control
Conditioned
Stress (MPa)
Peak Frequency (kHz)
Strain (%)
0
100
200
300
400
500
600
700
800
900
1000
0.5
1
1.5
2
2.5
3
3.5

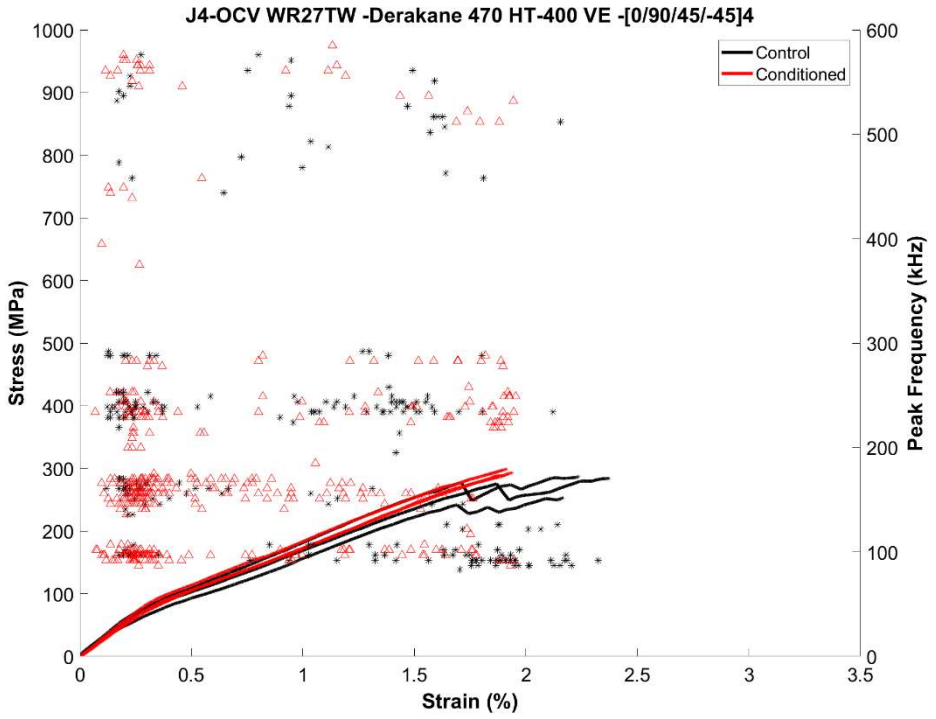
J4-OCV WR27TW -Derakane 470 HT-400 VE -[0/90/45/-45]4
Control
Conditioned
Stress (MPa)
Peak Frequency (kHz)
Strain (%)
0
100
200
300
400
500
600
700
800
900
1000
0.5
1
1.5
2
2.5
3
3.5

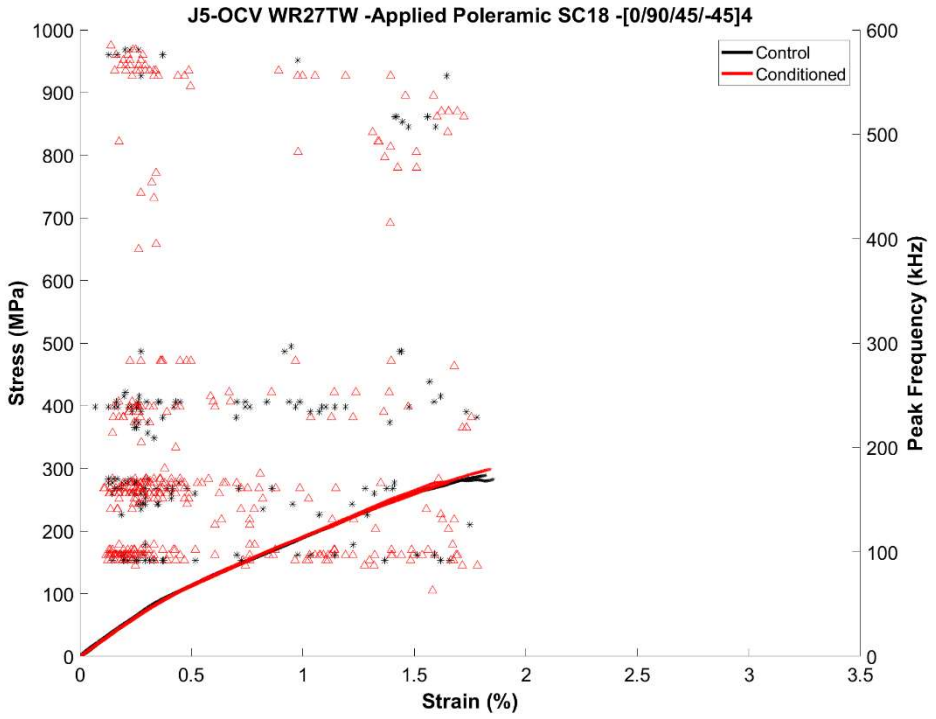
J5-OCV WR27TW -Applied Poleramic SC18 -[0/90/45/-45]4
Control
Conditioned
Stress (MPa)
Peak Frequency (kHz)
Strain (%)
0
100
200
300
400
500
600
700
800
900
1000
0.5
1
1.5
2
2.5
3
3.5

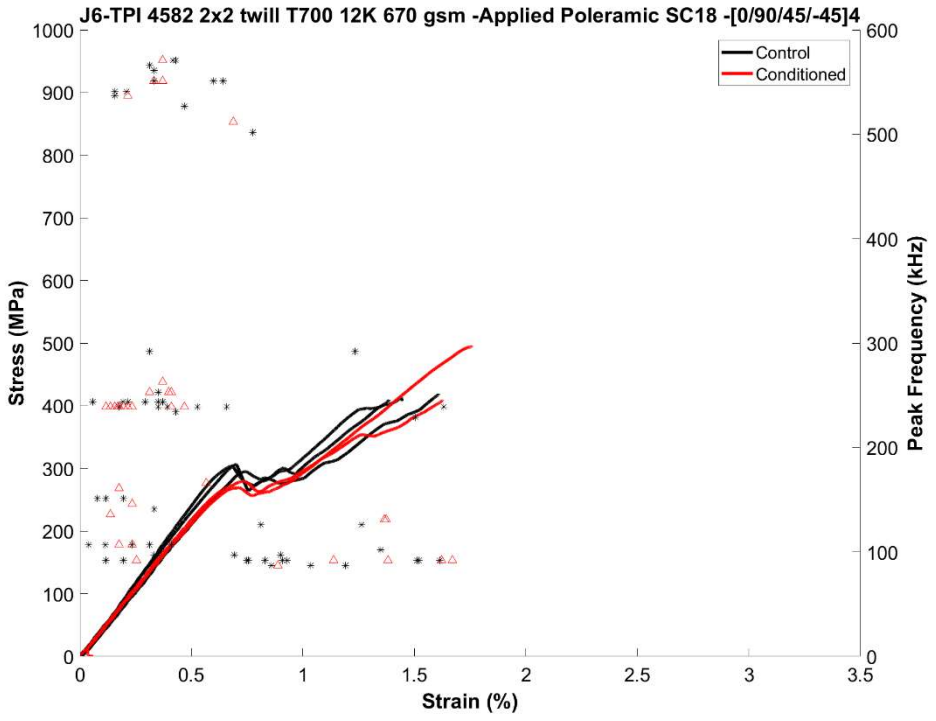
J6-TPI 4582 2x2 twill T700 12K 670 gsm -Applied Poleramic SC18 -[0/90/45/-45]4
Control
Conditioned
Stress (MPa)
Peak Frequency (kHz)
Strain (%)
0
100
200
300
400
500
600
700
800
900
1000
0.5
1
1.5
2
2.5
3
3.5

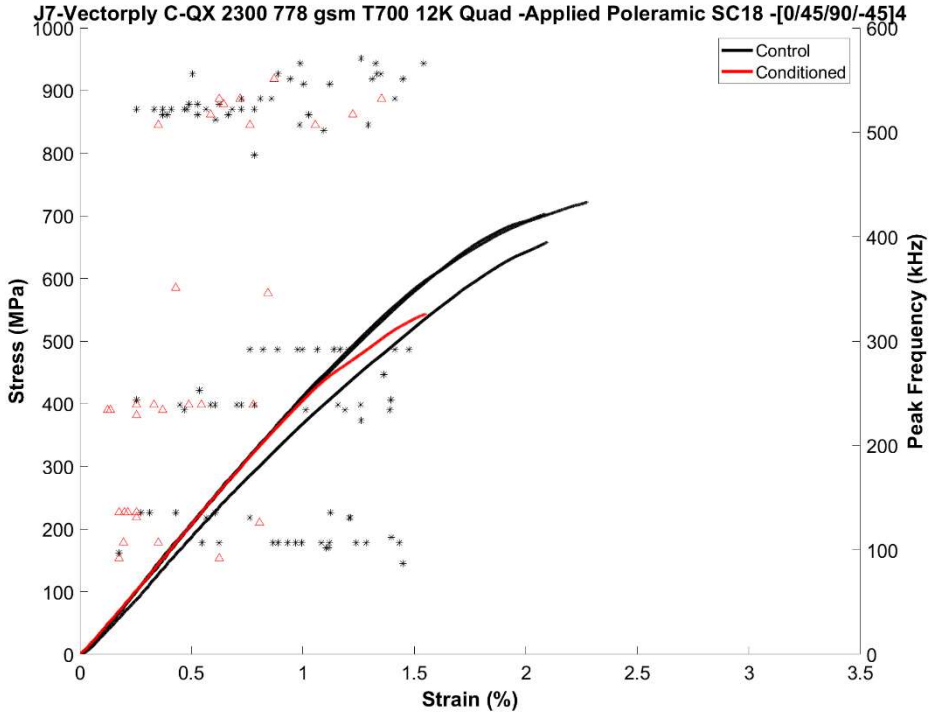
J7-Vectorply C-QX 2300 778 gsm T700 12K Quad -Applied Poleramic SC18 -[0/45/90/-45]4
Control
Conditioned
Stress (MPa)
Peak Frequency (kHz)
Strain (%)
0
100
200
300
400
500
600
700
800
900
1000
0.5
1
1.5
2
2.5
3
3.5

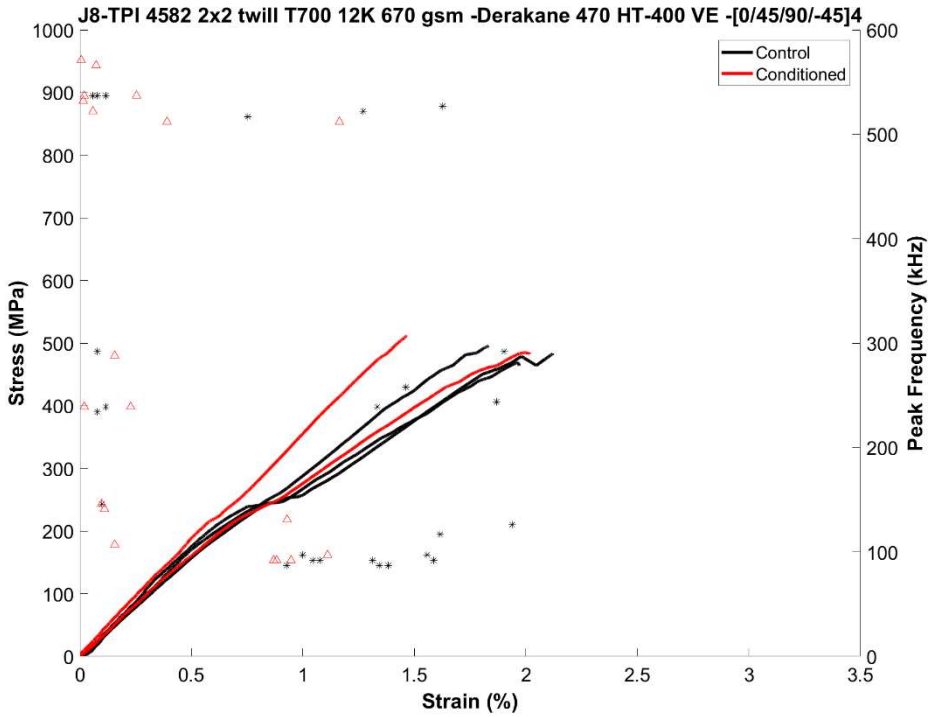
J8-TPI 4582 2x2 twill T700 12K 670 gsm -Derakane 470 HT-400 VE -[0/45/90/-45]4
Control
Conditioned
Stress (MPa)
Peak Frequency (kHz)
Strain (%)
0
100
200
300
400
500
600
700
800
900
1000
0.5
1
1.5
2
2.5
3
3.5

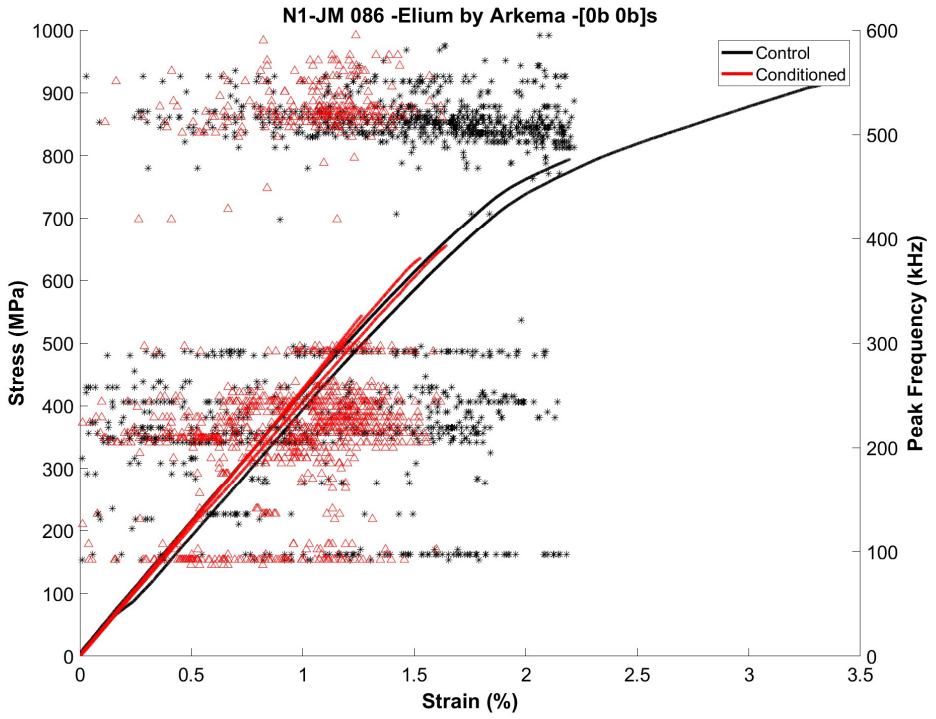
N1-JM 086 -Elium by Arkema -[0b 0b]s
Control
Conditioned
Stress (MPa)
Peak Frequency (kHz)
Strain (%)
0
100
200
300
400
500
600
700
800
900
1000
0.5
1
1.5
2
2.5
3
3.5

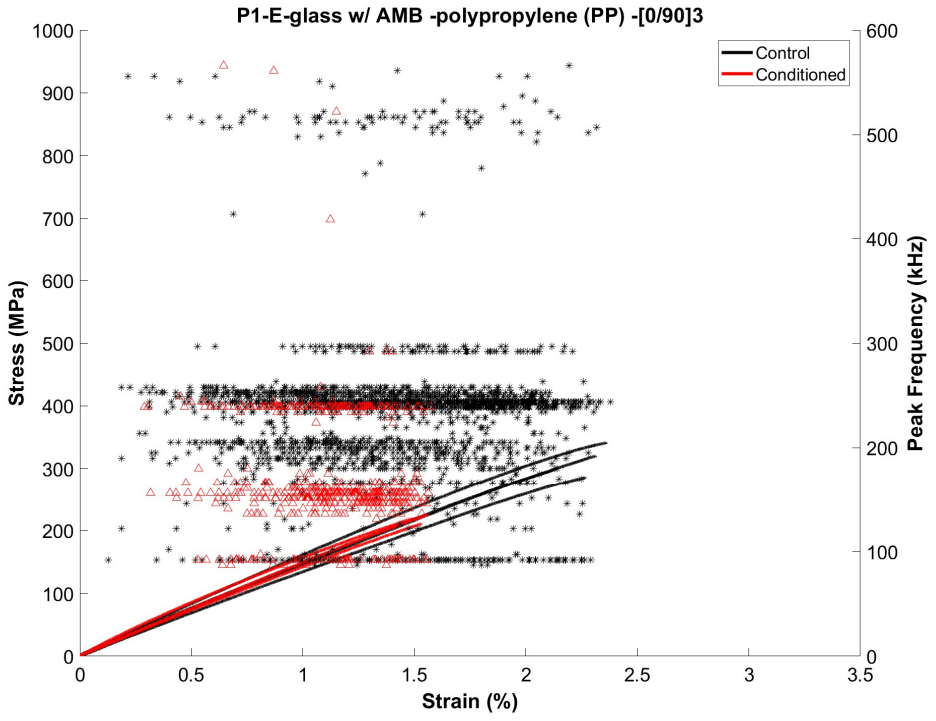
P1-E-glass w/ AMB -polypropylene (PP) -[0/90]3
Control
Conditioned
Stress (MPa)
Peak Frequency (kHz)
Strain (%)
0
100
200
300
400
500
600
700
800
900
1000
0.5
1
1.5
2
2.5
3
3.5

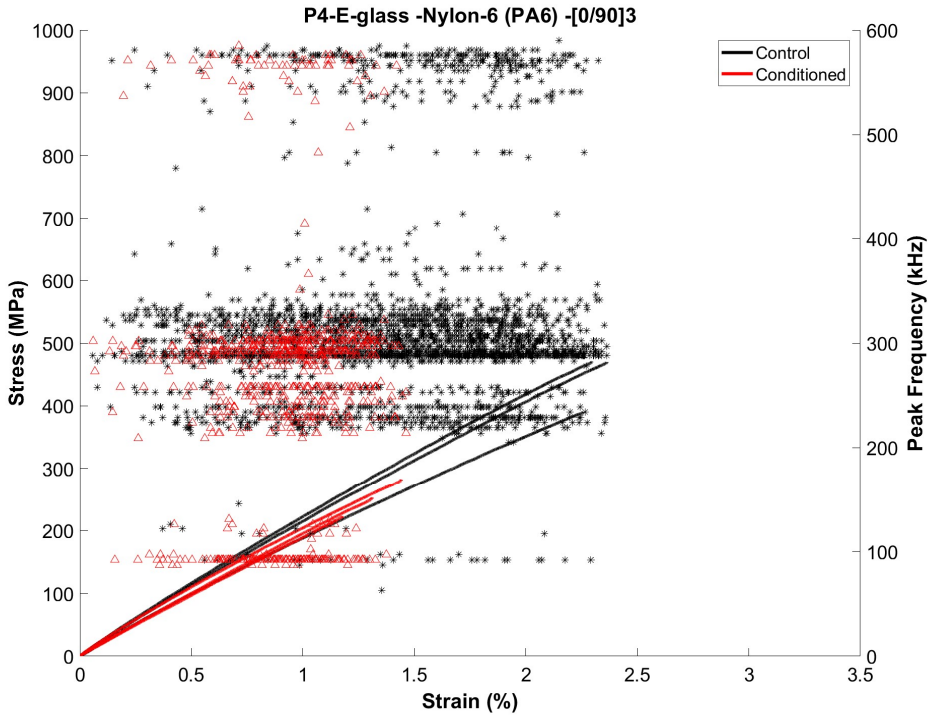
P4-E-glass -Nylon-6 (PA6) -[0/90]3
Control
Conditioned
Stress (MPa)
Peak Frequency (kHz)
Strain (%)
0
100
200
300
400
500
600
700
800
900
1000
0.5
1
1.5
2
2.5
3
3.5

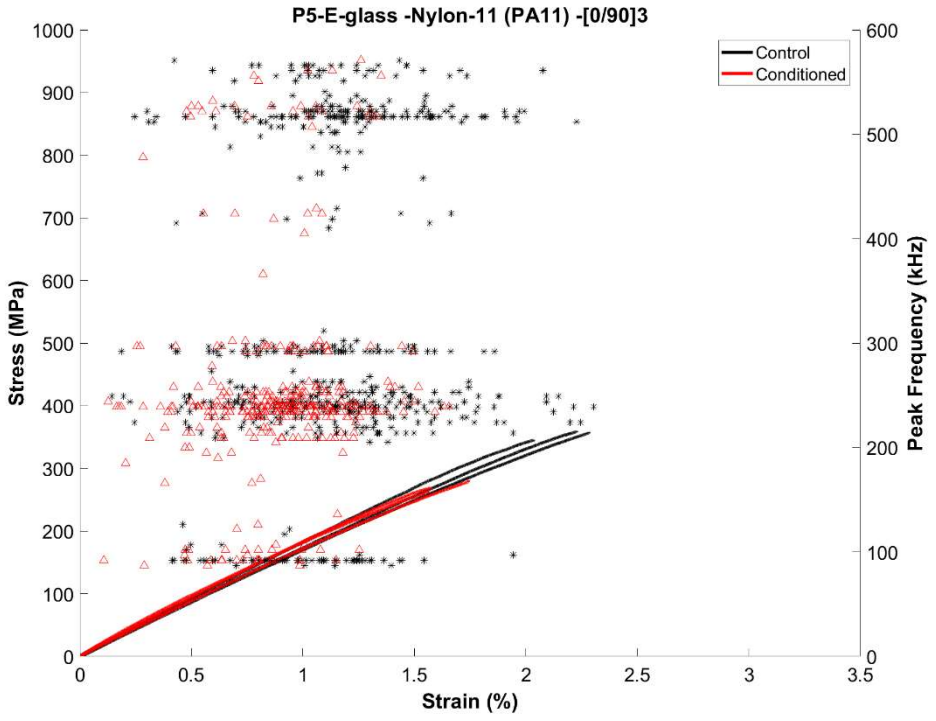
P5-E-glass -Nylon-11 (PA11) -[0/90]3
Control
Conditioned
Stress (MPa)
Peak Frequency (kHz)
Strain (%)
0
100
200
300
400
500
600
700
800
900
1000
0.5
1
1.5
2
2.5
3
3.5

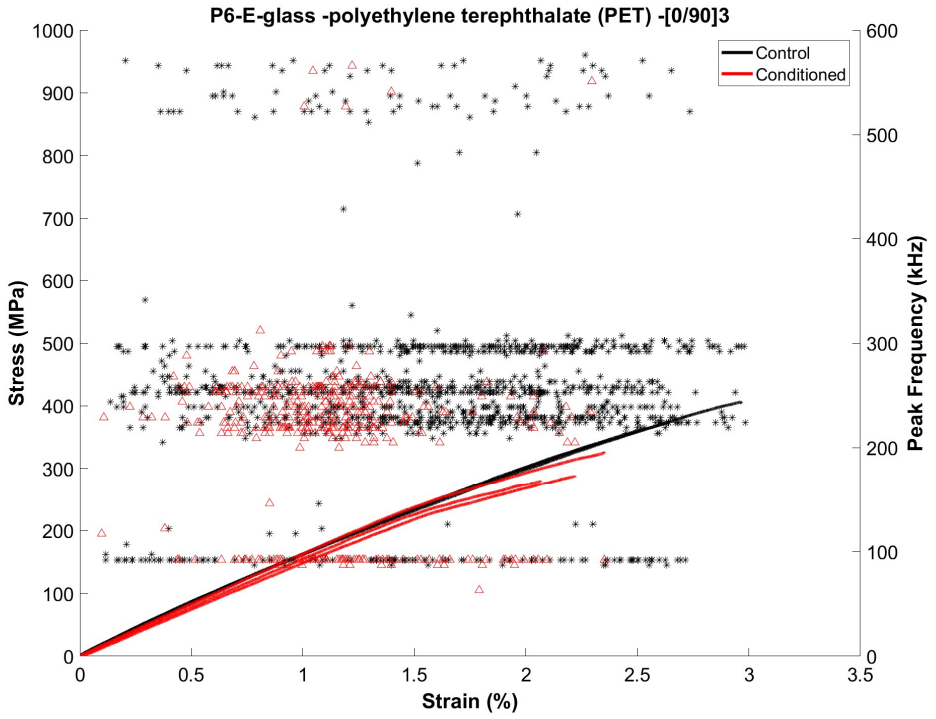
P6-E-glass -polyethylene terephthalate (PET) -[0/90]3
Control
Conditioned
Stress (MPa)
Peak Frequency (kHz)
Strain (%)
0
100
200
300
400
500
600
700
800
900
1000
0.5
1
1.5
2
2.5
3
3.5

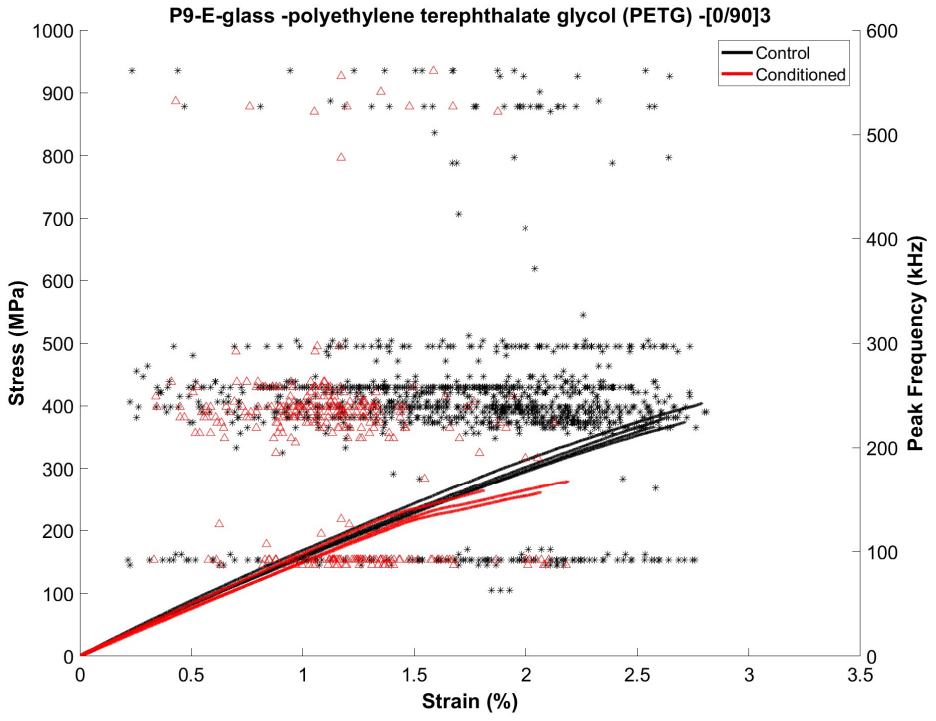
P9-E-glass -polyethylene terephthalate glycol (PETG) -[0/90]3
Control
Conditioned
Stress (MPa)
Peak Frequency (kHz)
Strain (%)
0
100
200
300
400
500
600
700
800
900
1000
0.5
1
1.5
2
2.5
3
3.5

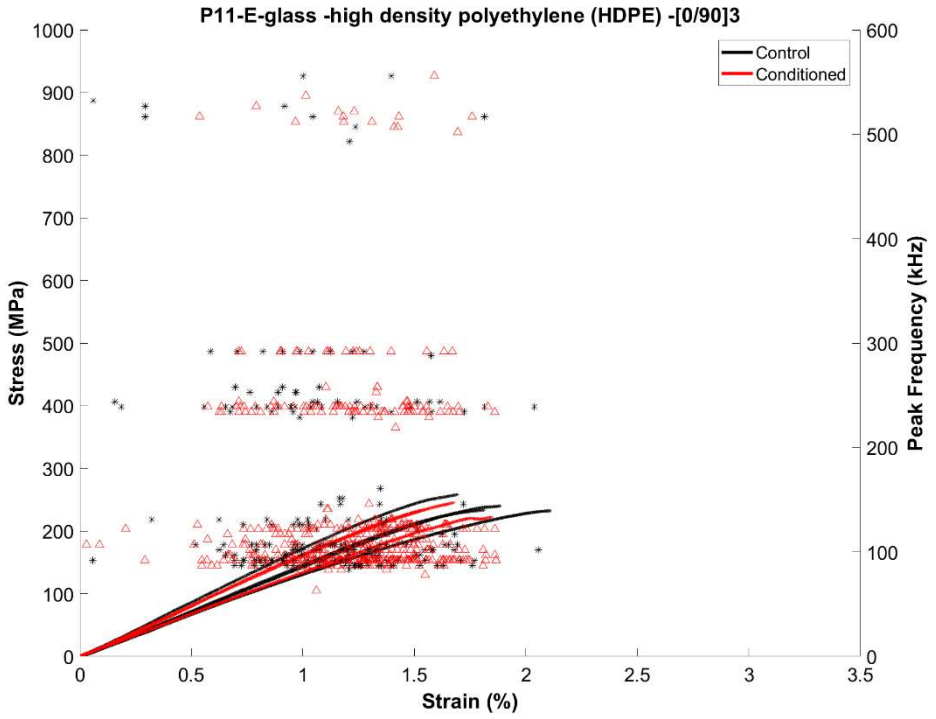
P11-E-glass -high density polyethylene (HDPE) -[0/90]3
Control
Conditioned
Stress (MPa)
Peak Frequency (kHz)
Strain (%)
0
100
200
300
400
500
600
700
800
900
1000
0.5
1
1.5
2
2.5
3
3.5

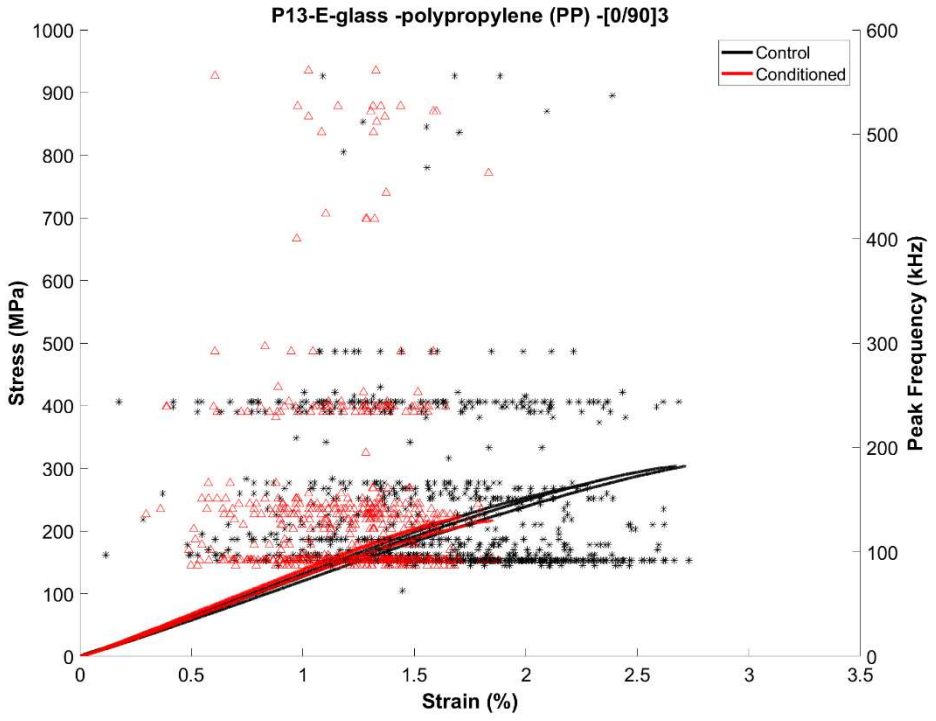
P13-E-glass -polypropylene (PP) -[0/90]3
Control
Conditioned
Stress (MPa)
Peak Frequency (kHz)
Strain (%)
0
100
200
300
400
500
600
700
800
900
1000
0.5
1
1.5
2
2.5
3
3.5

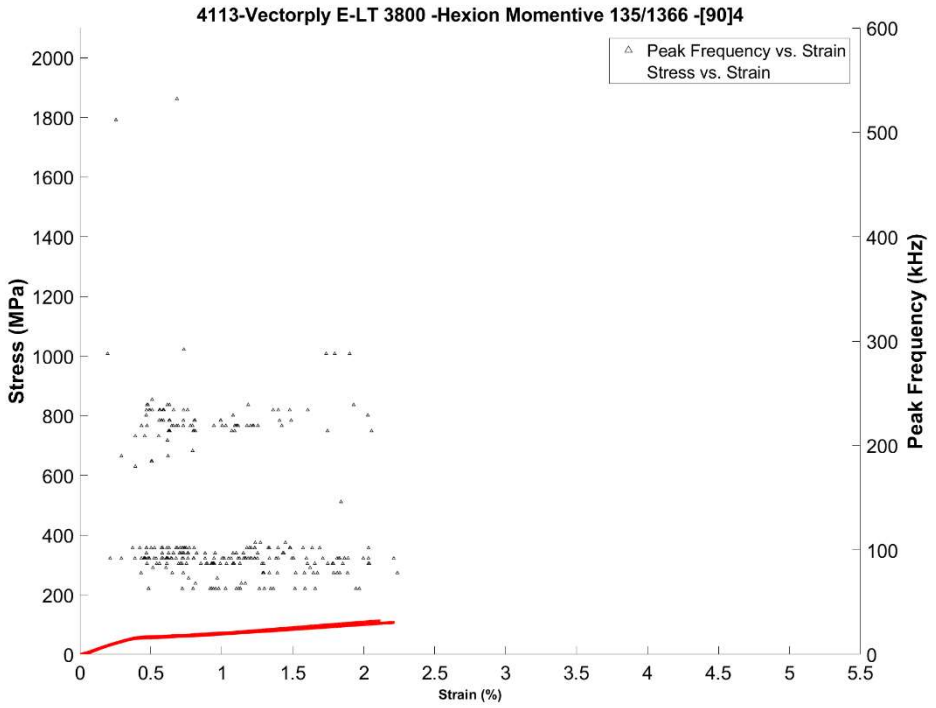
4113-Vectorply E-LT 3800 -Hexion Momentive 135/1366 -[90]4
Peak Frequency vs. Strain
Stress vs. Strain
Stress (MPa)
Peak Frequency (kHz)
Strain (%)
0
200
400
600
800
1000
1200
1400
1600
1800
2000
100
300
500
0.5
1
1.5
2
2.5
3
3.5
4
4.5
5
5.5

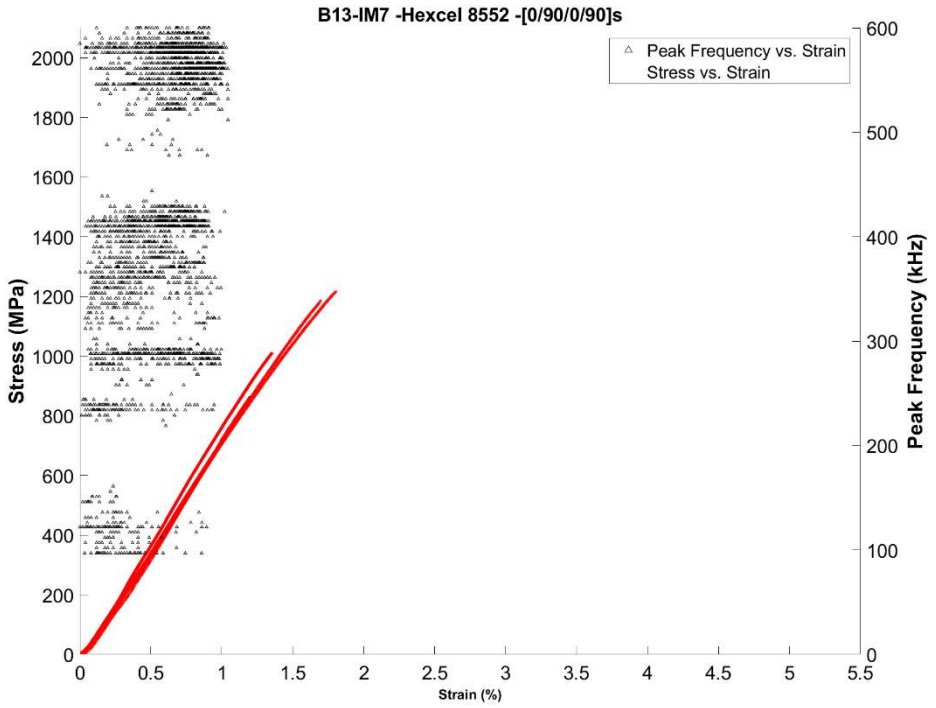
B13-IM7 -Hexcel 8552 -[0/90/0/90]s
Peak Frequency vs. Strain
Stress vs. Strain
Stress (MPa)
Peak Frequency (kHz)
Strain (%)
0
200
400
600
800
1000
1200
1400
1600
1800
2000
100
300
500
0.5
1
1.5
2
2.5
3
3.5
4
4.5
5
5.5

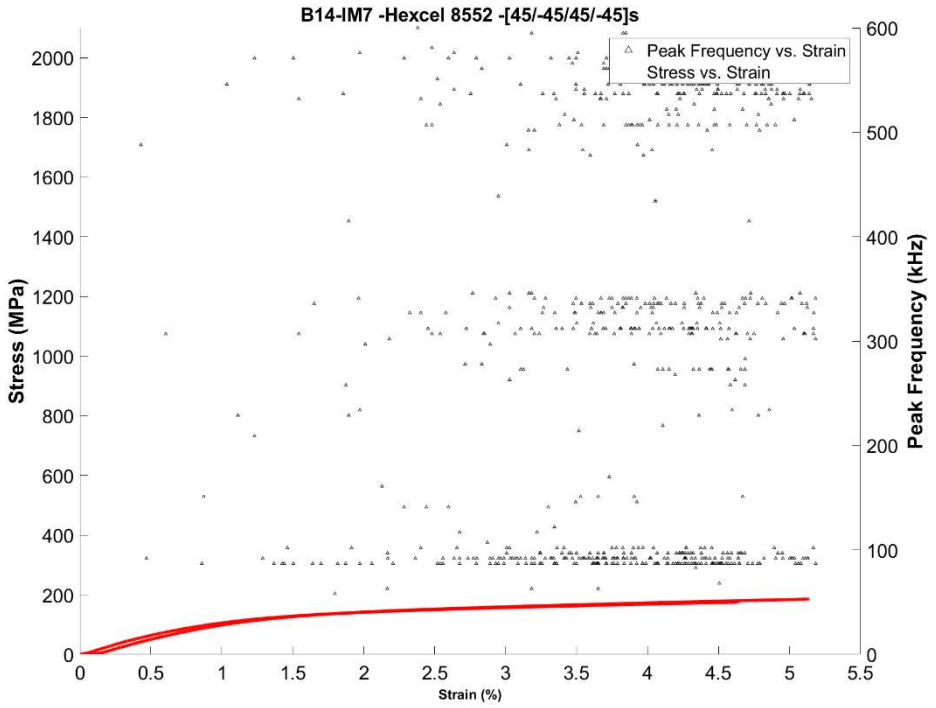
B14-IM7 -Hexcel 8552 -[45/-45/45/-45]s
Peak Frequency vs. Strain
Stress vs. Strain
Stress (MPa)
Peak Frequency (kHz)
Strain (%)
0
200
400
600
800
1000
1200
1400
1600
1800
2000
0
100
200
300
400
500
600
0
0.5
1
1.5
2
2.5
3
3.5
4
4.5
5
5.5

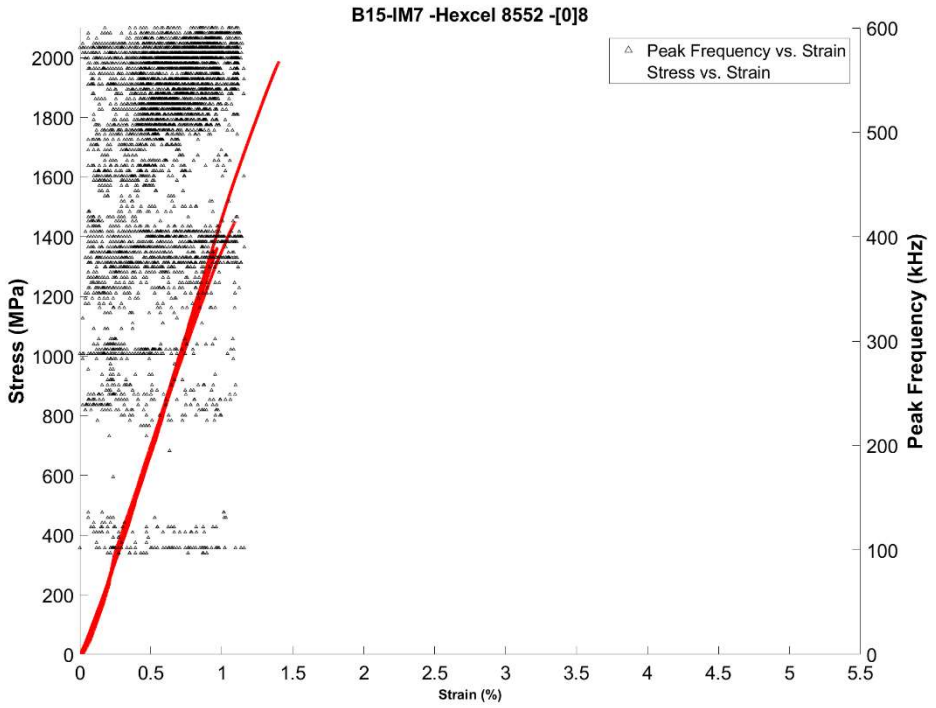
B15-IM7 -Hexcel 8552 -[0]8
Peak Frequency vs. Strain
Stress vs. Strain
Stress (MPa)
Peak Frequency (kHz)
Strain (%)
0
200
400
600
800
1000
1200
1400
1600
1800
2000
0
100
200
300
400
500
600
0
0.5
1
1.5
2
2.5
3
3.5
4
4.5
5
5.5

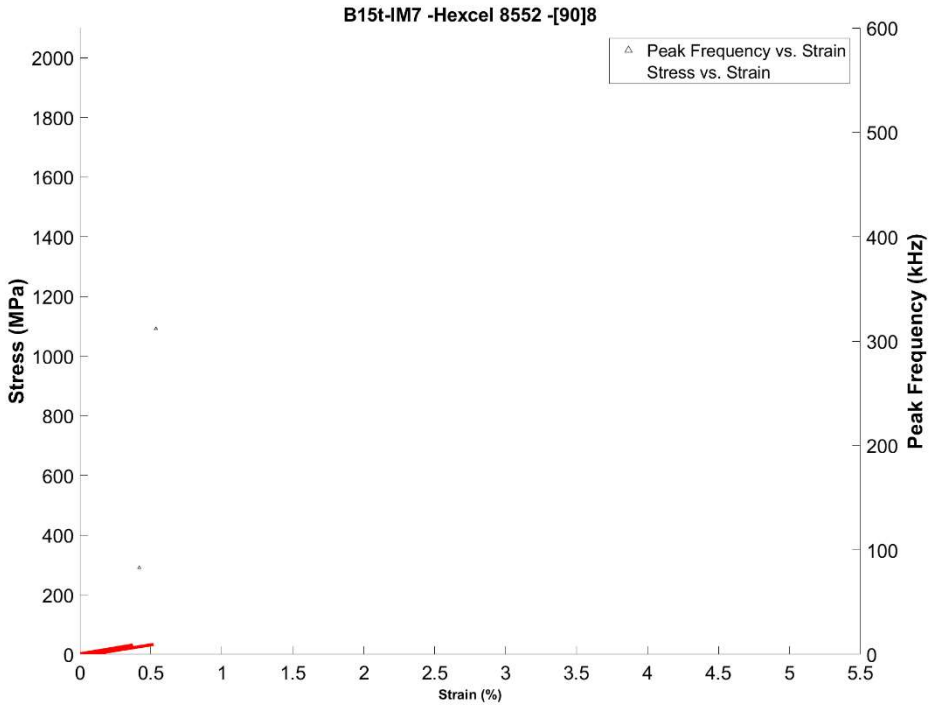
B15t-IM7 -Hexcel 8552 -[90]8
Peak Frequency vs. Strain
Stress vs. Strain
Stress (MPa)
Peak Frequency (kHz)
Strain (%)
0
200
400
600
800
1000
1200
1400
1600
1800
2000
0
100
200
300
400
500
600
0
0.5
1
1.5
2
2.5
3
3.5
4
4.5
5
5.5

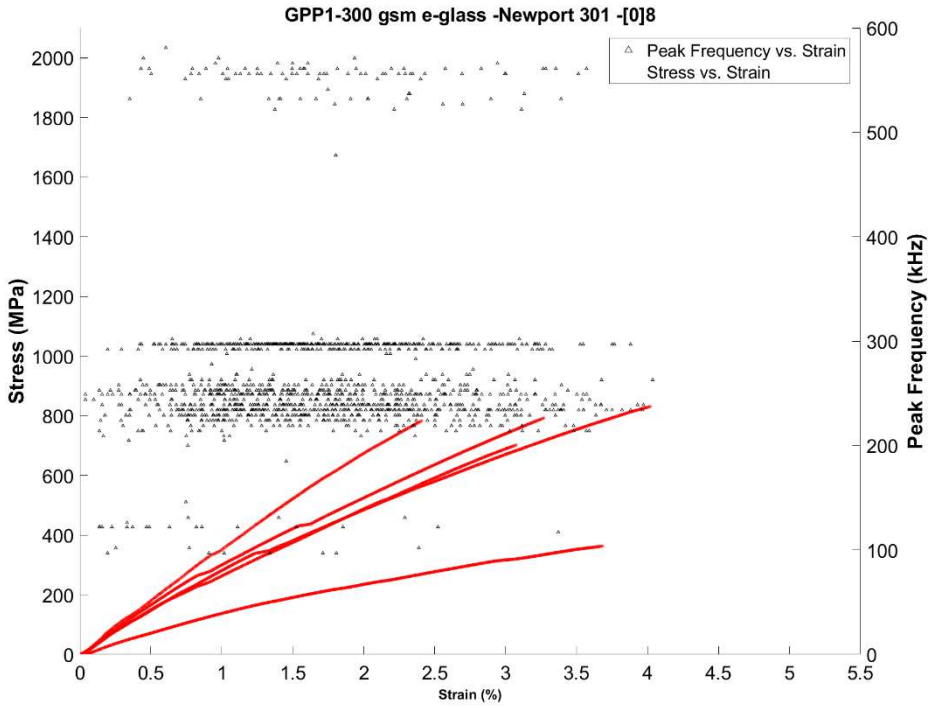
GPP1-300 gsm e-glass -Newport 301 -[0]8
Peak Frequency vs. Strain
Stress vs. Strain
Stress (MPa)
Peak Frequency (kHz)
Strain (%)
0
200
400
600
800
1000
1200
1400
1600
1800
2000
0
100
200
300
400
500
600
0
0.5
1
1.5
2
2.5
3
3.5
4
4.5
5
5.5

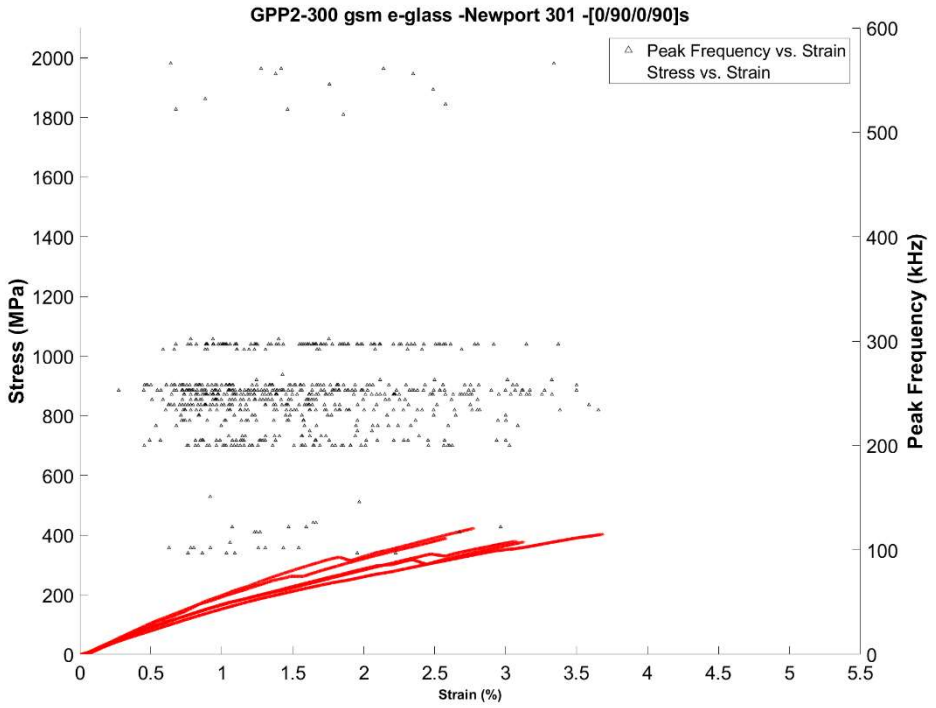
GPP2-300 gsm e-glass -Newport 301 -[0/90/0/90]s
Peak Frequency vs. Strain
Stress vs. Strain
Stress (MPa)
Peak Frequency (kHz)
Strain (%)
0
200
400
600
800
1000
1200
1400
1600
1800
2000
100
300
500
0.5
1
1.5
2
2.5
3
3.5
4
4.5
5
5.5

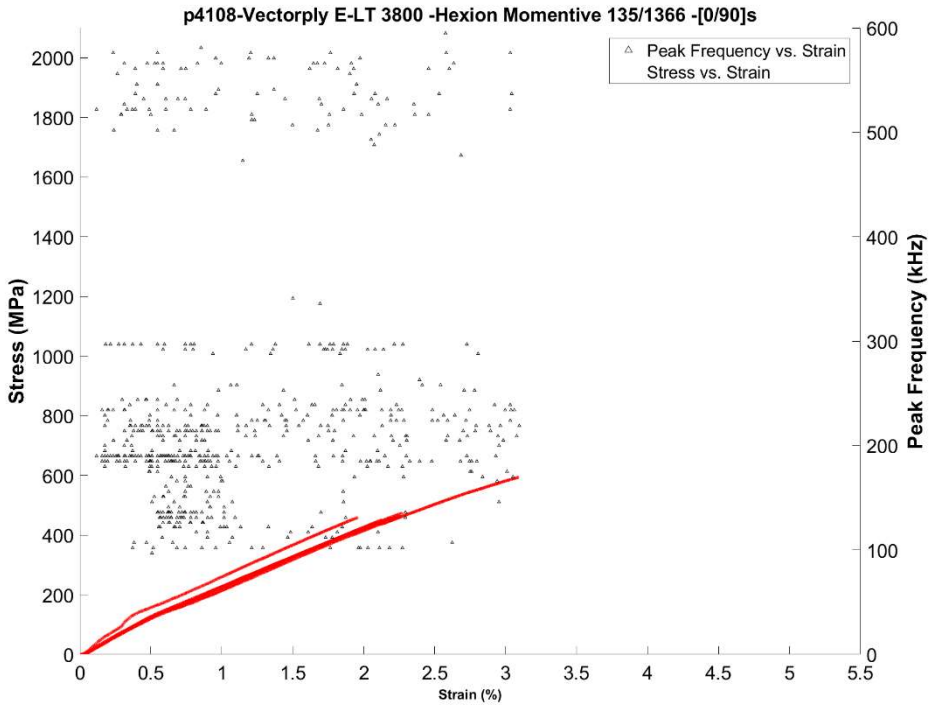
p4108-Vectorply E-LT 3800 -Hexion Momentive 135/1366 -[0/90]s
Peak Frequency vs. Strain
Stress vs. Strain
Stress (MPa)
Peak Frequency (kHz)
Strain (%)
0
200
400
600
800
1000
1200
1400
1600
1800
2000
100
300
500
0.5
1
1.5
2
2.5
3
3.5
4
4.5
5
5.5

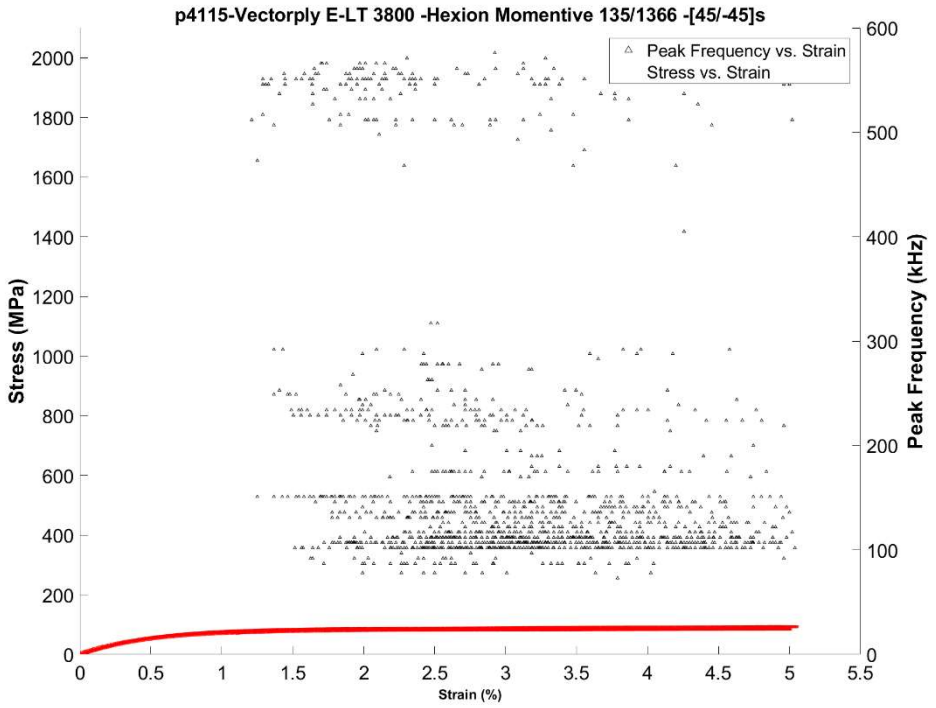
p4115-Vectorply E-LT 3800 -Hexion Momentive 135/1366 -[45/-45]s
Peak Frequency vs. Strain
Stress vs. Strain
Stress (MPa)
Peak Frequency (kHz)
Strain (%)
0
200
400
600
800
1000
1200
1400
1600
1800
2000
0
100
200
300
400
500
600
0
0.5
1
1.5
2
2.5
3
3.5
4
4.5
5
5.5

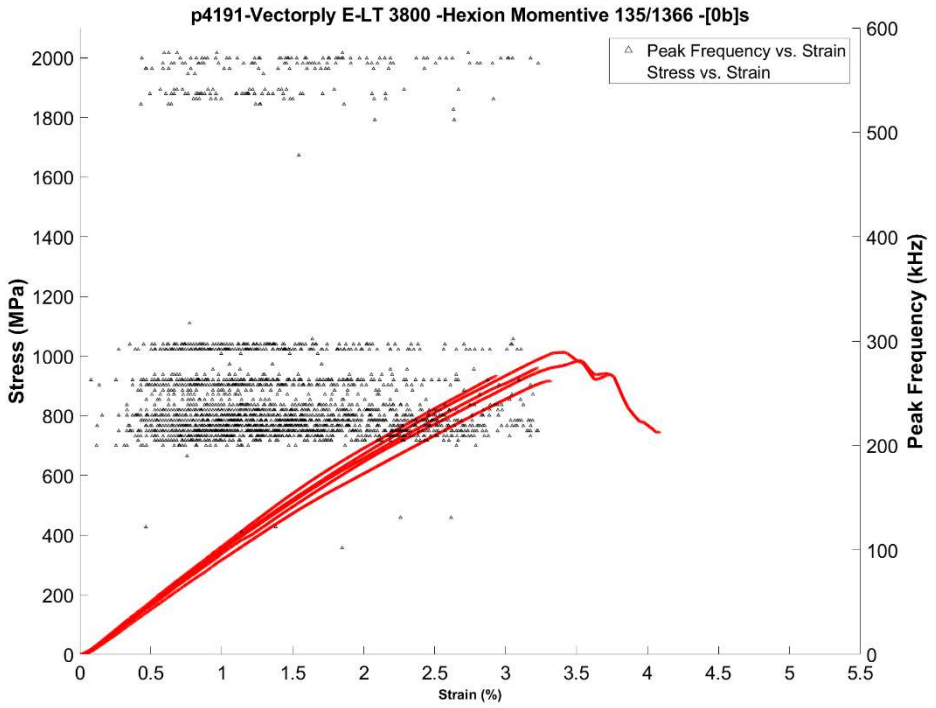
p4191-Vectorply E-LT 3800 -Hexion Momentive 135/1366 -[0b]s
Peak Frequency vs. Strain
Stress vs. Strain
Stress (MPa)
Peak Frequency (kHz)
Strain (%)
0
200
400
600
800
1000
1200
1400
1600
1800
2000
0
100
200
300
400
500
600
0
0.5
1
1.5
2
2.5
3
3.5
4
4.5
5
5.5